THE REPORT TO
THE CALIFORNIA DEPARTMENT OF
TRANSPORTATION

LONG-TERM STRUCTURAL PERFORMANCE MONITORING OF TWO HIGHWAY BRIDGES

PHASE I: INSTRUMENTATION

RTA-59A0155

by

Maria Q. Feng, Associate Professor
and
Doo-Kie Kim, Post-doctoral Researcher

DEPARTMENT OF CIVIL AND ENVIRONMENTAL ENGINEERING
UNIVERSITY OF CALIFORNIA, IRVINE

FEBRUARY, 2001

Technical Report Documentation Page

1. Report No.	2. Government Accession No.	3. Recipient's Catalog No.
FHWA A/CA/UCI-01-01		

4. Title and Subtitle	5. Report Date
Long-Term Structural Performance Monitoring of Two Highway Bridges Phase I: Instrumentation	February 26, 2001
	6. Performing Organization Code UC, Irvine
7. Author's	**8. Performance Organization Report No.**
Maria Q. Feng and Doo-Kie Kim	FHWA A/CA/UCI-01-01
9. Performing Organization Name and Address	**10. Work Unit No. (TRAIS)**
Civil and Environmental Engineering 4165 Engineering Gateway University of California, Irvine Irvine, CA 92697	**11. Contract or Grant No.** RTA-59A0155
12. Sponsoring Agency Name and Address	**13. Type of Report and Period Covered**
California Department of Transportation (Caltrans) 1801 30th Street Sacramento, CA 95816	Final Report
	14. Sponsoring Agency Code

15. Supplementary Notes

16. Abstract

In this project, sensor systems for long-term structural performance monitoring have been installed on two new highway bridges in Orange County, California: the Jamboree Road Overcrossing and the West Street On-Ramp. They include accelerometers, strain gauges, pressure sensors, displacement sensors, installed or embedded at strategic locations of both super- and sub-structures. Data recorders and power supplies have also been installed at the bridge sites.

Although the major focus of this Phase I project is on the sensor installation, preliminary vibration measurement and data analysis have been performed on these two instrumented bridges. On the Jamboree Road Overcrossing, Ambient vibration data have been collected, based on which natural frequencies and mode shapes have been extracted using various methods and compared with those obtained by the preliminary finite element analysis. On the West Street On-Ramp, braking and bumping vibration tests have been carried out using a water truck in addition to ambient vibration tests. Natural frequencies and mode shapes have been derived and the results by the breaking and bumping vibration tests have been compared.

17. Key Words	18. Distribution Statement
Instrumentation, Structural performance monitoring, bridge, accelerometer, embedded strain gauge, displacement sensor, soil pressure sensor, vibration measurement, frequency, mode shape	No restrictions. This document is available to the public through the National Technical Information Service, Springfield, Virginia 22161

19. Security Classif. (of this report)	20. Security Classif. (of this report)	21. No. of Pages	22. Price
Unclassified	Unclassified		

Form DOT F 1700.7 (2-86)

DISCLAIMER: The opinions, findings, and conclusions expressed in this publication are those of the authors and not necessarily those of the STATE OF CALIFORNIA

ABSTRACT

In this project, sensor systems for long-term structural performance monitoring have been installed on two new highway bridges in Orange County, California: the Jamboree Road Overcrossing and the West Street On-Ramp. They include accelerometers, strain gauges, pressure sensors, displacement sensors, installed or embedded at strategic locations of both super- and sub-structures. Data recorders and power supplies have also been installed at the bridge sites. Although the major focus of this Phase I project is on the sensor installation, preliminary vibration measurement and data analysis have been performed on these two instrumented bridges. On the Jamboree Road Overcrossing, Ambient vibration data have been collected, based on which natural frequencies and mode shapes have been extracted using various methods and compared with those obtained by the preliminary finite element analysis. On the West Street On-Ramp, braking and bumping vibration tests have been carried out using a water truck in addition to ambient vibration tests. Natural frequencies and mode shapes have been derived and the results by the breaking and bumping vibration tests have been compared.

ACKNOWLEDGEMENT

This instrumentation program of highway bridges was funded jointly by the Federal Highway Administration (FHWA) and the California Department of Transportation (Caltrans) under Contract #59A0155.

This program was monitored by Mr. Li-Hong Sheng of Caltrans, as Program Manager. Great support for the instrumentation was attained by Mr. Leonard M. Fiji of Caltrans. Professor Chung-Bang Yun at Korea Advanced Institute of Science and Technology provided valuable technical advices.

Tokyo Sokushin Inc., FCI Constructors, and Silverado Constructors offered in-kind support in embedding and installing the sensors and data acquisition systems during the construction of bridges. District 12 of Caltrans provided traffic control and lifting equipment for the sensor installation and data collection.

This project would have been impossible without the assistance and the support mentioned above, for which the authors wish to cordially express their sincere gratitude.

TABLE OF CONTENTS

LIST OF FIGURES

LIST OF TABLES

Chapter 1

INTRODUCTION

1.1 Background

Monitoring technology can play an important role in securing system integrity, minimizing maintenance cost, and maintaining longevity of highway bridges. Meanwhile, it can also provide verifications of current design/analysis and suggest their improvement for retrofit and future construction. Monitoring technology consists of two aspects: (1) instrumentation of bridges with sensors such as accelerometers and strain gauges and more importantly, (2) methodologies for obtaining meaningful information concerning the structural performance, if any, from the measured data.

The Eastern Transportation Corridor is one of the three design/build/operate toll roads in southern California. All of the bridges in the Corridor are designed based on a two-level seismic performance design criterion, which greatly influence the structural proportion between the super- and sub-structures. In general, the sub-structures become stiffer and larger than those designed by the current Caltrans criteria. The consequence of this change has not been evaluated yet. It will be of great interest to monitor and evaluate the long-term structural performance of such bridges under not only seismic but also service

loads, and to compare their performance with that of the bridges designed by the current Caltrans approach.

In the current Phase I project, monitoring systems including accelerometers, strain gauges, pressure sensors, and displacement sensors have been installed on two new highway bridges in Orange County, California: the Jamboree Road Overcrossing and the West Street On-Ramp. Both are three-span concrete box-girder bridges located in Orange County, California. The former is on the Eastern Transportation Corridor and designed based on the two-level seismic performance criterion, and the latter is on the I-5 Corridor and designed by the current Caltrans approach. A further Phase II study will develop methodologies for bridge performance monitoring using these two instrumental bridges.

1.2 Objectives and Tasks

The primary objectives of this two-year project are to (1) install automated structural monitoring systems involving strain gauges, pressure sensors, displacement sensors, accelerometers, data recorders, and power supplies on the Jamboree Road Overcrossing and the West Street On-Ramp, and (2) to perform preliminary data collection, processing, and analysis.

Major tasks of this project include: (1) finite element analysis of the two bridges to determine the optimal locations of sensors; (2) installation of a variety of sensors on each of the two bridges; (3) installation of an automated data acquisition system and a power supply unit on each of the bridges; (4) collection of data under different traffic conditions; and (5) preliminary data analysis and comparison.

Chapter 2

DESCRIPTION OF BRIDGES

The Jamboree Road Overcrossing is located on Rt. 261 of the Eastern Transportation Corridor in Irvine and the West Street On-Ramp is on I-5 Corridor near Disneyland in Anaheim, both in Orange County, California. Figure 2.1 is a map showing their locations.

2.1 Jamboree Road Overcrossing

2.1.1 Description

The Jamboree Road Overcrossing is a typical three-span continuous cast-in-place prestressed post-tension box-girder bridge in the Eastern Transportation Corridor (Figure 2.2). The total length of the bridge is 110.9 m (366 ft.), in which the lengths of spans are 35.5, 46.1, and 30.3 m. (114, 152, and 100 feet) from span 1 to span 3 (Figure 2.3). The bridge is supported on two monolithic single columns and sliding bearings on both abutments (Figures 2.4). The sliding bearings (Figure 2.5) allow creep, shrinkage, and thermal expansion or contraction. The typical cross section of the box-girder is shown in

Figure 2.6. It is noted that the columns are not on the center line of the super-structure as shown in Figure 2.7 and the bridge has a skewed abutment 4 as shown in Figure 2.8.

The Eastern Transportation Corridor is one of the three design/build/operate toll roads in southern California. All of the bridges in the Corridor are designed based on the new two-level seismic performance design criteria, which greatly influence the structural proportion between the super- and sub-structures. In general, the sub-structures become stiffer and larger than those designed by the current Caltrans criteria (TCA, 1996; Caltrans, 1996). The consequence of this change has not been evaluated yet. It will be of great interest to monitor and evaluate the long-term structural performance of such bridges under not only seismic but also service loads, and to compare their performance with that of the bridges designed by the current Caltrans approach.

During the proposal stage of this project, the Jamboree Road Overcrossing was one of a few bridges that were scheduled for completion of construction at the end of the proposed project, thus providing an excellent opportunity for embedding strain sensors in concrete and a pressure sensor in the abutment during the construction. However, the corridor construction was finished before the funding was approved and contract executed by Caltrans. As a result, only accelerometers and a displacement sensor were installed after the completion of construction on the Jamboree Road Overcrossing.

2.1.2 Preliminary Finite Element Analysis

For a preliminary finite element analysis of the Jamboree Road Overcrossing, a 3 dimensional (3D) finite element model as shown in Figure 2.9 was developed. The

super- and sub-structures were modeled as 3D frame elements. The cross section area and moment of inertia for each element were calculated from the design drawings and listed in Table 2.1.

The most difficult part of modeling was to develop realistic and accurate footing and bearing models and to determine their stiffness parameters. Considering that the use of the model is for analyzing the bridge response to operational (traffic) loads, the bridge pile footings and bearings were modeled as linear horizontal, vertical, and rotational springs as shown in Figure 2.9. In this analysis, the foundation stiffness values were assumed as $1.0\times10^{5}\,kip/\,ft$ for the horizontal spring, and $1.0\times10^{7}\,kip\cdot ft/rad$ for the rotational spring, based on ATC-32 (1996). The bearing stiffness values at both ends of the bridge were assumed as $1.366\times10^{4}\,kip/\,ft$ for the horizontal spring, and $2.130\times10^{5}\,kip\cdot ft/rad$ and $8.521\times10^{5}\,kip\cdot ft/rad$ for the rotational springs at left and right ends of a deck, based on FHWA (1996). It is noted that the values for the rotational springs were taken considering the skewness of the deck.

The computed natural frequencies, derive from the analytical model with the boundary spring elements, are shown in Table 2.2, and the computed first mode shapes are plotted in Figure 2.10 for the vertical direction and in Figure 2.11 for the transverse direction, together with those measured from ambient vibration tests to be described later.

2.2 West Street On-Ramp

2.2.1 Description

The West Street On-Ramp is a three-span continuous and curved cast-in-place prestressed post-tension box-girder bridge in the I-5 Corridor near Disneyland in Anaheim, California (Figure 2.12). The total length of the bridge is 496′-6″, in which the lengths of spans are 150′-2″, 197′-3″, and 149′-1″ from span 1 to span 3 (Figure 2.13). The bridge is supported by two fixed columns and sliding bearings on both abutments (Figures 2.14). The sliding bearings allow creep, shrinkage, and thermal expansion or contraction. The typical cross section of the box-girder is shown in Figure 2.15. It is noted that the bridge is curved and with a 12% super-elevation.

2.2.2 Preliminary Finite Element Analysis

For a preliminary finite element analysis of the West Street On-Ramp, a 3-dimensional (3D) finite element model as shown in Figure 2.16 was developed. The super- and sub-structures were modeled as 3D frame elements. The values of the area and moment of inertia for each element were calculated from the design drawings and listed in Table 2.3. The moments of inertia and areas represent the characteristics of the stiffness and the mass matrices of the structure. A total of 202 beam-column elements for the super-structure and 16 frame elements in each column were used. The inclination of the girder was considered using the transformation of the girder local axes. Considering that the model is for the analysis of the bridge response under operational (traffic) loads, the

bridge bearings were modeled as linear horizontal, vertical, and rotational springs as shown in Figure 2.17. The bearing stiffness values at both ends of a deck were assigned according to the FHWA (1996) as 65,861 kip/ft for the longitudinal springs, and 129,170 kip/ft and 148,000 kip/ft for the transverse and rotational springs, respectively.

The natural frequencies and periods computed using this analytical model with the boundary spring elements are shown in Table 2.4, and the computed mode shapes are plotted in Figure 2.17.

Chapter 3

MONITORING SYSTEM

The monitoring system installed at the West Street On-Ramp involves not only accelerometers, but also strain gauges embedded in concrete. Long-term strain and acceleration monitoring is expected to provide verifications of current design/analysis and suggest their improvement for retrofit and future construction. The sensors were installed at both super- and sub-structures. Instrumentation of sub-structures is important, since they turned out to be one of the most vulnerable structural components of highway bridges under damaging earthquakes.

3.1 Sensor

3.1.1 Accelerometer

Uni-axial, bi-axial, and tri-axial force-balance servo-type accelerometers as shown in Figure 3.1 were permanently installed on both bridges. Their specification are listed in Table 3.1. The frequency response functions of the accelerometers in Figures 3.2 and 3.3 indicate that the accelerometers can measure dynamic signals in a frequency range from

0.5 Hz through 30 Hz. The accelerometers were installed on the bottom of the bridge box girder. Figure 3.4 shows a tri-axial accelerometer installed on the bridge.

The accelerometers were installed at the strategic locations of these bridges, which were based on the preliminary finite element analyses described in Chapter 2. The locations of accelerometers were selected as sensitive ones in mode shapes obtained by preliminary finite element analysis, and they are shown in Figures 3.5 and 3.6 at the Jamboree Road Overcrossing, and in Figures 3.7 and 3.8 at the West Street On-Ramp. The accelerometers were placed along the center line of the bottom of the girder to minimize the torsional effect of the bridge box girder.

3.1.2 Strain Gauge

Strain gauges shown in Figures 3.9 and 3.10, which are micro-displacement sensors, were permanently embedded in concrete members of the West Street On-Ramp. Each end of a strain gauge was completely welded to a dummy reinforcing bar as shown in Figures 3.11, 3.12 and 3.13. The specification of the strain gauges are shown in Table 3.2. These sensors were embedded to measure the dynamic strains induced by bending moments. The locations of strain gauges are shown in Figures 3.16 and 3.17.

The strain is determined based on the change of the distance between two ends of the gauge:

$$\mu \text{ strain} = \frac{\Delta L}{L} \times 10^{-6} \tag{3.1}$$

The calibration test of the strain gauges was performed by applying a load on one end while fixing the other end of the gauge, as shown in Figure 3.14. The relationship between the load and the strain is as follows:

$$\sigma = \frac{F}{S} = \frac{F}{283.5} \ [kg/mm^2] \tag{3.2}$$

$$\sigma = E \times \varepsilon = 20000[kg/mm^2] \times \varepsilon \tag{3.3}$$

$$\varepsilon = \frac{dL}{L} = \frac{\sigma}{20000[kg/mm^2]} = \frac{F/283.5[mm^2]}{20000[kg/mm^2]} = \frac{F}{567 \times 10^4 \ [kg]} \tag{3.4}$$

The calibration test results are shown in Tables 3.3 and 3.4.

The installation procedures of strain gauges are summarized in the following:

1. Weld each end of a strain gauge to a dummy steel rebar.

2. Since there are some electrical parts inside the strain gauge, the high temperature more than 50°C should be prohibited. The water-wetted cloth was winded around the whole strain meter during the welding, as shown in Figure 3.11.

3. Arrange the dummy rebar, so that the cable drawer mouth of the strain gauge faces inside, as shown in Figure 3.15.

3.1.3 Displacement Sensor

In order to measure the displacement of the concrete box girder with respect to the abutment due to shortening, creep, shrinkage, as well as seismic excitations, a displacement sensor was installed at the expansion joint for each bridge. The information on the displacement sensor is shown in Table 3.5, and Figures 3.18 - 3.20. The location of displacement sensor is shown in Figure 3.21 at the Jamboree Road Overcrossing and in Figure 3.22 at the West Street On-Ramp.

3.1.4 Soil Pressure Sensor

To measure the soil pressure at an abutment during earthquakes, a soil pressure sensor (Figures 3.23 and 3.24) was installed on the back wall of the abutment at the West Street On-Ramp as shown in Figure 3.25. The specification of the pressure sensor are shown in Table 3.6. The location of the sensor is shown in Figure 3.22.

3.2 Data Recorder

A 16-channel data recorder was installed at the Jamboree Road Overcrossing as shown in Figure 3.26, while a 24-channel data recorder was installed at the West Street On-Ramp as shown in Figure 3.27. The specification of the recorders are shown in Table 3.7. They can be triggered either manually or automatically by earthquake ground motion.

Each recorder is equipped with a flash memory card. When the flash memory card in full, either the oldest record or the record with the smallest average amplitude will be automatically over-written. For seismic response measurement, the latter is more reasonable.

The recorder is automatically triggered for seismic response measurement. The tri-axial accelerometer at the bottom of column 3 was set up for triggering, and the triggering acceleration for each direction is 0.002g. In other words, once the acceleration in one of three directions at the bottom of the column exceeds 0.002g, the monitoring system will automatically begin to record data from the sensors.

3.3 Power Supply

In the West Street On-Ramp, the factory electric voltage available at the bridge site is transformed into domestic voltage by a transformer, and then the electrical power is used for the monitoring system. The transformer is shown in Figure 3.28, and its specification is shown in Table 3.8. Given the complexity of today's networked systems there is a high probability that power failure caused by earthquakes may result in data corruption or equipment failure. Power disturbances during an earthquake could also result in damaging voltages or current surges being passed along to the bridge monitoring system. Uninterruptible power supply (UPS) systems were installed at both of the West Street On-Ramp and the Jamboree Overcrossing, which can provide excellent protection against most power disruptions, even for those caused by lightning. When power fails, the UPS system will provide emergency backup power to the monitoring system for a certain

period depending on the capacity of its rechargeable batteries. The UPS unit installed at the West Street On-Ramp is shown in Figure 3.29, and its specifications are listed in Table 3.9. It can provide power backup for 10 minutes. In addition to the regular power electrical power supply, a solar power supply system was installed at the Jamboree Road Overcrossing, as shown in Figure 3.30. The batteries shown in Figure 3.31 are charged by the solar panels during daytime and provide power to the monitoring system at nights. Figure 3.32 is a schematic diagram of the solar power supply system.

3.4 Installation

The system configurations of the monitoring systems are shown in Figures 3.33 and 3.34 respectively for the Jamboree Road Overcrossing and the West Street On-Ramp. Figure 3.35 is a photo showing the block of the traffic under the Jamboree Road Overcrossing bridge for sensor installation. Figures 3.36 and 3.37 show the installation of the accelerometers on the bottom of the box girder using a cherry picker.

Figure 3.38 shows the strain gauges being installed together with rebars before pouring concrete at the West Street On-Ramp.

Chapter 4

THEORY OF DATA PROCESSING

Processing of ambient vibration data measured at a structure is usually associated with the extraction of modal parameters including natural frequencies and mode shapes. The loads are normally unknown, and thus the modal parameter extraction is solely based on the measured responses only.

Several methods for extracting modal parameters without requiring information about input loads have been studied. The peak picking (PP), the random decrement (RD), and the frequency domain decomposition (FDD) methods are most widely used methods based on frequency domain analysis. And the Ibrahim time domain (ITD) and the eigen-system realization algorithm (ERA) methods are based on time domain analysis (Ibrahim et al., 1977; Juang, 1994).

The major advantage of the frequency domain-based methods compared to the time domain-based ones is their user-friendliness. They are fast, simple to use, and give the user a feeling of the data he or she is dealing with. On the other hand, the most important advantage of the time domain-based method is that they can consider the nonlinear responses of structures. This chapter reviews the theoretical background of the modal parameter extraction methods in the frequency domain which are used in this project.

4.1 Peak Picking Method

The *peak picking* (or *peak amplitude*) method has been used for a long time (e.g. Bendat and Piersol, 1993; Ewins, 1999). It is effective for structures whose frequency response functions (FRF) exhibit well-separated modes. It is not suitable for very lightly-damped structures because accurate measurements around resonance are difficult to obtain, and is not suitable for very heavily-damped structures either, because the measurements around resonance are strongly influenced by more than one mode. Although all these appear to limit the application of the method, it is highly useful in obtaining initial estimates of the required parameters, thereby speeding up the analysis using more general methods such as the curve fitting method, the random decrement method, and the frequency domain decomposition method.

This method involves the following steps:

1. Individual resonance peaks are detected on the FRF plot, and the frequency of each peak is taken as the natural frequency of each mode (ω_i).

2. The value of each FRF peak is noted as $\rho_{i,\max}$ and the frequency bandwidth at $\rho_{i,\max}/\sqrt{2}$ is noted as $\Delta\omega_i (= \omega_{ib} - \omega_{ia})$. The damping of each mode can be estimated from the following formulae:

$$\xi_i = 2(\omega_{ib}^2 - \omega_{ia}^2)/\omega_i^2 \cong 2\Delta\omega_i/\omega_i \qquad (4.1)$$

3. Mode shapes are obtained by solving the following equations:

$$\rho_{i,\max}^{jk} = \left| \frac{\phi_{ji}\phi_{ki}}{2\omega_i^2 \xi_i} \right| \tag{4.2}$$

It must be noted that the estimation of the modal parameters using the peak picking method depends heavily on the accuracy of the peak value $\rho_{i,\max}$, which, unfortunately, are difficult to measure with good accuracy. Usually the measurement errors are concentrated around the resonance region, especially for lightly-damped structures. Errors may also arise because the modes are not well separated. Even with clearly separated modes, it is often found that the neighboring modes do contribute a noticeable amount to the total response at the resonance of the mode being analyzed.

4.2 Random Decrement Method

In this project, the random decrement (RD) technique, sometimes referred to as *Randomdec*, was used to reduce the effect of vibration noises on the estimation of modal parameters from the vibration measurement data. The fundamental concept of the random decrement technique (Cole, 1968; Yang et al., 1985; Asmussen and Brincker 1996) is based on the fact that the random response of a structure is composed of a deterministic part and a random part under white noise excitation. By averaging sufficient sample responses, the random part associated with the random excitation will average out, leaving the deterministic part. It has been shown that the remaining deterministic part is a *free decay response* and is called *randomdec signature*, from which the modal parameters can be easily extracted. The randomdec signature $z(\tau, x)$ can be obtained as

$$z(\tau, x) = \frac{1}{N}\sum_{i=1}^{N} y(\tau + t_i, x) \tag{4.3}$$

where $y(t, x)$ is measured data at point x and time t; t_i is a time instance satisfying certain initial conditions described below; and N is the number of data sets.

The random response is decomposed into segments in a way such that each segment starts with the same initial conditions. The randomdec signature is defined as the average of these segments. Figure 4.1 illustrates a randomdec signature derived from a random response divided into segments with the same initial amplitudes and the same initial slopes.

4.3 Frequency Domain Decomposition Method

The peak peaking (PP) method gives reasonable estimates of natural frequencies and mode shapes if the modes are well separated. Otherwise, it is very difficult or impossible to use this method. The frequency domain decomposition (FDD) method, which utilizes the singular value decomposition of the power spectral density (PSD) matrix and was originally developed for extracting operational deflection shapes in mechanical vibrating systems (Otte et al., 1990), may be used to separate close modes, thus obtaining better estimates (Yun et al, 2000).

The FDD technique is an extension of the PP technique. The PP approach is based on simple signal processing using the Discrete Fourier Transform (DFT), and is using the fact that well separated modes can be estimated directly from the FRF matrix at resonance peaks. In the FDD technique, the PSD matrix is first formed from the

measured data using a simple signal processing by DFT. However, instead of using the PSD matrix directly like the FRF in the PP approach, the PSD matrix is decomposed at each frequency line using the Singular Value Decomposition (SVD). By doing so, the PSD matrix is decomposed into a set of auto spectral density functions, each corresponding to a single degree of freedom (SDOF) system. This is exactly true in the case where the loading is white noise, the structure is lightly damped, and the mode shapes of close modes are geometrically orthogonal. If these assumptions are not satisfied, the decomposition into SDOF systems becomes an approximation, but still the results are significantly more accurate than those of the classical approaches (Brinker et al., 2000). The singular vectors in the SVD are used as estimates of the mode shape vectors, and the natural frequencies are estimated by taking each individual SDOF auto spectral density function back to the time domain by inverse DFT. The frequency and damping are simply estimated from the crossing times and the logarithmic decrement of the corresponding SDOF auto correlation function.

The FDD method is summarized as the following steps:

1. The PSD $\mathbf{G}_{yy}(j\omega)$ is estimated from vibration measurements.

2. Estimations of the output PSD $\mathbf{G}_{yy}(j\omega)$ at discrete frequencies $\omega = \omega_i$ is then decomposed by taking the SVD of the matrix

$$\mathbf{G}_{yy}(j\omega_i) = \mathbf{U}_i \mathbf{S}_i \mathbf{U}_i^H \tag{4.4}$$

where the matrix $\mathbf{U}_i = [\mathbf{u}_{i1}, \mathbf{u}_{i2}, \Lambda, \mathbf{u}_{im}]$ is a unitary matrix holding the singular vector $\mathbf{u}_{ij}$, and $\mathbf{S}_i$ is a diagonal matrix holding the scalar singular values s_{ij}.

3. If only the k th mode is dominating near a peak corresponding to the k th mode in the spectrum, the first singular vector becomes

$$\boldsymbol{\varphi} = \mathbf{u}_{i1} \tag{4.5}$$

and the corresponding singular value is the auto PSD function of the corresponding SDOF system.

4. Near a peak corresponding to the k th mode in the spectrum, this mode or possible close modes may be dominating. This PSD function is identified around the peak by comparing the mode shape estimate $\boldsymbol{\varphi}$ with the singular vectors for the frequency lines around the peak. The modal assurance criterion (MAC) value can be used to find a singular vector corresponding to the singular value.

Chapter 5

TEST ON JAMBOREE ROAD OVERCROSSING

5.1 Ambient Vibration Test

When estimating dynamic properties of large civil engineering structures such as bridges and buildings from vibration measurement, possibilities to control and measure the loading on the structures are rather limited. For a bridge which carries traffic loads 24 hours a day, the traffic-induced ambient vibration will be a dominating signal. That is one of the reasons that ambient vibration tests have gained an increasing interest and popularity during the recent years as a tool for monitoring large civil engineering structures (e.g., Abdel-Ghaffer and Scanlan, 1985; Harik et al., 1997; Feng et al., 1998). In comparison to forced vibration techniques, the ambient vibration techniques present the remarkable advantage of not requiring heavy and expensive equipment for exciting the structure. The dynamic properties of the structure can be rather accurately estimated on the basis of the measurements of structural ambient responses. Dynamic property extraction using ambient vibration measurements requires special data processing techniques to deal with relatively small amplitudes of ambient vibrations contaminated with noises without the knowledge of input forces. In this project, the peak picking, the

random decrement, and the frequency domain decomposition methods have been used for processing ambient vibration measurements at the Jamboree Road Overcrossing.

5.2 Measurement Data

The locations of the accelerometers are shown in Figures 3.5 and 3.6. The accelerations at the various locations on the bottom of the box-girder and the column were measured with a sampling frequency 100 Hz. The maximum continuous recording duration is 70 minutes with a 1-minute recess every 10 minutes.

Typical time histories of accelerations of the super-structure in the vertical direction are shown in Figure 5.1, in which time delays are noticed among the accelerations at different locations. A vehicle passes from abutment 4 to abutment 1 with an average vehicle speed of 84.3km/h(50mph), and the average time that it takes for a vehicle to completely pass through the bridge is 4.93sec. The first excitation frequencies of vehicles for a simply supported beam can be roughly computed using the span length and the average vehicle speed as follow:

$$\frac{74.2\ ft/sec}{114\ ft} = 0.65\ Hz \qquad \text{: for the length of span 1}$$

$$\frac{74.2\ ft/sec}{152\ ft} = 0.49\ Hz \qquad \text{: for the length of span 2}$$

$$\frac{74.2\ ft/sec}{100\ ft} = 0.74\ Hz \qquad \text{: for the length of span 3}$$

Though the excitation frequencies are calculated with the assumption of a simply supported beam, all these excitation frequencies are very low, which do not seem to affect heavily the modal parameters of the bridge measured from ambient vibrations.

The typical time histories of accelerations of the super-structure in the transverse direction are shown in Figure 5.2, in which, time delays are also noticed. The amplitudes of accelerations in the transverse direction are relatively smaller than those in the vertical direction because of the traffic loads mainly induce vibrations in the vertical direction.

The typical time histories of accelerations of the super-structure in the longitudinal direction is shown in Figure 5.3 and typical accelerations at the bottom of column 3 are shown in Figure 5.4. The amplitudes of these are relatively small comparing to those of the super-structure in the vertical and the transverse directions.

The relative displacement between the super-structure and the abutment was measured using the displacement sensor at the same sampling frequency in the longitudinal direction. A typical recorded displacement time history is shown in Figure 5.5.

5.3 Data Processing

Totally, 82 data sets measured in the daytime were processed, in which the time length of each data set is 10 minutes. The peak picking (PP) and the frequency domain decomposition (FDD) methods were used to extract modal parameters from the averaged vibration data with 25 percent overlapping. The random decrement (RD) method was also applied to obtain the parameters from the randomdec vibration data which was

obtained under a prescribed initial condition of positive zero crossing. The total number of sampling data in the averaged and the randomdec data is 4096 (= 40.96 sec).

Figure 5.6 shows the time history of a typical recorded vertical acceleration in the middle of span 2 (at JA4) at the Jamboree Road Overcrossing. Figures 5.7 and 5.8 are the time histories of the averaged and the randomdec accelerations at the same location respectively. Randomdec acceleration exhibits its free vibration decay since the data sets have been sampled with the approximately same initial conditions compared to those in the averaged acceleration.

Figures 5.9-5.11 show the power spectral density (PSD) functions of the averaged and the randomdec vertical accelerations used for the PP, the RD, and the FDD analyses. Figure 5.12 shows the PSD function of an averaged transverse acceleration used for the FDD analysis. Figures 5.13-5.15 show mode shapes in the vertical and longitudinal directions derived by the PP, the RD, and the FDD methods. Figure 5.16 shows mode shapes in the transverse direction derived by the FDD method. The peak values in the PSD functions decrease as frequency increases, so picking peak values become more difficult for each subsequent mode.

It is observed that the high and the horizontal modes contain more noises than the low and the vertical modes since traffic loads mainly excite vertical vibration and the frequency contents of the loads are relatively low. Observing the mode shapes, those estimated by the FDD method agree better with those from the finite element analysis than those estimated by the PP and the RD methods.

Figure 5.17 shows the PSD function of an averaged displacement measurement at the abutment. The frequency contents of the displacement are lower than those of the acceleration, and no remarkable peaks are noticeable.

The natural frequencies (six in the vertical and three in the transverse directions) derived analytically and experimentally are shown together in Table 5.1. The difference as shown in the parentheses between the analytical and the experimental natural frequencies suggests the need for updating the initial finite element model using the experimental results.

Chapter 6

TEST ON WEST STREET ON-RAMP

6.1 Post Tension Test

During the post tension of the West Street On-Ramp, concrete strains at various locations of the bridge were measured using the embedded strain gauges, and their time histories are shown in Figures 6.1 and 6.2. Long-term strain monitoring and analysis will be performed in the future.

6.2 Braking Vibration Test

Braking vibration tests using a water truck were carried out at the final constructional stage of the West Street On-Ramp before it opened to traffic. Braking forces were applied by the water truck at the middle point of each span in the longitudinal direction to induce bridge vibration. The water truck is shown in Figure 6.3, which weighs approximately 150kN when fully loaded. The locations of accelerometers installed on the bridge are shown in Figures 3.7 and 3.8. The sampling frequency is 100 Hz, the same as that used at the Jamboree Road Overcrossing .

Typical time histories of accelerations measured at various locations on the super-structure are shown in Figure 6.4 for the vertical direction and in Figure 6.5 for the transverse direction, in which the braking force was applied at the middle of span 2. The amplitudes of accelerations in the transverse direction are relatively smaller than those in the vertical direction. Among all the transverse accelerations, the acceleration of the super-structure near abutment 1 exhibits the largest amplitude due to the skewness of the abutment and the longitudinal direction of the applied braking force. Typical time histories of accelerations of the super-structure in the longitudinal direction is shown in Figure 6.6 and typical accelerations at the bottom of column 2 are shown in Figure 6.7. The amplitudes of these accelerations are smaller than those of the super-structure in the vertical and the transverse directions. Among the accelerations at the bottom of column 2, the acceleration in the transverse direction has the largest amplitude, demonstrating the torsional effects of the deck.

Typical time histories of strains are shown in Figure 6.8 for the super-structure and in Figure 6.9 for the bottom of column 2. The amplitudes of the strains exhibit similar trends to those of the accelerations, while the strain data appear more noise contaminated.

The relative displacement of the super-structure with respect to the abutment and the soil pressure on the abutment back wall were also measured at sampling frequency of 100 Hz. Typical displacement and soil pressure time histories measured at abutment 1 are shown in Figures 6.10 and 6.11. The displacement at time instance of about 35 sec showed a sharp movement when the braking force was applied.

6.3 Bumping Vibration Test

Bumping vibration tests using the same water truck were also carried out on the West Street On-Ramp. Impact forces were applied by the water truck while driving over a bumper at the middle of each span. Typical time histories of accelerations of the super-structure are shown in Figure 6.12 for the vertical direction and in Figure 6.13 for the transverse direction, in which the bumping forces were applied at the middle of span 2 at time instant of approximately 56 sec and at the middle of span 1 at approximately 98 sec. The amplitudes of accelerations in the transverse direction are relatively smaller than those in the vertical direction. Typical time histories of accelerations of the super-structure in the longitudinal direction are shown in Figure 6.14 and typical accelerations at the bottom of column 2 are shown in Figure 6.15. The amplitudes of these accelerations are smaller than those of the super-structure in the vertical and the transverse directions. Among the accelerations at the bottom of column 2, the acceleration in the transverse direction exhibits the largest amplitude, demonstrating the torsional effects of the deck. More importantly, the amplitudes of the accelerations in the bumping vibration tests were greater than those in the braking vibration tests.

Typical time histories of strains are shown in Figure 6.16 for the super-structure and in Figure 6.17 for the bottom of column 2. The amplitudes of the strains exhibit similar trends to those of the accelerations, but the strains appear more noise contaminated than the accelerations. More importantly, the amplitudes of the strains in the bumping vibration tests were greater and more clear than those in the braking vibration tests.

Typical displacement and soil pressure time histories measured at abutment 1 are shown in Figures 6.18 and 6.19. The displacement showed sharp movements when the bumping forces were applied.

6.4 Data Processing

Four sets of data from the braking vibration tests and three sets of data from the bumping vibration tests were processed, in which the time length of each data set is 10 minutes and all the data were collected at night with the traffic under the bridge blocked. The frequency domain decomposition (FDD) method was used to extract modal parameters from the averaged vibration data with 25 percent overlapping. The sampling rate was 0.01sec and the time length of the averaged data 40.96 sec.

Figures 6.20 and 6.21 show the power spectral density (PSD) functions of the averaged accelerations measured during the braking vibration tests in the vertical and the transverse directions respectively. Figures 6.22 and 6.23 show the power spectral density (PSD) functions of the averaged accelerations measured during the bumping vibration tests in the vertical and the transverse directions respectively. The first and the second natural frequencies are detected in the vertical and in the transverse directions simultaneously since the vertical and the transverse modes are highly coupled.

It is noted that the natural frequencies derived from the braking vibration tests are different from those from the bumping vibration tests. As shown in the comparison in Table 6.1, the natural frequencies estimated from the bumping vibration tests are up to 3.5 percent smaller than those from the braking vibration tests, although these tests were

performed under the same experimental conditions. This can be explained by the nonlinear characteristics of a concrete: larger deformation corresponds to the smaller elasticity. The deformation of the structure is reciprocally proportional to the smaller elasticity. The magnitudes of the bumping loads are larger than the braking loads and as a result larger bridge responses are induced in the bumping vibration tests than in the braking vibration tests.

Chapter 7

CONCLUDING REMARKS

Long-term structural performance monitoring can play an important role in securing system integrity, minimizing the maintenance cost, and maintaining longevity of highway bridges. Meanwhile, it can also provide verifications of current design/analysis and suggest their improvement for retrofit and future construction.

The focus of this project is on the installation of sensor systems on two new highway bridges for their long-term performance monitoring: the Jamboree Road Overcrossing and the West Street On-Ramp, both in Orange County, California. The sensor system includes data recorders, power supply and back-up units, accelerometers, embedded strain gauges, pressure sensors, and displacement sensors.

Preliminary data collection and analysis were performed after the completion of the installation. On the Jamboree Road Overcrossing, traffic-induced ambient vibrations were measured several times. The acceleration amplitudes in the vertical direction were larger than those in the transverse direction. The peak picking method, the random decrement method, and the frequency domain decomposition method were used to extract modal parameters including natural frequencies and mode shapes from the ambient vibration data. The modal parameters were also compared with those obtained by the

preliminary finite element analysis. The results showed that the high and the horizontal modes were more contaminated by noise than the low and the vertical modes, and the frequency domain decomposition method was found as the best among the three methods.

On the West Street On-Ramp, braking and bumping vibration tests were carried out using a fully loaded water truck. The acceleration responses exhibited similar trends to those in the Jamboree Road Overcrossing. The modal parameters were estimated by the frequency decomposition method. The vertical and the transverse modes appeared to be coupled, and the natural frequencies derived from the braking vibration tests were smaller than those from the bumping vibration tests, because the braking loads are smaller that the bumping loads.

With the sensor systems permanently installed on these two highway bridges, their long-term structural performance will be continuously monitored in the future. Methodologies for assessing the structural health conditions based on the monitored data will be developed.

REFERENCE

Abdel-Ghaffer, A.M. and Scanlan, R.H., "Ambient Vibration Studies of Golden Gate Bridge. I: Suspended Structure," *Journal of Engineering Mechanics, ASCE*, Vol.111, No.4, pp.463-482, 1985.

Asmussen, J.C. and Brincker, R., "Estimation of Frequency Response Function by Random Decrement," *Proceedings of International Modal Analysis Conference*, pp.246-252, 1996.

ATC, *Improved Seismic Design Criteria for California Bridges: Provisional Recommendations*, Report ATC-32, Redwood City, California, 1996.

Bendat, J.S. and Pierso, A.G., *Engineering Application of Correlation and Spectral Analysis*, John Wiley & Sons, New York, USA, 1993.

Brinker, R., Zhang, L. and Andersen, P., "Modal Identification from Ambient Response Using Frequency Domain Decomposition," *Proceedings of 16th International Modal Analysis Conference*, San Antonio, Texas, USA, Feb., 6-10, 2000, 625-630.

California Department of Transportation, *Seismic Design Criteria V.1.1*, July, 1996.

Cole, H.A., "On-The-Line Analysis of Random Vibrations," *AIAA* Paper, no.68-288, 1968.

Ewins, D.J., *Modal Testing: Theory, Practice and Application*, Wiley, John & Sons, 1999.

Feng, M.Q., Kim, J.M. and Xue, H., "Identification of a Dynamic System Using Ambient Vibration Measurements," *Journal of Applied Mechanics, ASME*, Vol.65, No.4, pp.1010-1021, 1998.

Harik, I.E., Allen, D.L., Street, R.L., Guo, M., Graves, R.C., Harrison, J. and Gawry, M.J., "Free and Ambient Vibration of Brent-Spence Bridge," *Journal of Structural Mechanics, ASCE*, Vol.123, No.9, pp.1262-1268, 1997.

Ibrahim, S.R. and Mikulcik, E.C., "A Method for the Direct Identification of Vibration Parameters from the Free Responses," *Shock and Vibration Bulletin*, No.47, Part4, Sept. 1977, pp.183-198.

Juang, J.N., *Applied System Identification*, Prentice Hall, Englewood Cliffs, New Jersey, USA, 1994.

Lee, A. and Robertson, I.N., *Implementation and Long-Term Monitoring of the North Halawa Valley Viaduct*, UHM/CE/95-8, University of Hawaii, 1995.

Otte, D., Ponseele, P.V.D. and Leuridan, J., "Operational Shapes Estimation as a Function of Dynamic Loads," *Proceedings of the 8th International Modal Analysis Conference*, 1990, pp.413-421.

SAP2000, *Integrated Finite Element Analysis and Design of Structures*, Computer and Structure, Inc., Berkeley, California, 1995.

Transportation Corridor Agencies, *Design Memorandum No. 6: Seismic Design Criteria and Commentary for Structures*, 1996.

U.S. Federal Highway Administration, *Seismic Design of Bridges Design Example No. 6: Three-Span Continuous CIP Concrete Box Bridge*, Report FHWA-SA-97-011, Federal Highway Administration, 1996.

Yang, J.C.S., Chen, J. and Dagalakis, "Damage Detection in Offshore Structures by the Random Decremental Technique," *Journal of Energy Resources Technology, ASME*, Vol. 106, 38-42, 1985.

Yun, C.B., Yi, J.H., Lee, J.J. and Kim, J.D., "Modal Parameter Identification Methods without Input Information: A Comparative Study," *The 1st International Conference on Structural Stability and Dynamics*, Dec 7-9, 2000, Taipei, Taiwan.

Table 2.1: Parameter Values of Jamboree Road Overcrossing

Elements		Area (ft^2)	Moments of inertia (ft^4)	
			I_Y	I_Z
Deck	1 – 20	64.0	349.2	6877.3
Column	22 – 26, 28 – 32	38.0	83.0	175.6
	21, 27	Rigid element	Rigid element	Rigid element

Table 2.2: Computed Natural Frequencies of Jamboree Road Overcrossing (Hz)

Modes	In the vertical direction	In the transverse direction
1	2.889	2.969
2	3.716	4.311
3	4.654	5.786
4	5.721	9.953
5	9.400	16.634
6	14.521	

Table 2.3: Parameter Values of West Street On-Ramp

Element	Area (ft^2)	Moments of inertia (ft^4)		
		I_X	I_Y	I_Z
Deck	69.46	526.9	1135.4	5481.1
Column	45.36	163.7	327.5	163.7

Table 2.4: Computed Natural Frequencies of West Street On-Ramp (Hz)

Mode	Period (sec)	Frequency (Hz)
1	0.510	1.959
2	0.389	2.570
3	0.351	2.842
4	0.347	2.874
5	0.276	3.621
6	0.210	4.755
7	0.201	4.956
8	0.158	6.319
9	0.127	7.834
10	0.114	8.727

Table 2.5: Modal Participation Mass Ratio Percentage

Mode	Direction		
	X	Y	Z
1	1.1019	4.1493	3.9076
2	3.2371	1.3977	0.1565
3	8.0432	27.1175	26.4922
4	5.6934	28.6083	33.9682
5	10.1402	2.4370	0.0112
6	2.6126	12.4557	0.0184
7	43.5554	9.8929	0.0227
8	17.5159	4.2111	0.0043
9	0.9440	0.2330	0.0004
10	0.0250	0.0266	0.1077

Figure 2.1: Locations of Jamboree Road Overcrossing and West Street On-Ramp

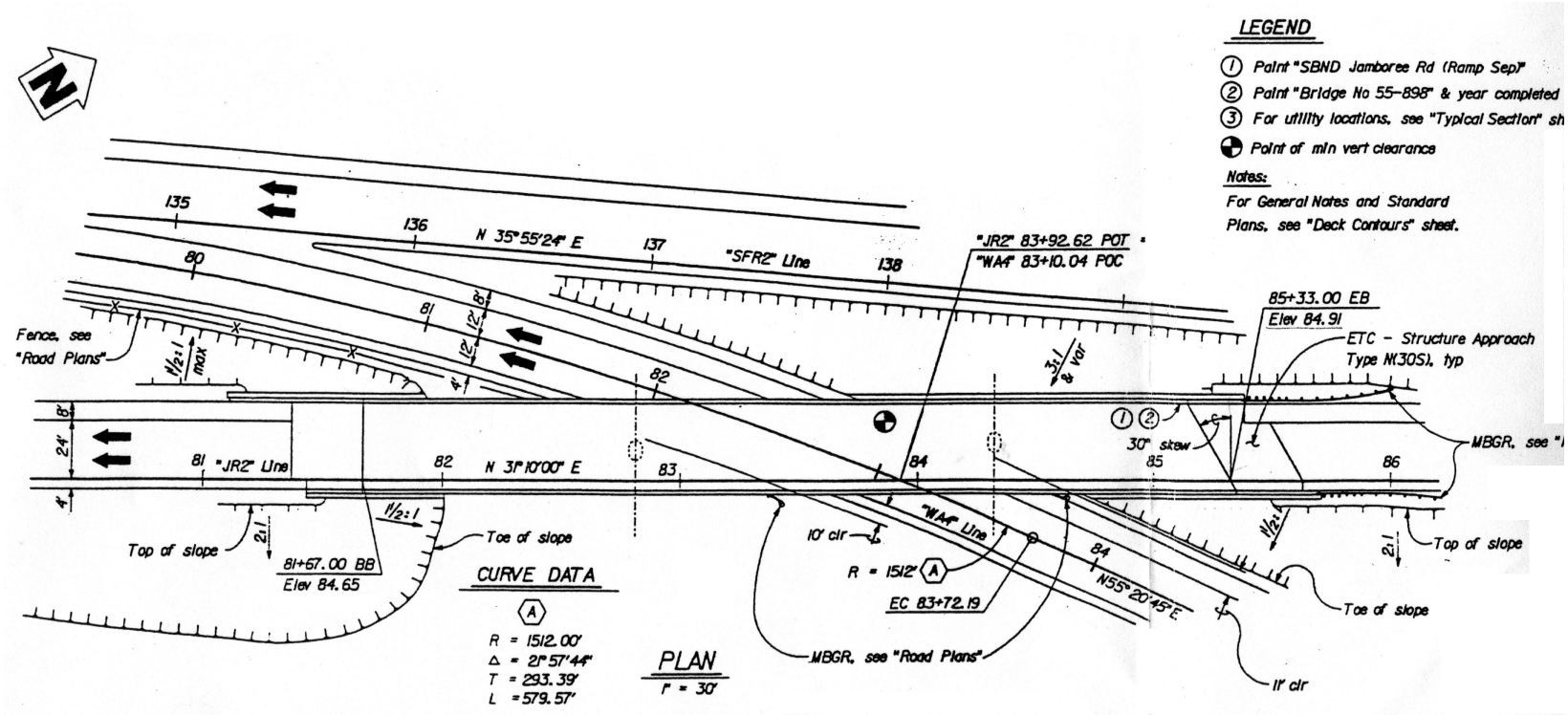

Figure 2.2: Jamboree Road Overcrossing; Plan

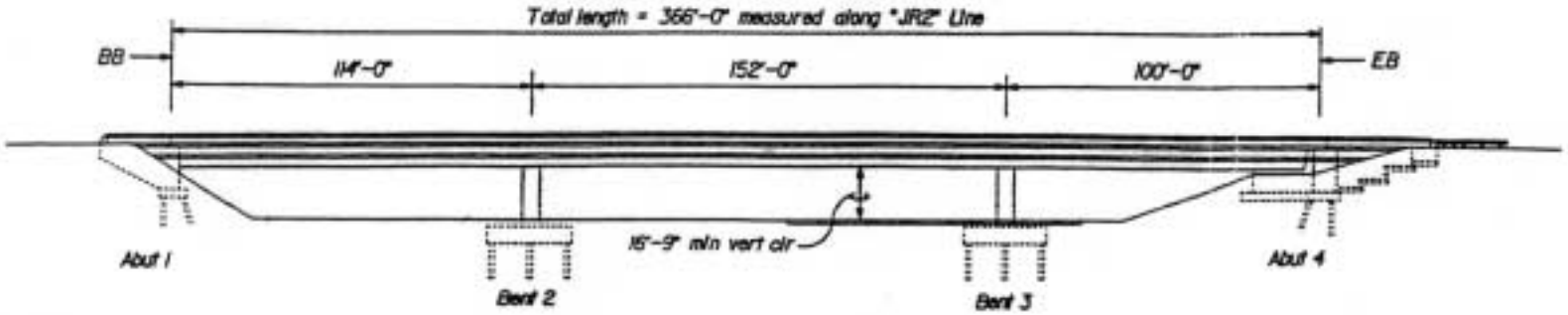

Figure 2.3: Jamboree Road Overcrossing; Elevation

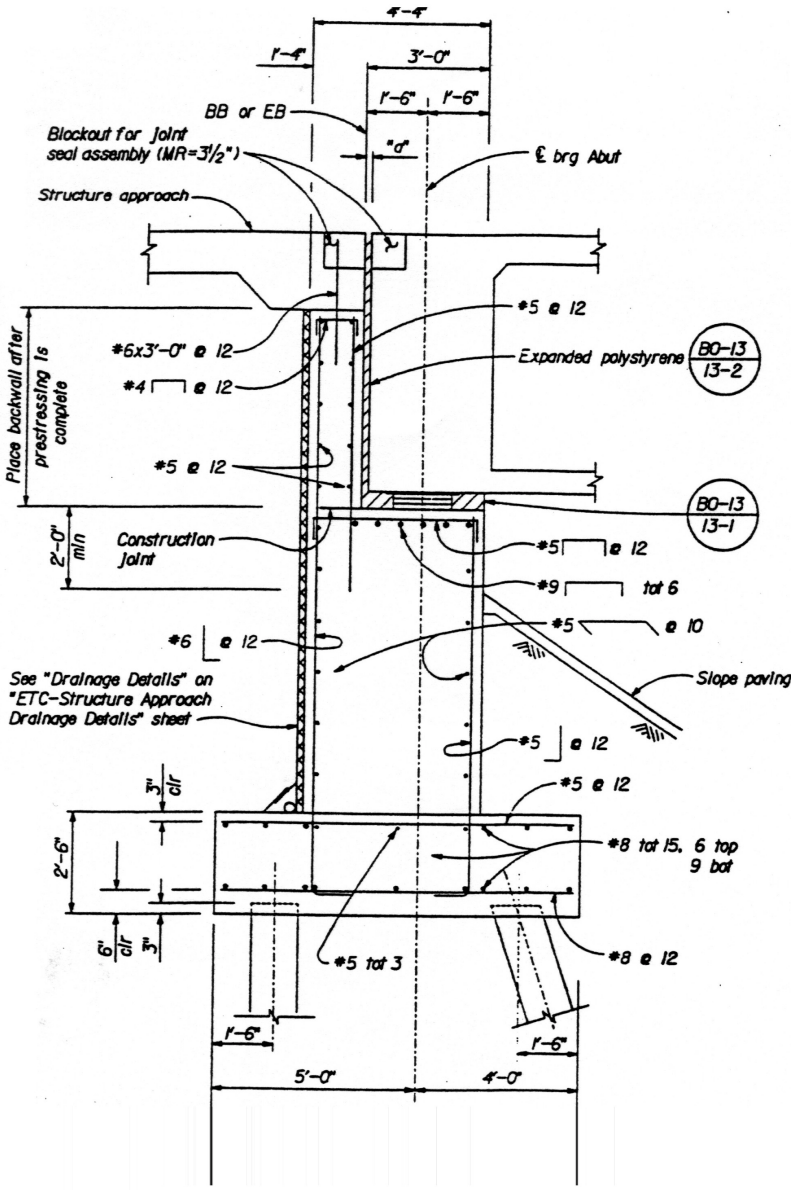

Figure 2.4: Typical Abutment Section at Jamboree Road Overcrossing

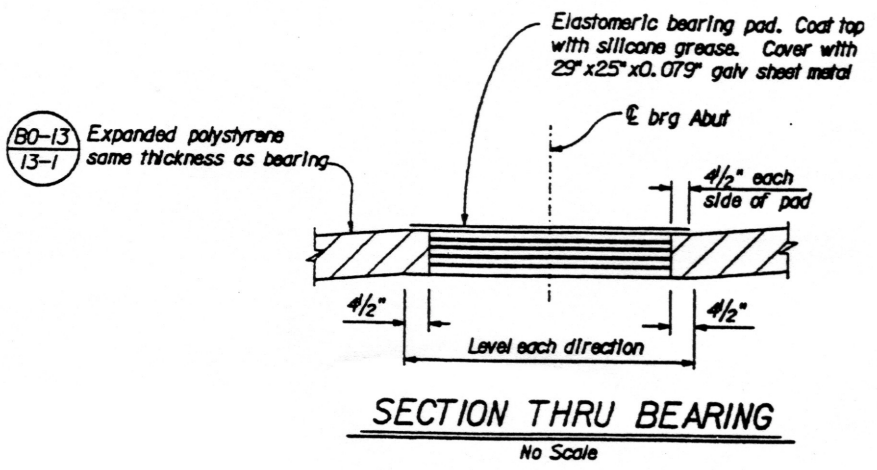

Figure 2.5: Elastomeric Bearing at an Abutment

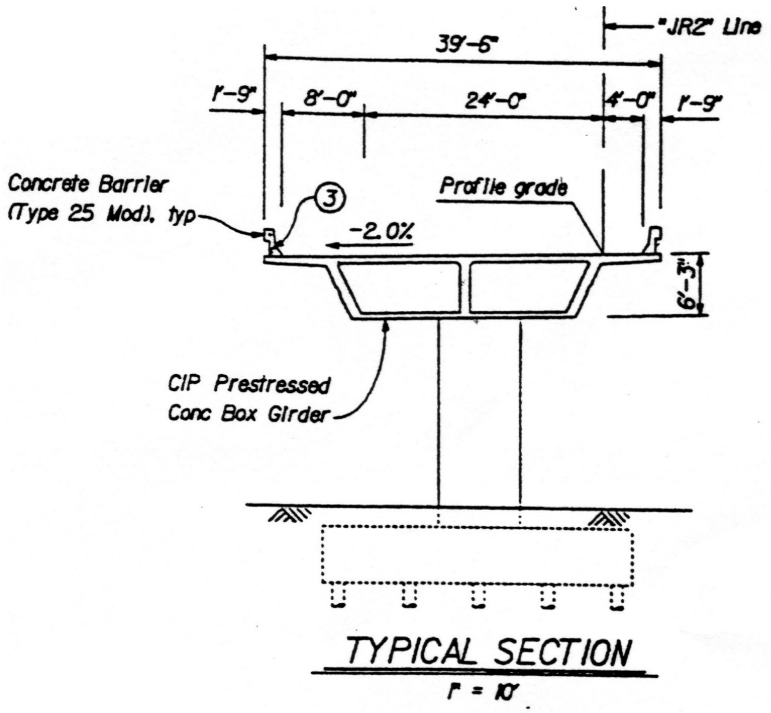

Figure 2.6: Typical Cross Section of a Box-Girder at Jamboree Road Overcrossing

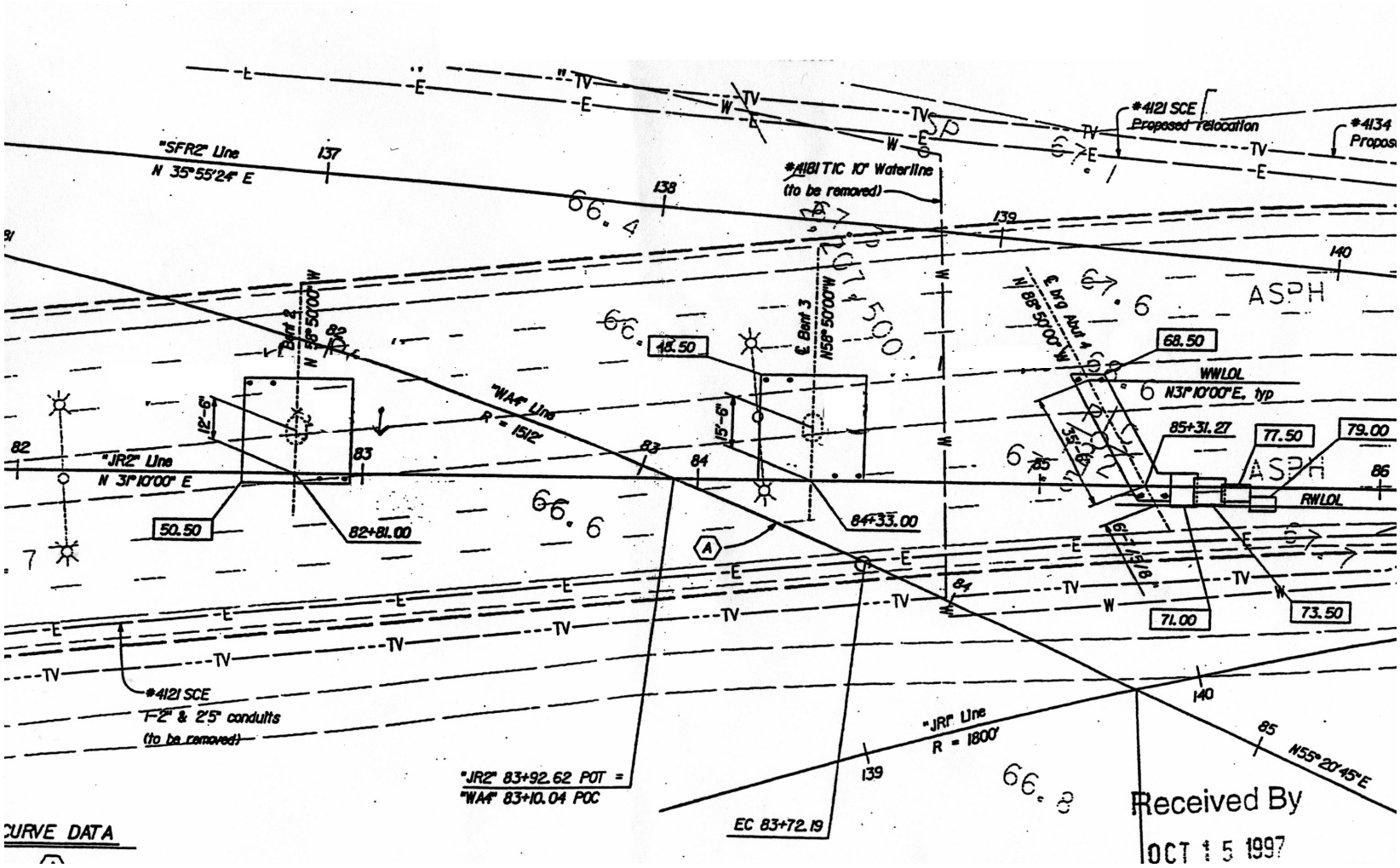

Figure 2.7: Location of Columns; Plan

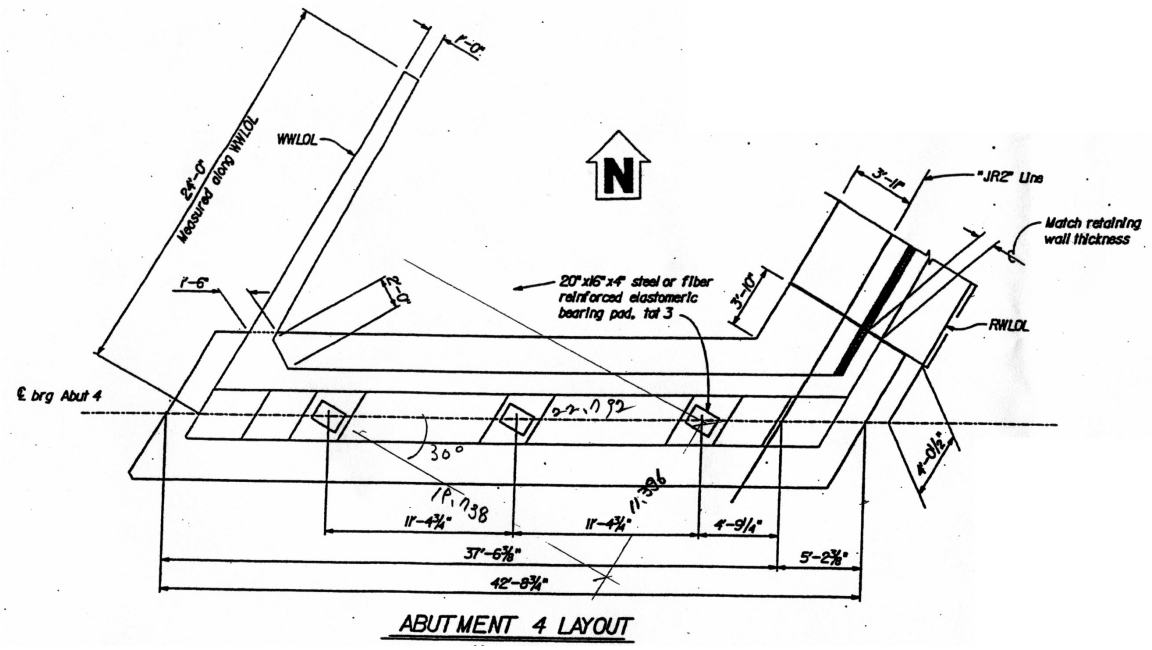

Figure 2.8: Super-Structure at Abutment 4; Plan

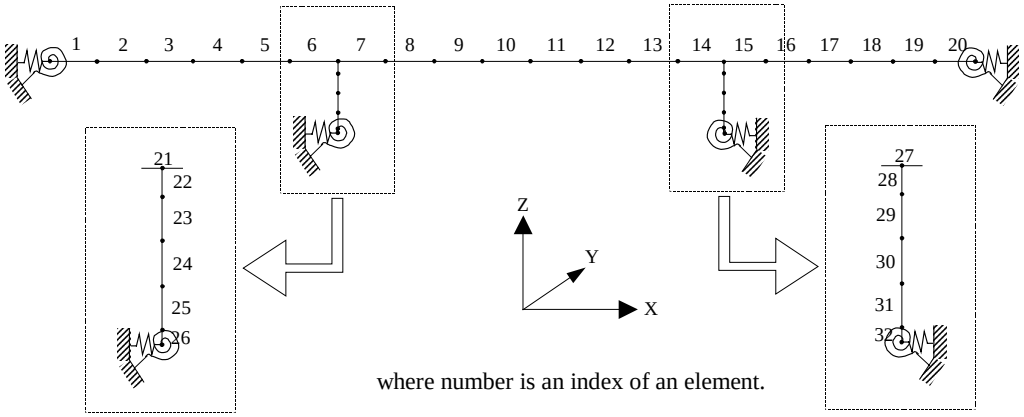

Figure 2.9: Finite Element Model of Jamboree Road Overcrossing

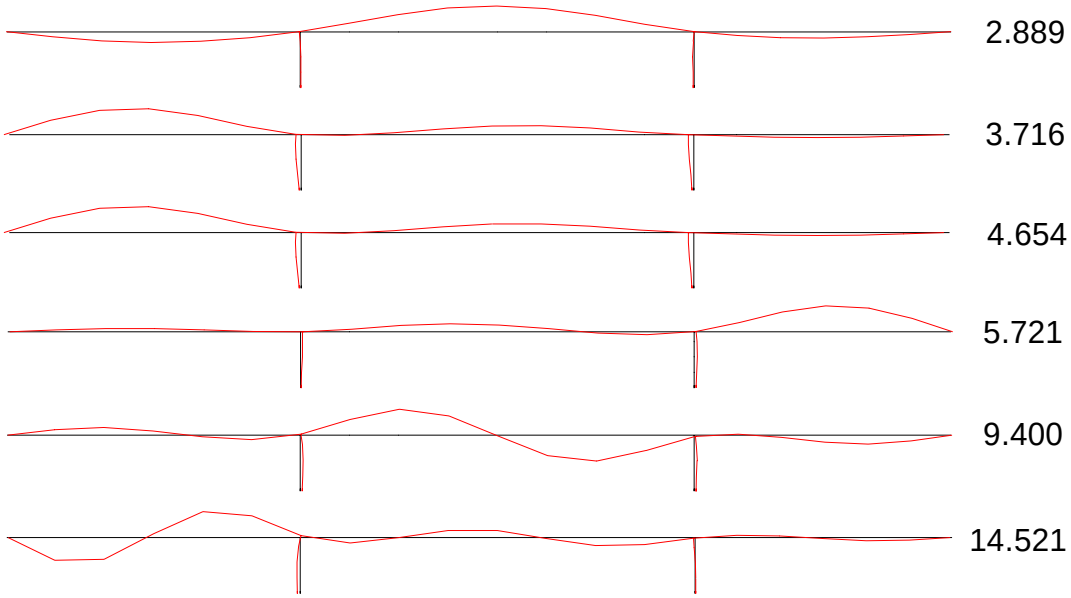

Figure 2.10: Mode Shapes of the 3D Finite Element Model
of Jamboree Road Overcrossing in the Vertical Direction (Hz)

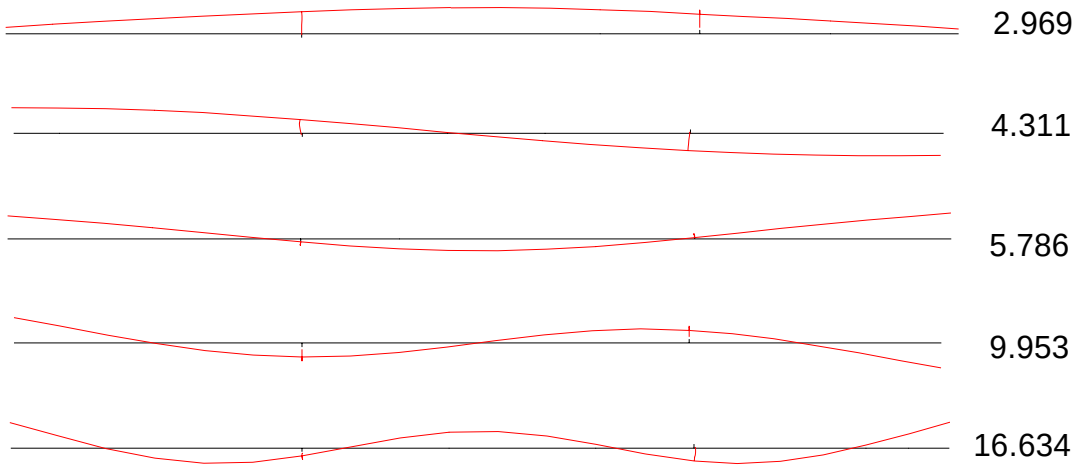

Figure 2.11: Mode Shapes of the 3D Finite Element Model
of Jamboree Road Overcrossing in the Transverse Direction (Hz)

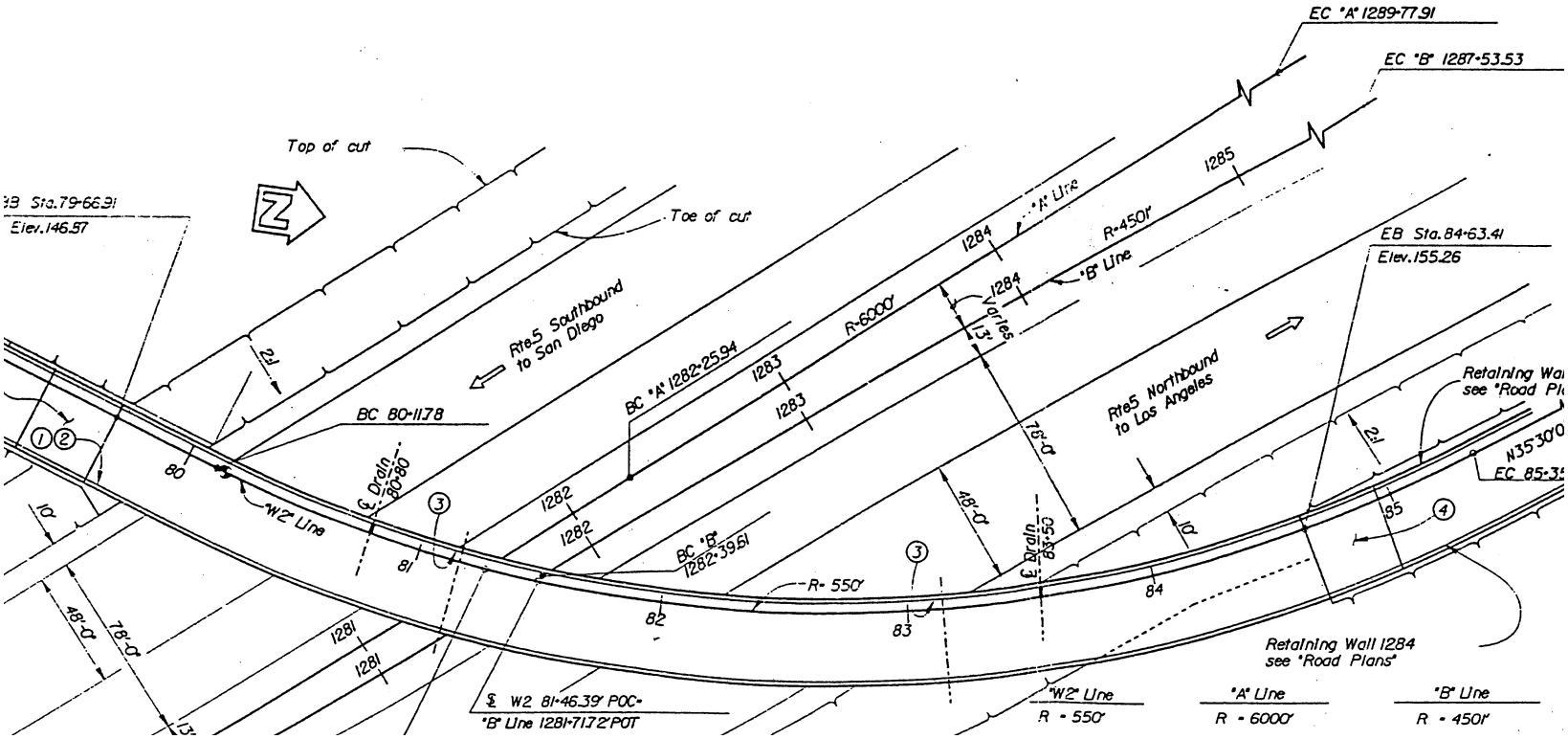

Figure 2.12: West Street On-Ramp; Plan

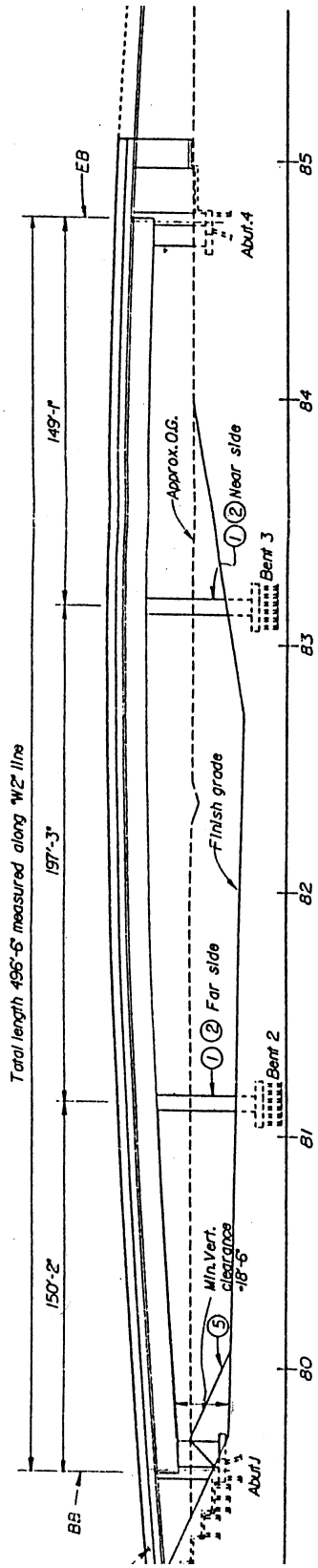

Figure 2.13: West Street On-Ramp; Elevation

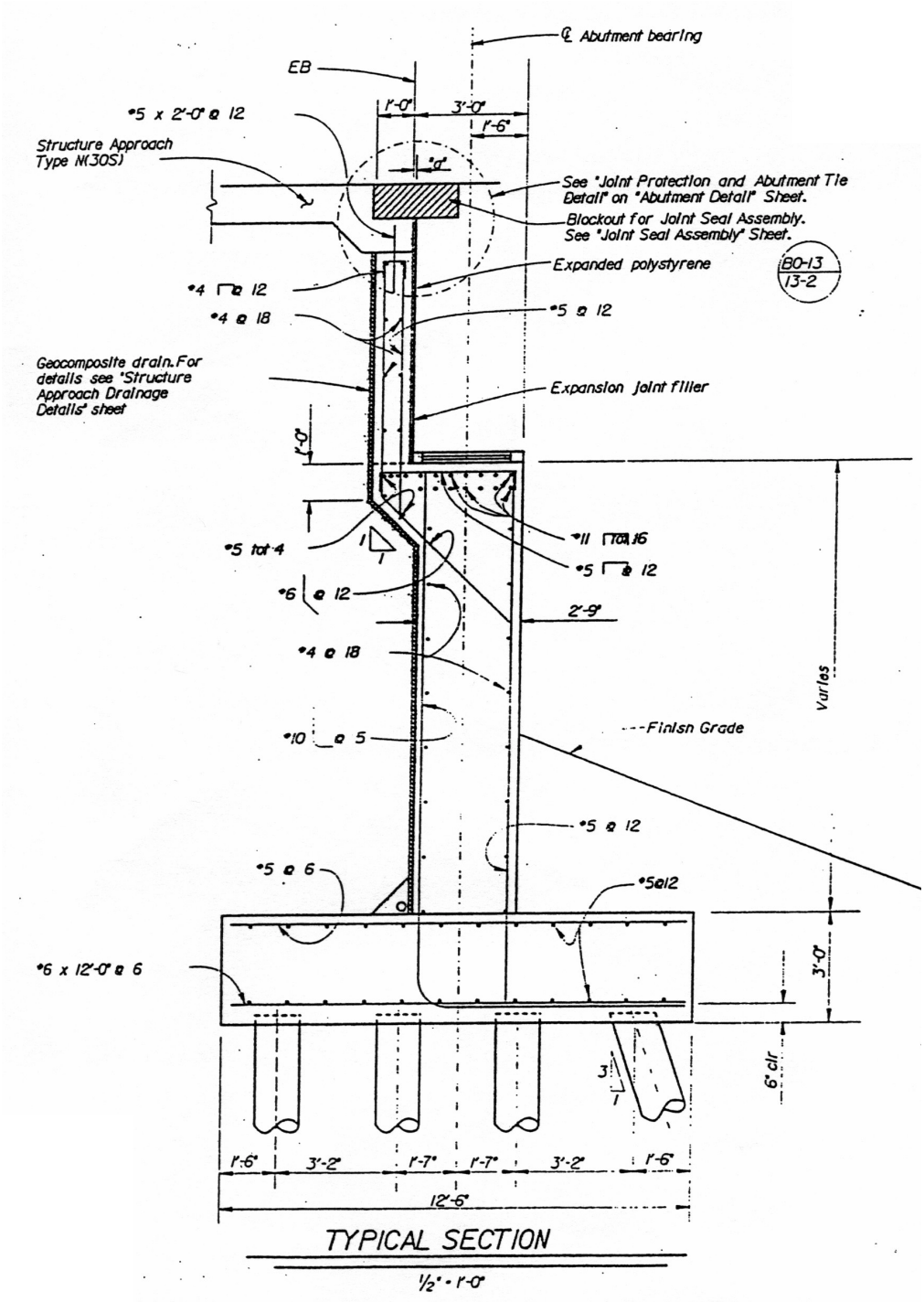

Figure 2.14: Typical Abutment Section at West Street On-Ramp

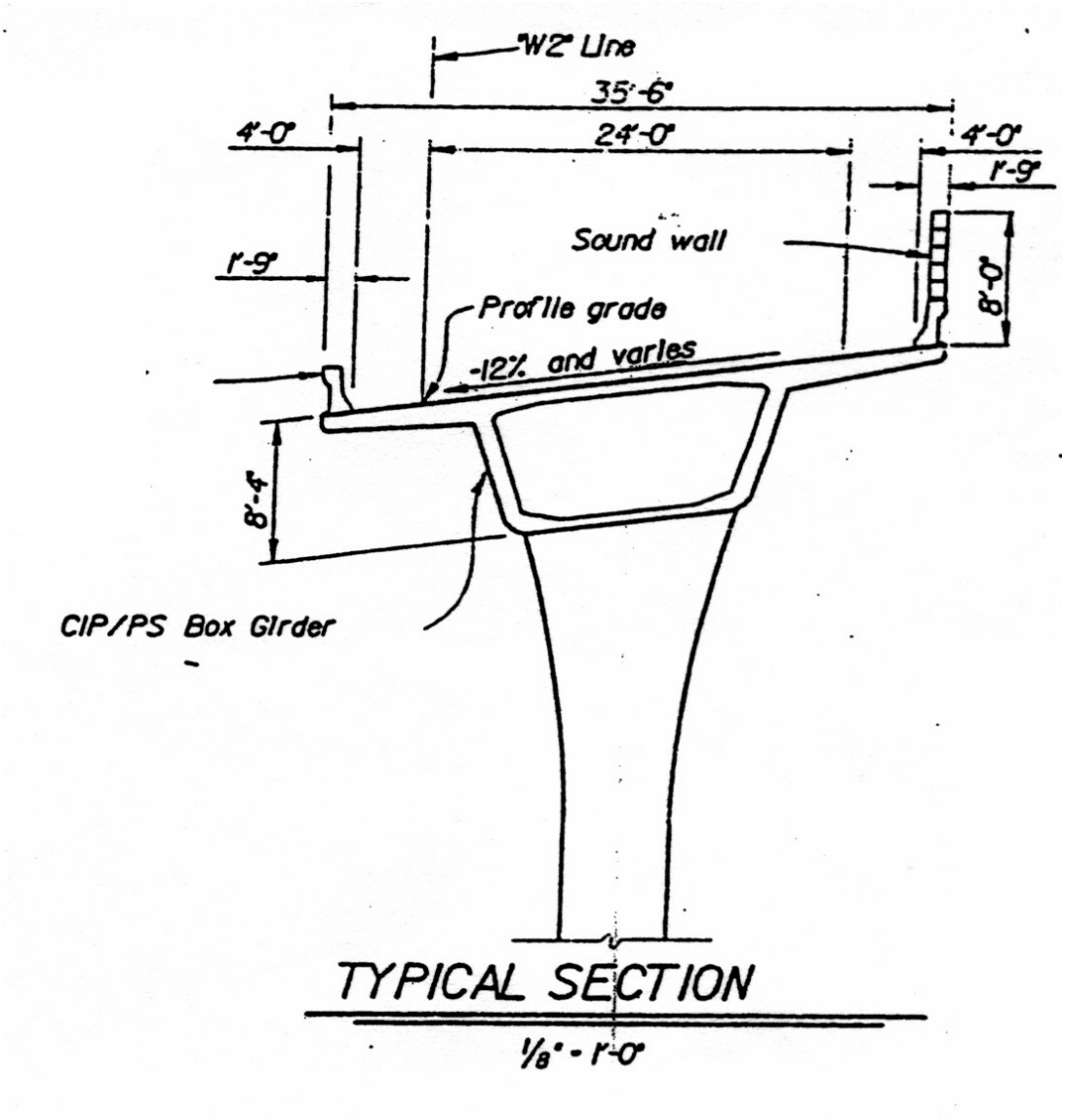

Figure 2.15: Typical Cross Section of a Box-Girder at West Street On-Ramp

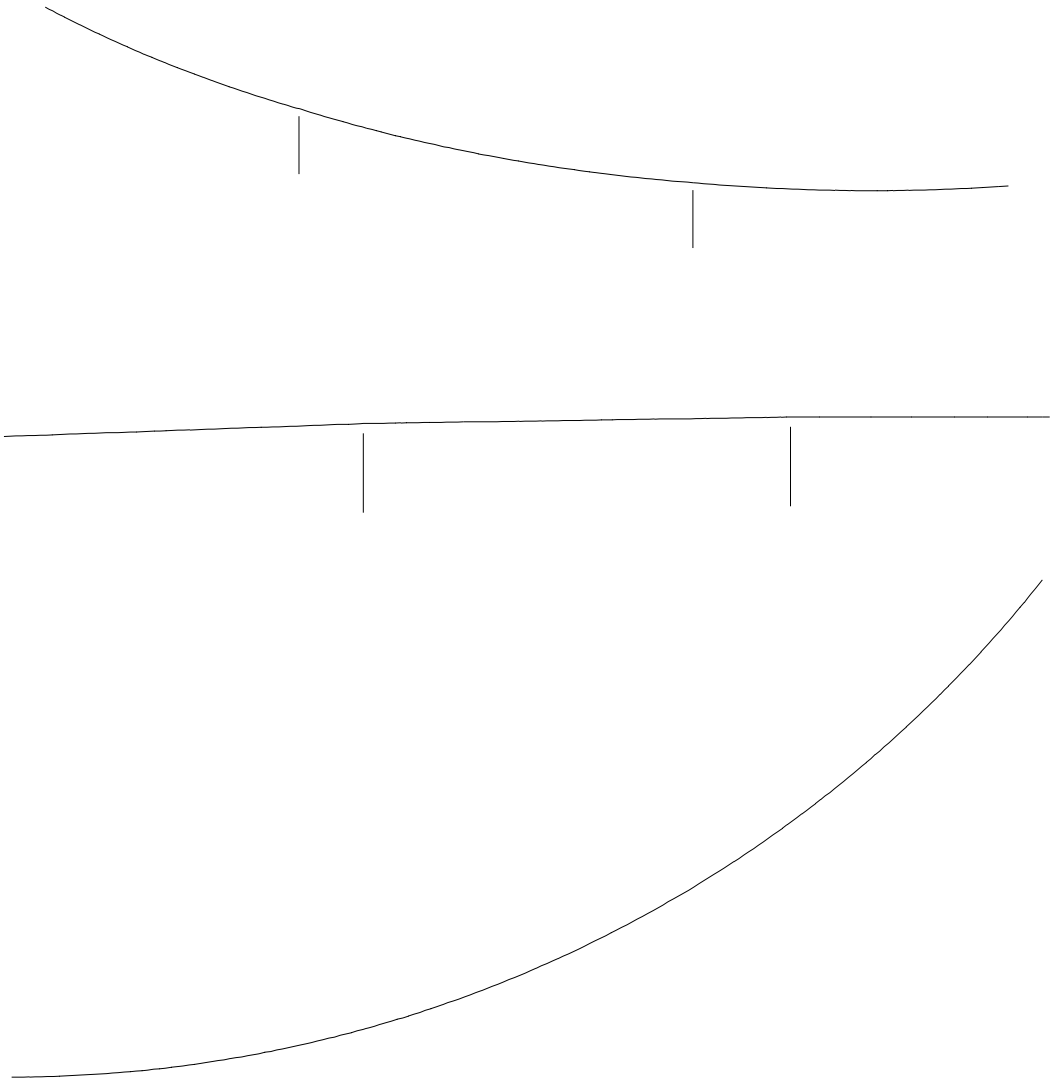

Figure 2.16: Finite Element Model of West Street On-Ramp

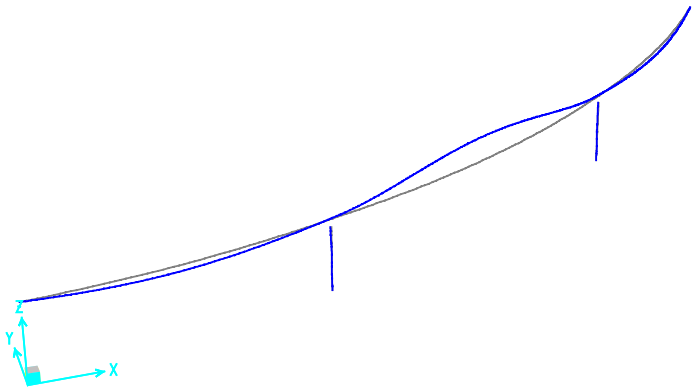

Mode 1

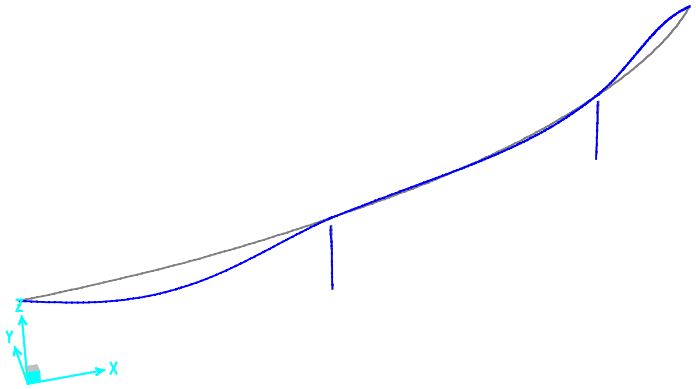

Mode 2

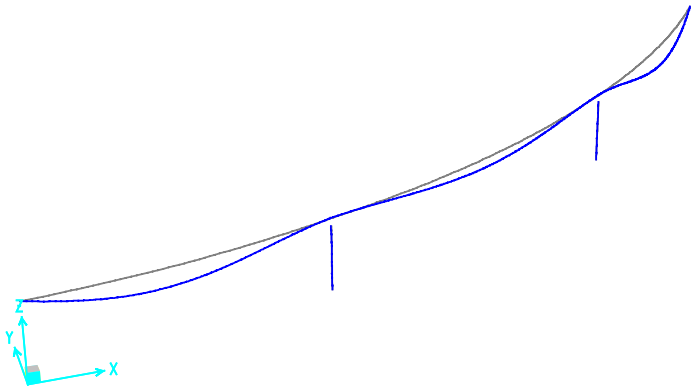

Mode 3

Figure 2.17: Mode Shapes of the 3D Finite Element Model of West Street On-Ramp (Continued)

Mode 4 (X-Z plane)

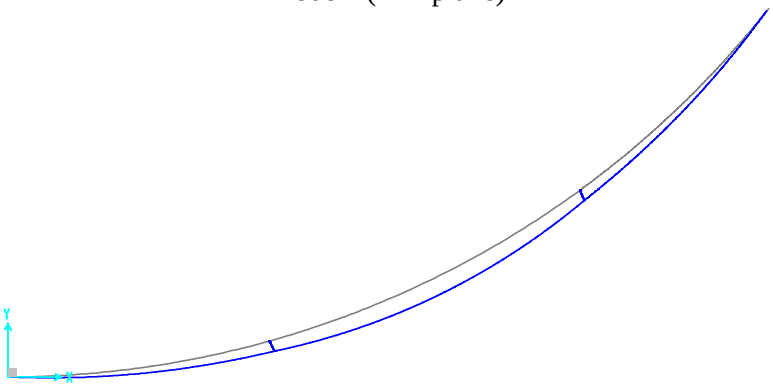

Mode 4 (X-Y plane)

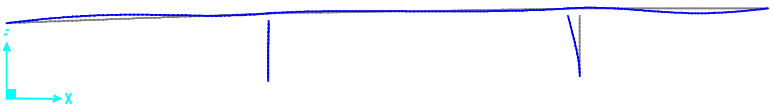

Mode 5 (X-Z plane)

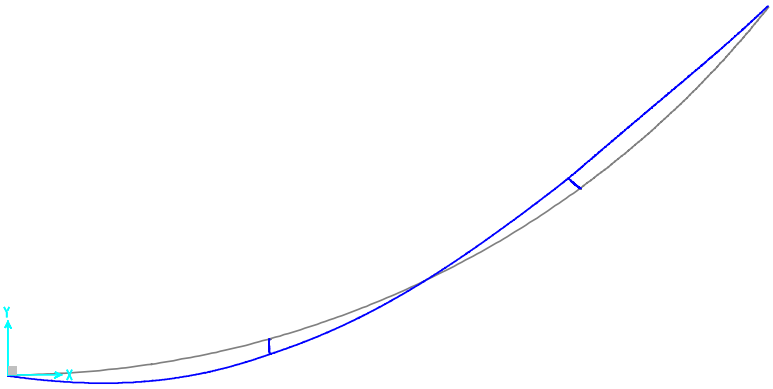

Mode 5 (X-Y plane)

Figure 2.17: Mode Shapes of the 3D Finite Element Model of West Street On-Ramp (Continued)

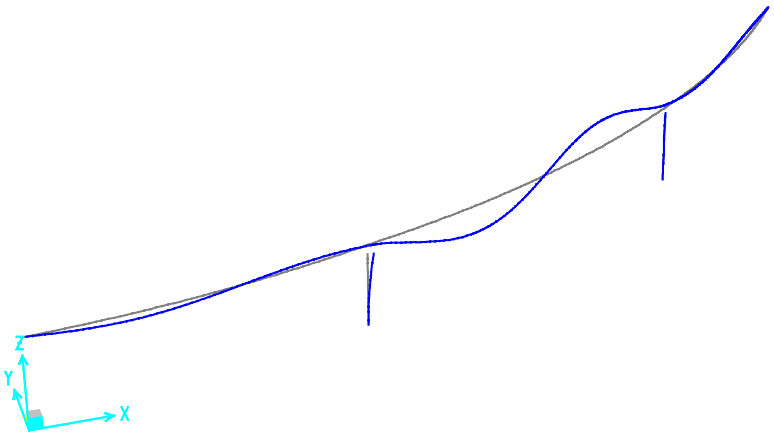

Mode 6

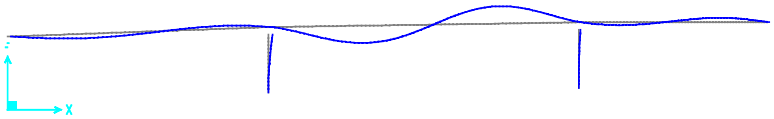

Mode 6 (X-Z plane)

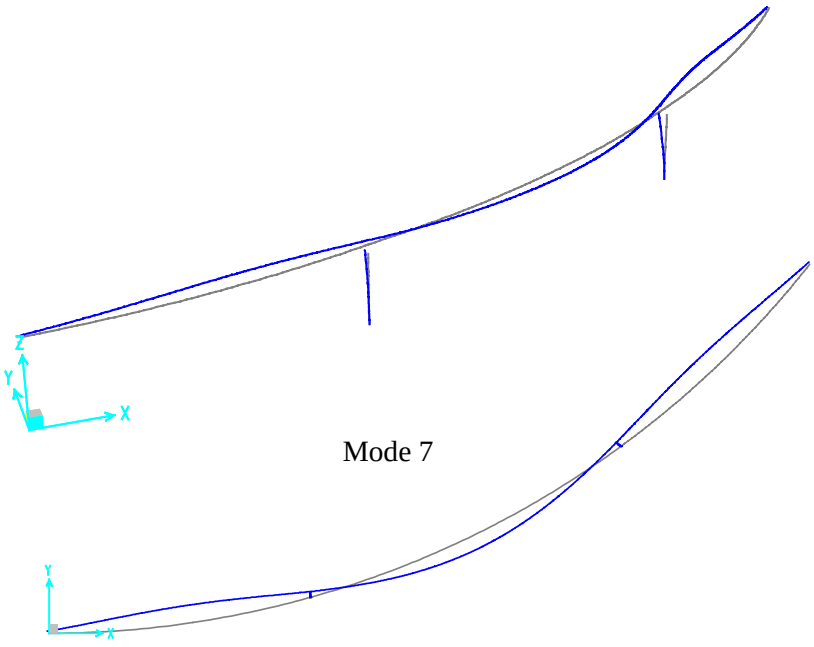

Mode 7

Mode 7(X-Y plane)

Figure 2.17: Mode Shapes of the 3D Finite Element Model of West Street On-Ramp

Table 3.1: Specifications of Force-Balance Servo Accelerometer

Parameter	Specification
1. Model	Uni-axial SV-155(H) SV-156(V)
	Bi-axial SV-255(H.H) SV-256(H.V)
	Tri-axial SV-355(H.H.V)
2. Bandwidth	DC to 100Hz (+3%, -10%)
	DC to 50Hz (± 1%)
3. Full Scale Range	±2000gal
4. Sensitivity	Current Output 5mV/gal
5. Load Resistance	10kΩ or more
6. Resolution	0.0001% of full range maximum
7. Linearity	0.03% of full range maximum
8. Damping Ratio	0.6 - 0.7
9. Sensitivity Axis to case Alignment	±0.3 degree maximum
10. Noise output	5mV rms maximum
11. Cross Axis Sensitivity	Smaller than 0.003 G/G(at 10Hz)
12. Calibration Coil	3.5μA/gal ±10%(140Ω±10%)
13. Input Voltage	±15VDC ±10%
14. Current Consumption	15mA Max./comp.
15. Operating Temperature	-20 °C - +70 °C
16. Thermal Coefficient of Sensitivity	0.02% per degree °C maximum
17. Thermal Coefficient of offset voltage	0.02% per degree °C
18. Shock survival	10G (Less than 0.1sec)
19. External Dimensions	SV-155 ϕ57×353
	SV-255P ϕ57×438
	SV-355 ϕ57×506
20. Case	Water proof 30kg/cm2
21. Cable	10G (Less than 0.1sec)

Table 3.2: Specifications of Strain Gauge

Parameter	Specification
1. Model	ES-500T
2. Strain range	±1000μ Srain
3. Average resolution	0.01μ Srain
4. Average sensitivity	0.55 mV/μStrain
5. Temperature coefficient	0.7×10^{-5}/°C (-20 to +60°C) 85μV/kg
6. Gauge length	500mm
7. Frequency response	DC – 50Hz
8. Cable	4 Conductor, shielded (Extensible length 300m)

Table 3.3: Calibration Test

Load (kg)		0	250	500	750	1000	1250	1500
Output (mV)	R1 (990479)	0	24.9	48.8	73.1	97.8	123.7	148.2
	R2 (990482)	0	23.0	48.2	73.4	97.1	122.4	146.9
	R3 (990485)	0	22.8	47.7	72.7	97.8	121.7	146.8
	R4 (990483)	0	23.8	47.8	73.2	97.2	122.7	146.7
	R5 (990480)	0	24.3	48.7	73.4	98.4	122.3	147.4
	R6 (990477)	0	23.2	46.8	70.5	94.7	117.8	141.6
	R7 (990478)	0	25.8	52.3	77.9	102.4	128.8	154.3
	R8 (990484)	0	22.9	47.8	71.8	96.8	120.8	145.8
	R9 (990481)	0	22.3	45.6	68.9	95.4	119.5	144.2
	R10 (990486)	0	22.9	47.9	73.0	97.5	123.9	147.9

Note:
1. Condition — Excitation Voltage: DC5V (±1%)
   Load Resistance : 10KΩ
2. Isolation — 10MΩ

Table 3.4: Sensitivity of Strain Gauge

	Volt/Load (mV/kg)	Volt/Strain (mV/μStrain)
No.990479	0.0984	0.558
No.990482	0.0973	0.552
No.990485	0.0970	0.550
No.990483	0.0974	0.552
No.990480	0.0980	0.556
No.990477	0.0942	0.535
No.990478	0.1031	0.585
No.990484	0.0964	0.547
No.990481	0.0945	0.536
No.990486	0.0977	0.554

Table 3.5: Specifications of Displacement Sensor

Parameter	Specification
1. Model	DP-50
2. Range	±20mm to ±100mm
3. Resolution	Infinite
4. Sensitivity	1V/10mm
5. Temperature coefficient	Max. ±3% (-20 to +60°C)
6. Frequency response	DC - 30Hz

Table 3.6: Specifications of Soil Pressure Sensor

Parameter	Specification
1. Model	BE-2KRS12 (Wall-surface soil pressure transducer)
2. Range	3kg/cm^2
3. Resolution	Infinite
4. Sensitivity	1V/kg/cm^2
5. Temperature coefficient	0.1% of F.S.
6. Frequency response	DC - 30Hz

Table 3.7: Specifications of Data Recorder

Parameter		Specification
Input	Channel number	24
	Maximum range	±10V
	AD converter resolution	22bit
	Dynamic range	114db
	Sampling frequency	50Hz,100Hz
	Anti-Alias Filter	Liner phase digital filter
	Delay	0 30 sec (step by 1 sec)
	Impedance	100kΩ
Recorder	Media	PCMCIA ATA type FLASH CARD 4MB, 10MB, 20MB, 40MB, 96MB (1 slot)
	Format type	MS-DOS
	Max recording time	About 44 minutes (100Hz sampling with 20MB card)
	Overwrite	1 : Preserve max-amplitude record 2 : Overwrite oldest record
	Length of one record	60 seconds
	Recording stop	Trigger off
	Memory erase	All records or specified record (external command)
	Record contents	1:Header a) ID number of the recorder b) Latest corrected time, c) Start recording time 2:Data
Trigger spec	Frequency	Band pass filter
	Trigger channel	Optional 3 channels
	Trigger level	1. 999mV, step by 1mV
	Trigger logic	AND, OR, AND, OFF
Display	Display type	LCD
	Items	Present time, Start recording time, Maximum value of input and record, Real time waveform
Console	Items	a)Delay, b)Trigger level, c)Trigger logic, d)Recording e)Calibration, f)Real time waveform
	Preserve setting duration	More than 90 days after shutdown
Clock	Internal clock	Year, Month, Day, Hour, Minute, Second
	Stability	TCX0 (±5*10, temperature –20-50°C)
	Calibration	GPS
	Accuracy	±0.005sec (with calibration)
Monitor Output	Channel :Optional 1 channel, Resolution :16 bit	
	Output voltage	±10V(load...above 10kΩ)
External Output]	Ext1 :RS-232C Baud rate ... 38400	
	Sensor power source :DC+-15V(1A) (Option)	
Power	Recorder : AC-100V(+-20%), Power current : 1A	
	Suspend :3 hours, Backup battery (max. current 5A)	
Dimension	Outside dimension	Width 480mm, Height 200mm, Depth 400mm (8kg)
Shockproof	7Hz, 1.5G, 3minutes (Both vertical and horizontal)	

Table 3.8: Specifications of Transformer

Parameter	Specification
1. Model	GE Industrial System, 9T51B0013
2. Type	Dry type control transformer
3. Primary voltage	240/480 V
4. Secondary voltage	120/240 V
5. Weight	55lbs
6. Stability	Temperature below 40°C, Free air circulation provided by one inch spacing 25-100Hz
7. Use	Max. 3kVA, 60Hz
8. Features and Benefits	Designed for wall mount application

Table 3.9: Specifications of Uninterrupted Power Supply (UPS)

Parameter	Specification
1. Output power capacity	300VA
2. Output voltage	AC-100V
3. Waveform type	Sine wave
4. Transfer time	Non interrupt
5. Input voltage	AC-115V
6. Input frequency	50 to 60Hz
7. Typical backup time	10 minutes on full load
8. Battery type	Sealed Lead-Acid battery condition
9. Control panel	LCD status display with load and battery
10. Audible alarm	Alarm when on low battery, over load and trouble
11. Dimension	150(W)×263(H)×450(D) (mm)
12. Net weight	20kg
13. Operating environment	0 to 40 , 0 to 95% RH.

Figure 3.1: Force-Balance Servo Accelerometer

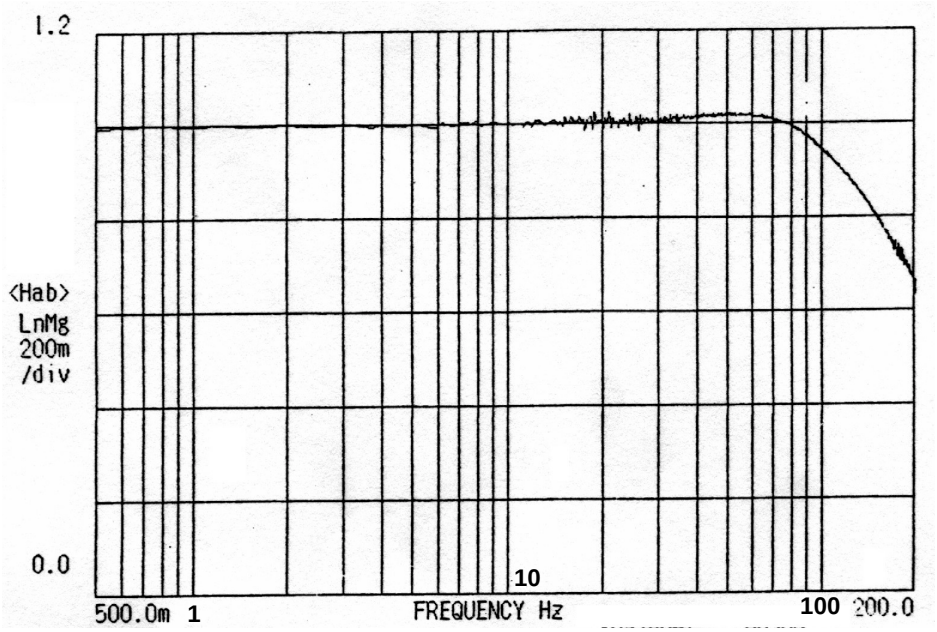

Figure 3.2: Frequency Response Function of
a Force-Balance Servo Accelerometer; Amplitude

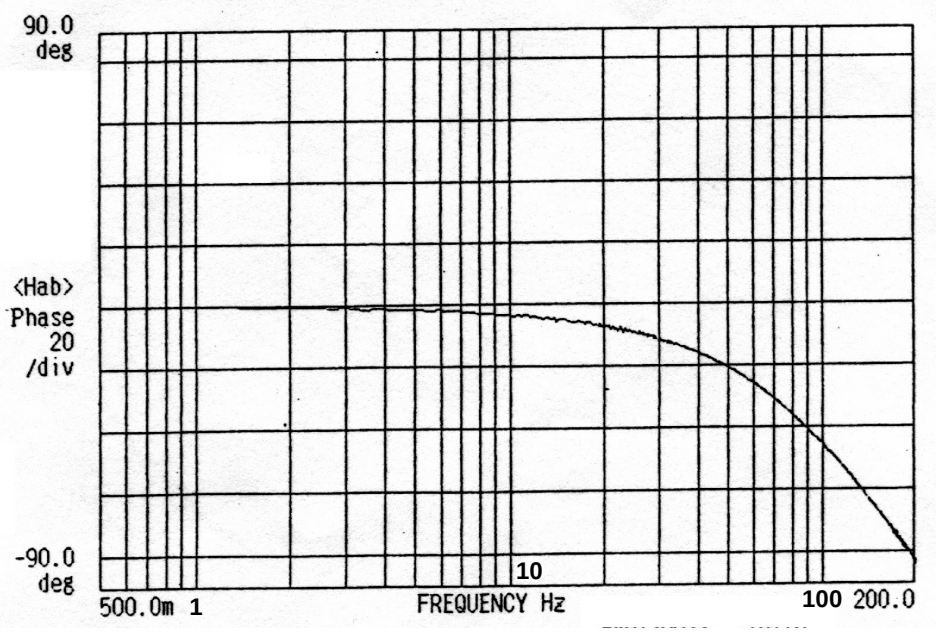

Figure 3.3: Frequency Response Function of
a Force-Balance Servo Accelerometer; Phase

Figure 3.4: Accelerometer installed on the Bottom of Super-Structure

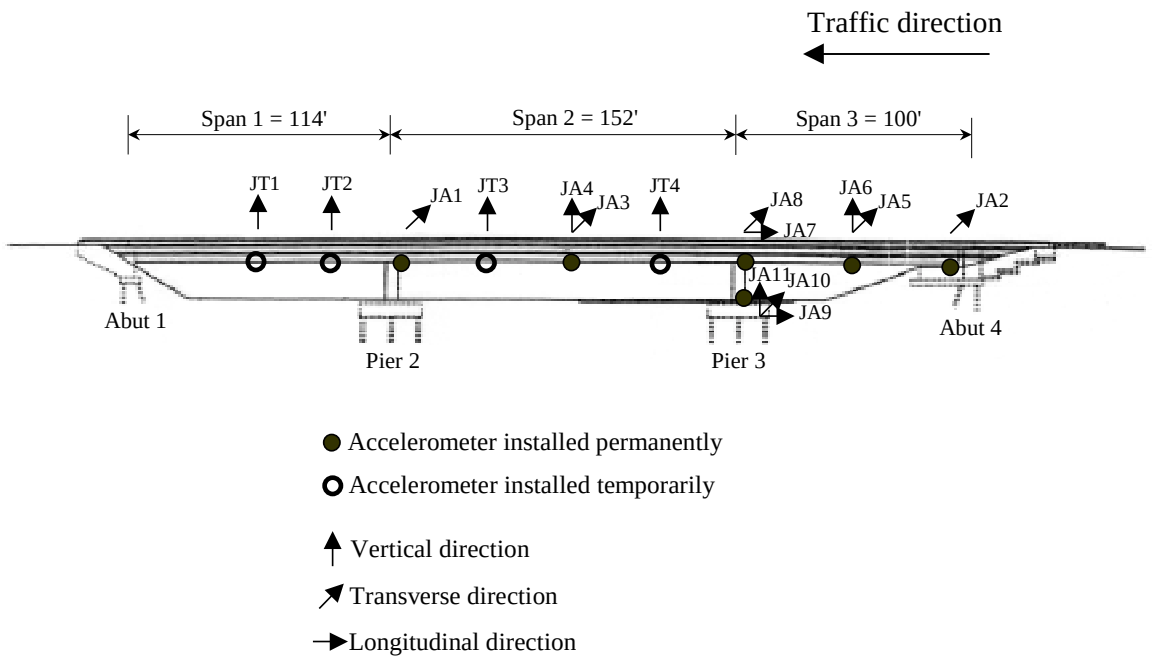

Figure 3.5: Accelerometer Arrangement at Jamboree Road Overcrossing; Elevation

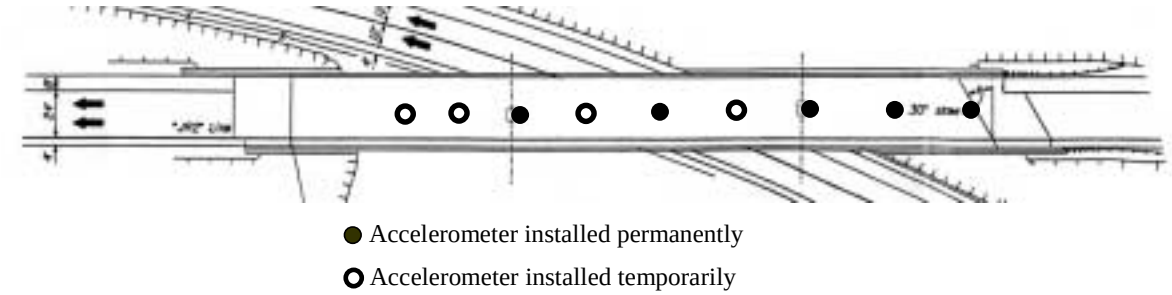

Figure 3.6: Accelerometer Arrangement at Jamboree Road Overcrossing; Plan

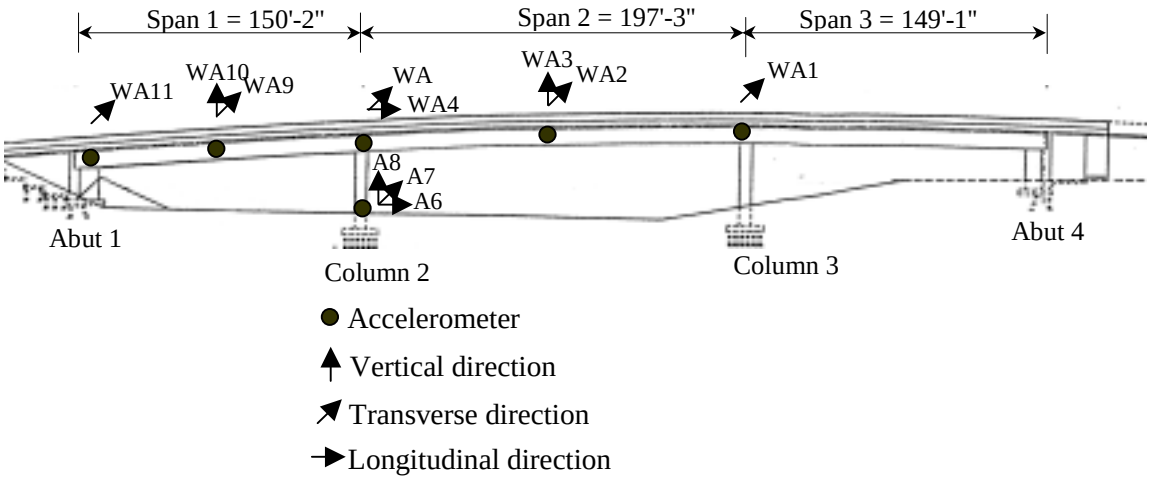

Figure 3.7: Accelerometer Arrangement at West Street On-Ramp; Elevation

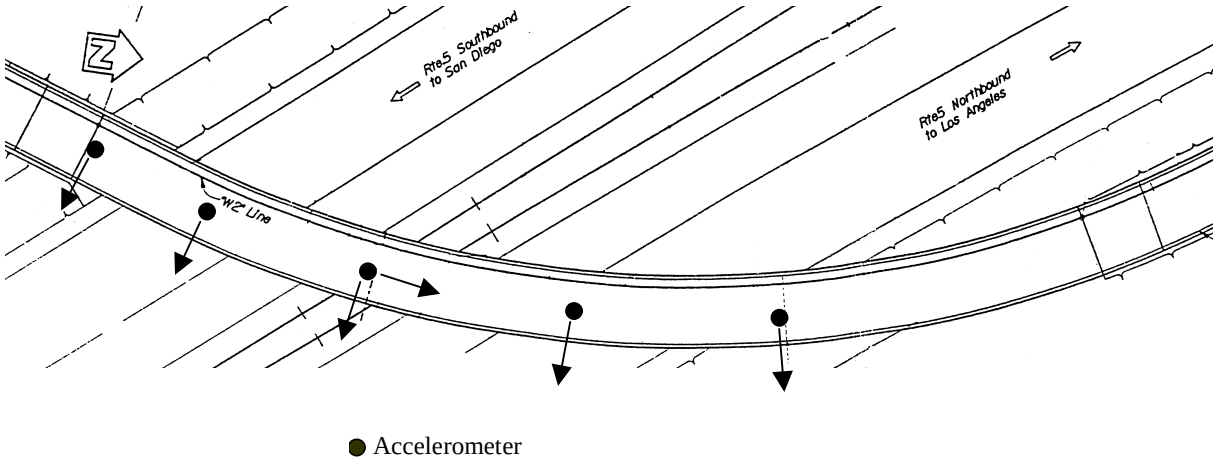

Figure 3.8: Accelerometer Arrangement at West Street On-Ramp; Plan

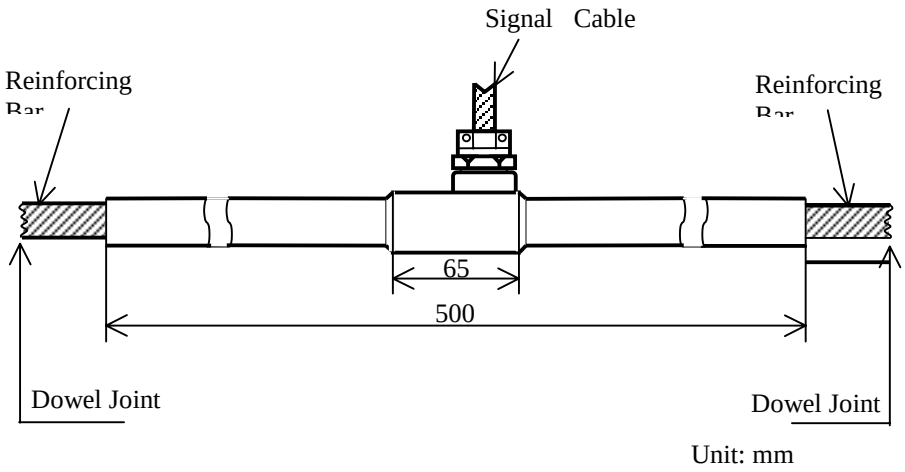

Figure 3.9: Rebar Strain Gauge; Outside View

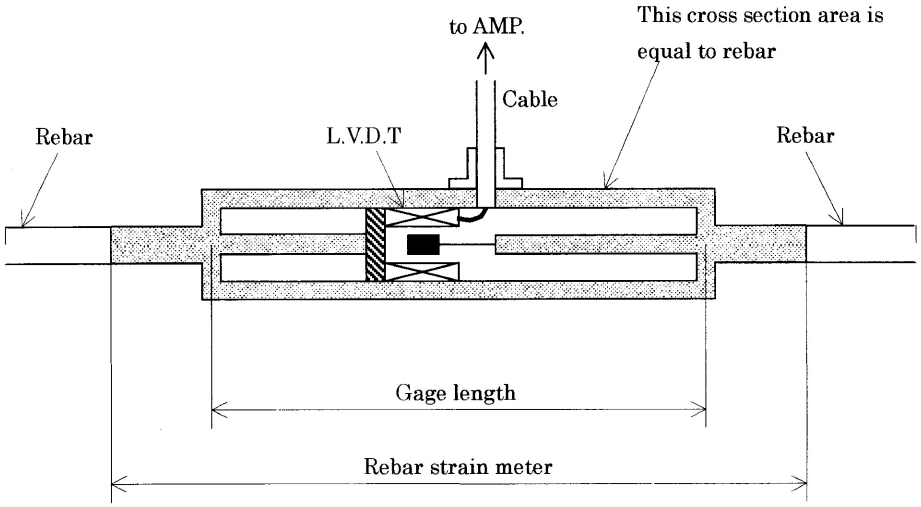

Figure 3.10: Rebar Strain Gauge; Inside View

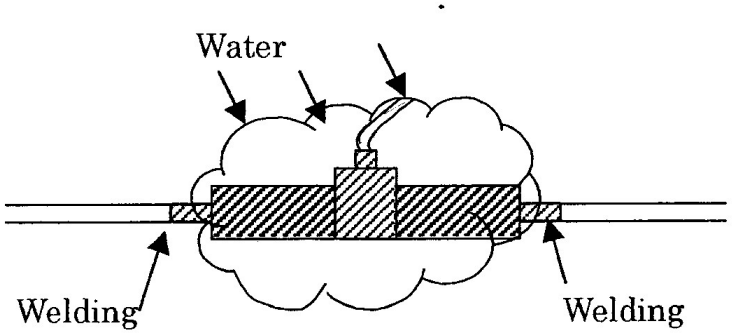

Figure 3.11: Strain Gauge on Dummy Rebar

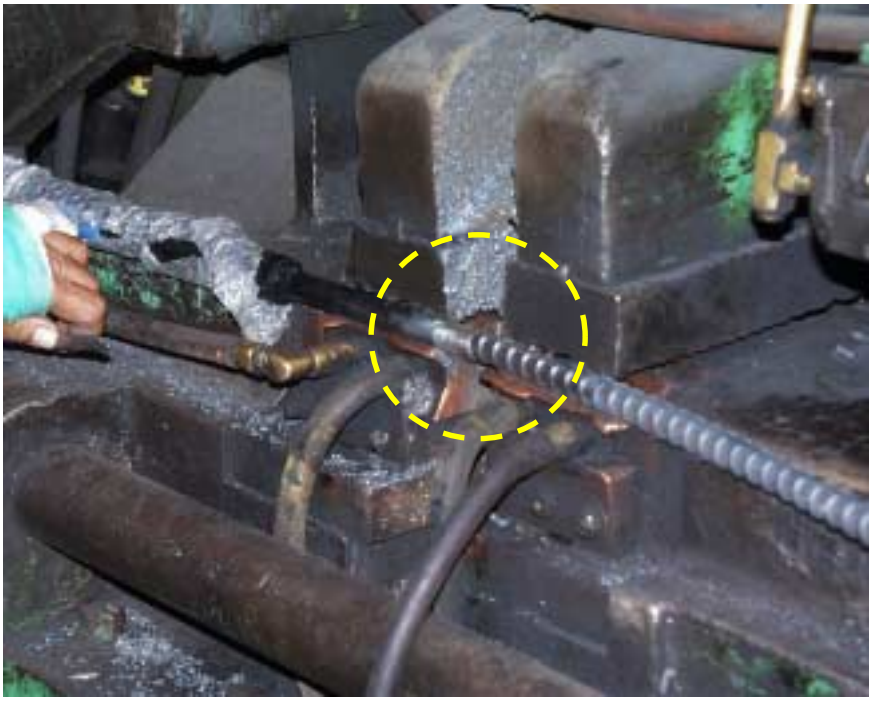

Figure 3.12: Welding of a Rebar Strain Gauge

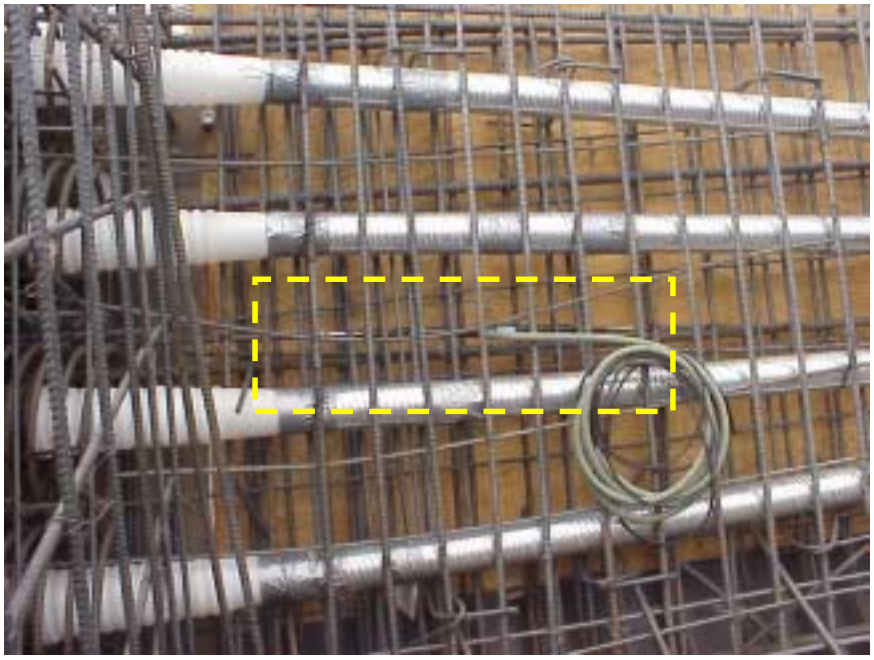

Figure 3.13: Strain Gauge Embedded in Super-Structure of West Street On-Ramp

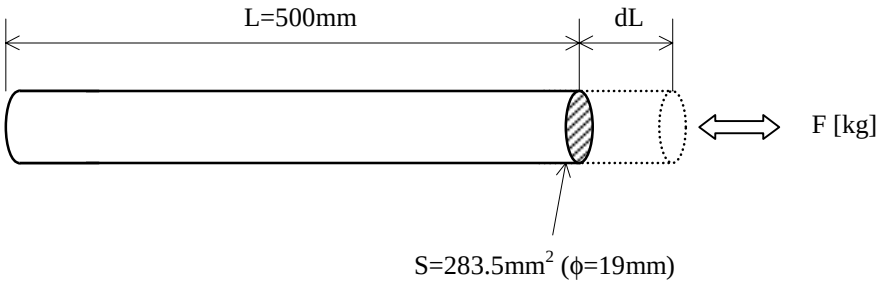

Figure 3.14: Calibration Test of Strain Gauge

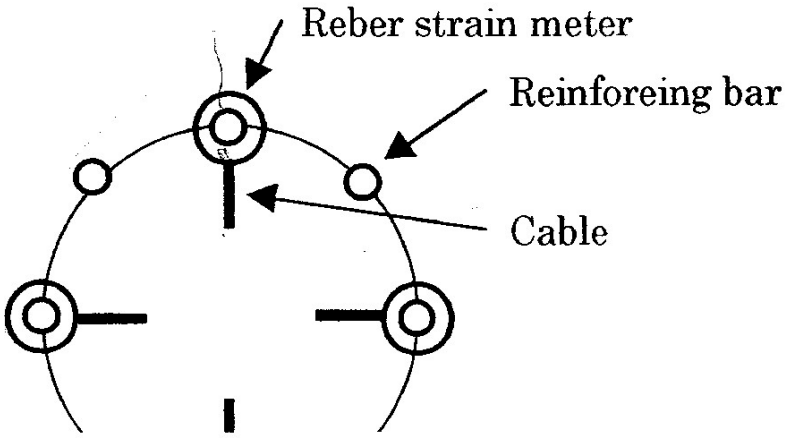

Figure 3.15: Arrange the Dummy Rebar

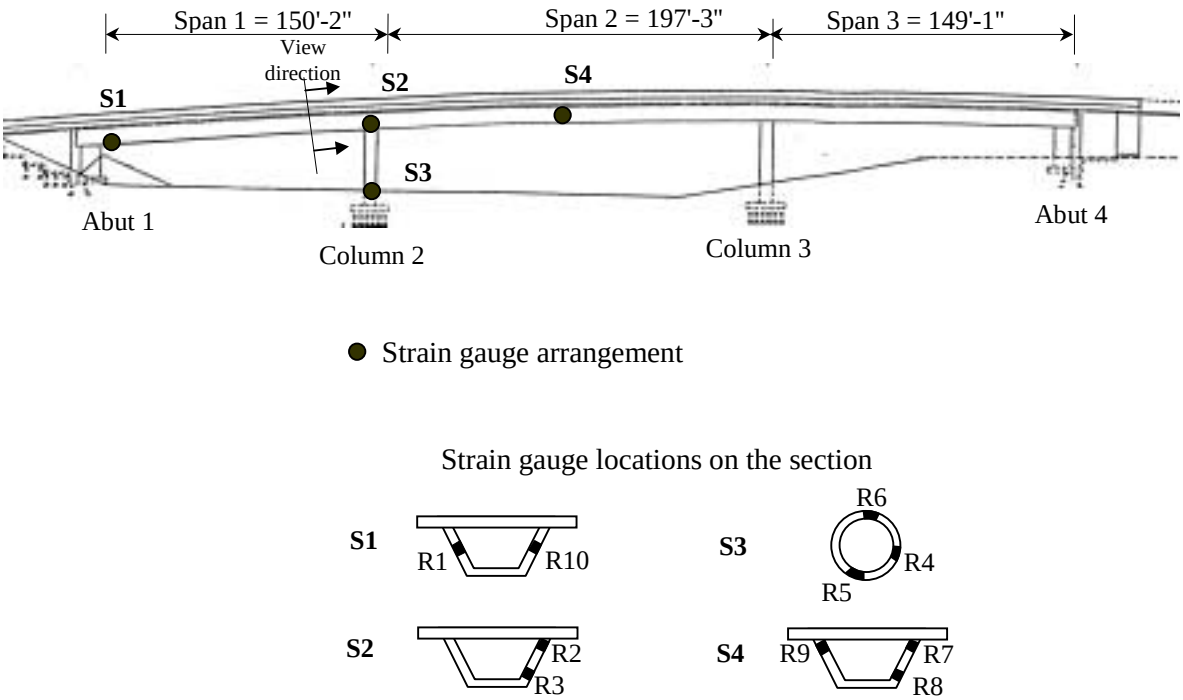

Figure 3.16: Strain Gauge Arrangement at West Street On-Ramp; Elevation

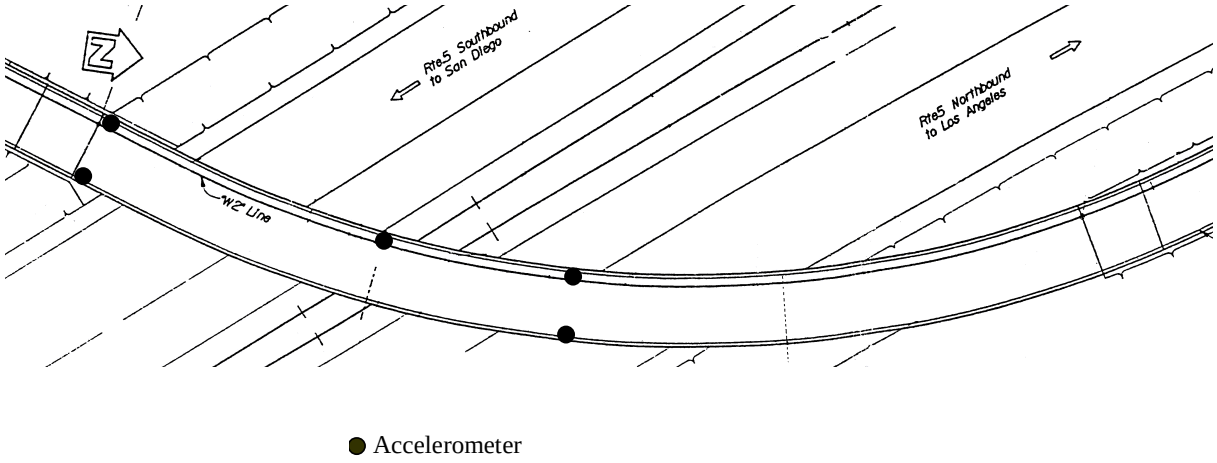

Figure 3.17: Strain Gauge Arrangement at West Street On-Ramp; Plan

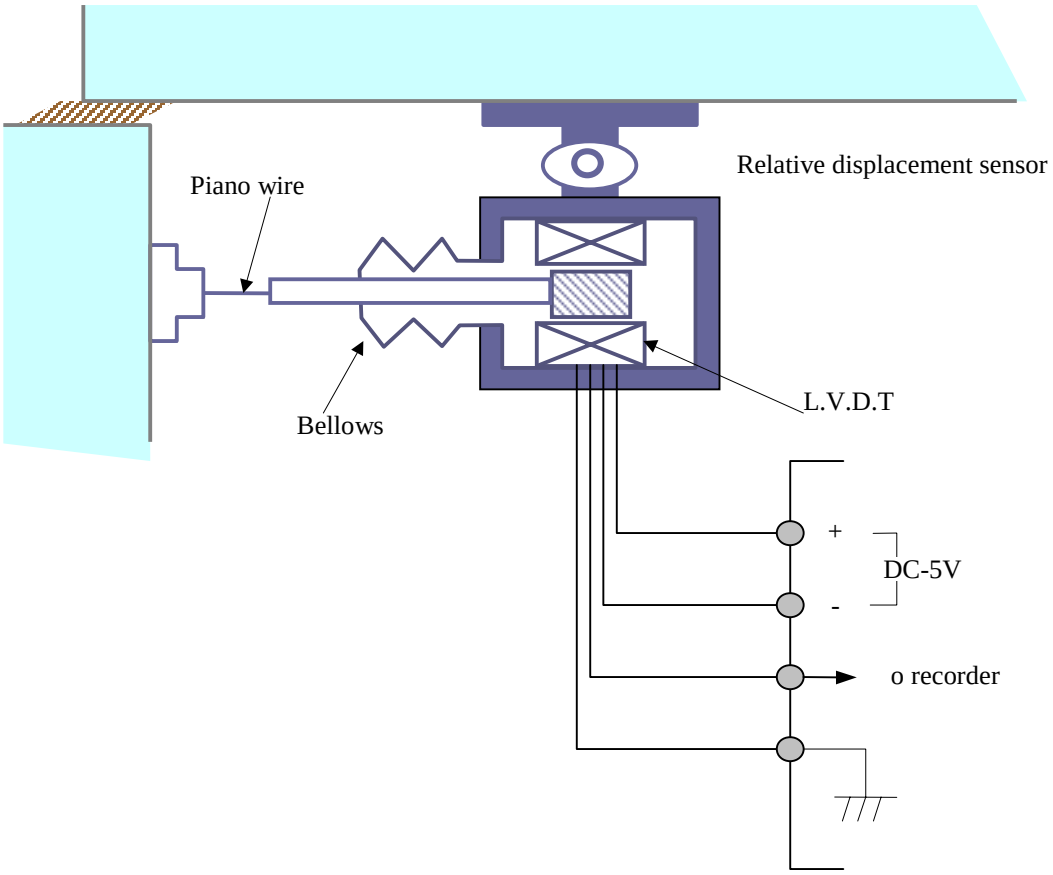

Figure 3.18: Displacement Sensor

Figure 3.19: Displacement Sensor at Jamboree Road Overcrossing

Figure 3.20: Displacement Sensor at West Street On-Ramp

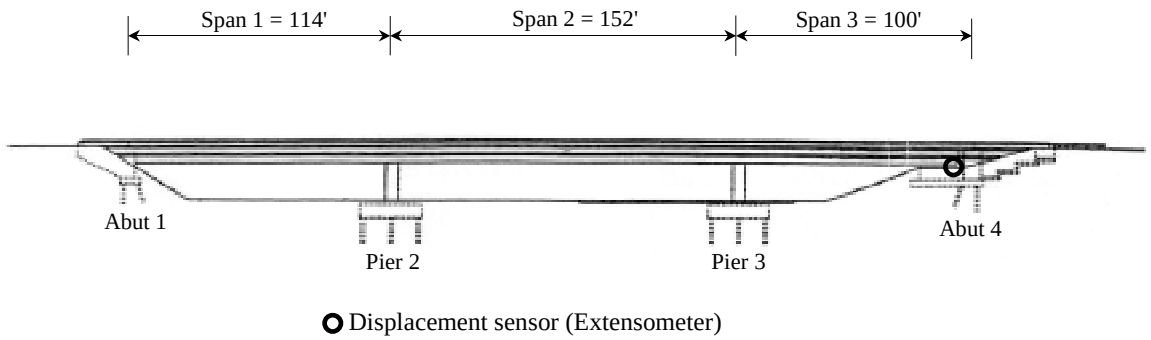

Figure 3.21: Displacement Sensor at Jamboree Road Overcrossing

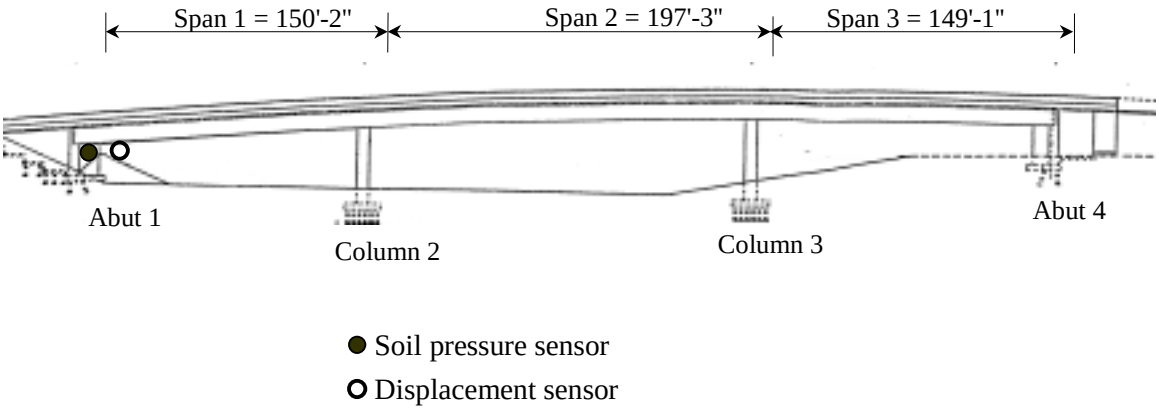

Figure 3.22: Displacement Sensor and Soil Pressure Sensor at West Street On-Ramp

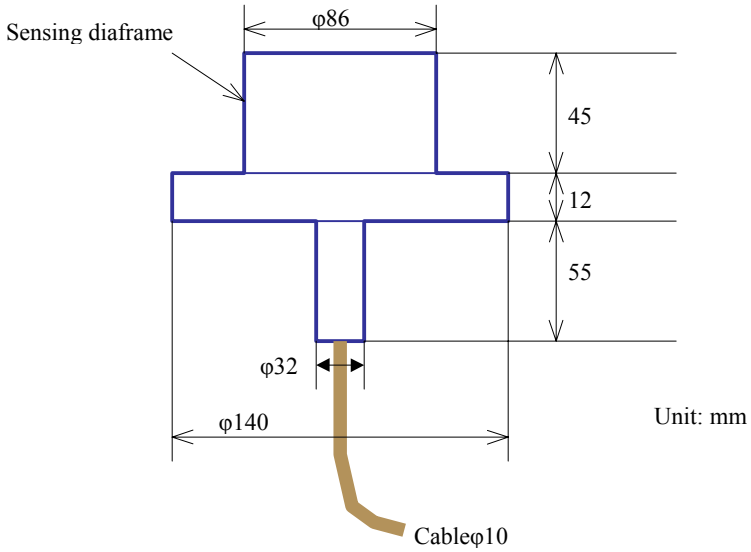

Figure 3.23: Soil Pressure Sensor; Outside View

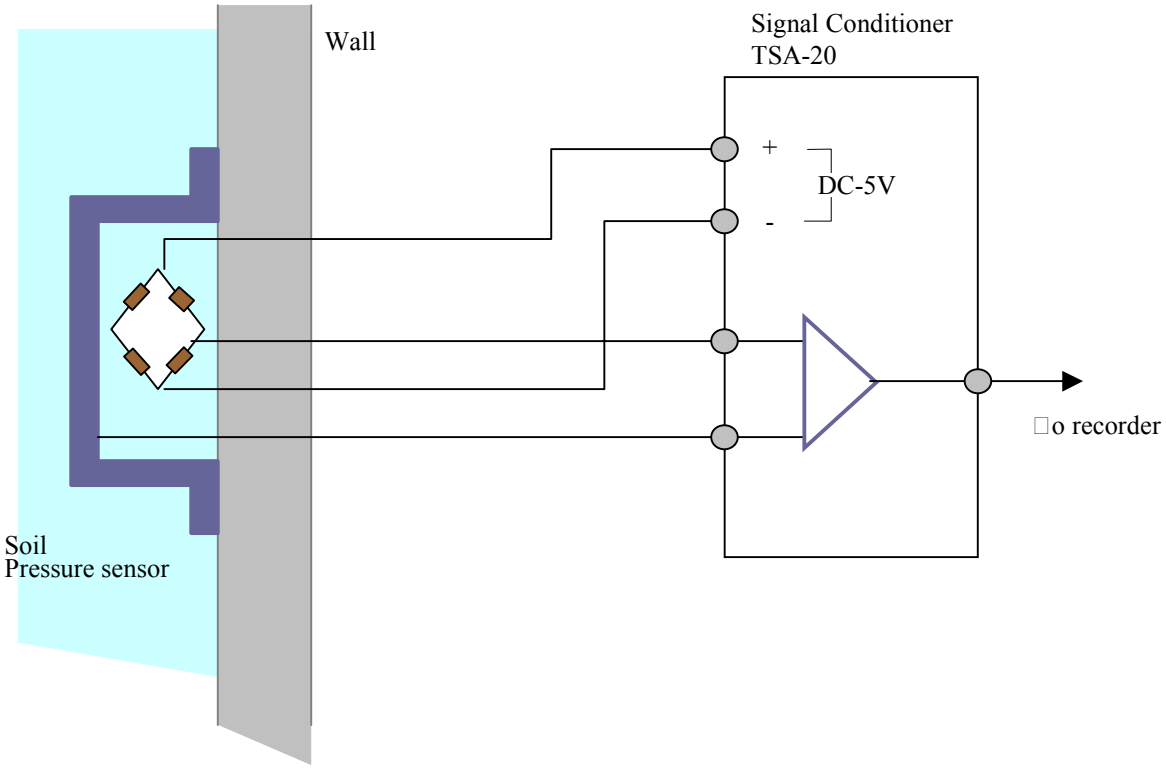

Figure 3.24: Soil Pressure Sensor; Inside View

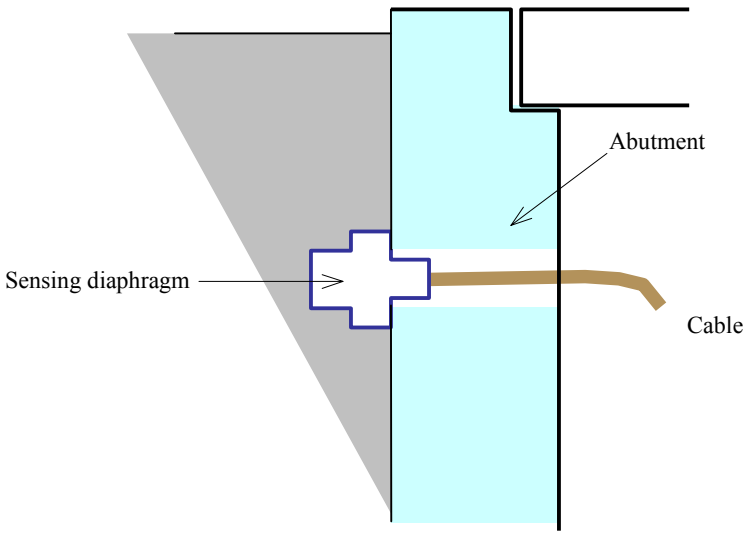

Figure 3.25: Installation of a Soil Pressure Sensor

Figure 3.26: Data Recorder Installed
on the Abutment Wall at Jamboree Road Overcrossing

Figure 3.27: Data Recorder Installed on the Inside Wall
of the Box Girder at West Street On-Ramp

Figure 3.28: Transformer

Figure 3.29: Uninterrupted Power Supply; Front and Back Sides

Figure 3.30: Solar Panel at Jamboree Road Overcrossing

Figure 3.31: Storage Battery of Solar Power Supply System
at Jamboree Road Overcrossing

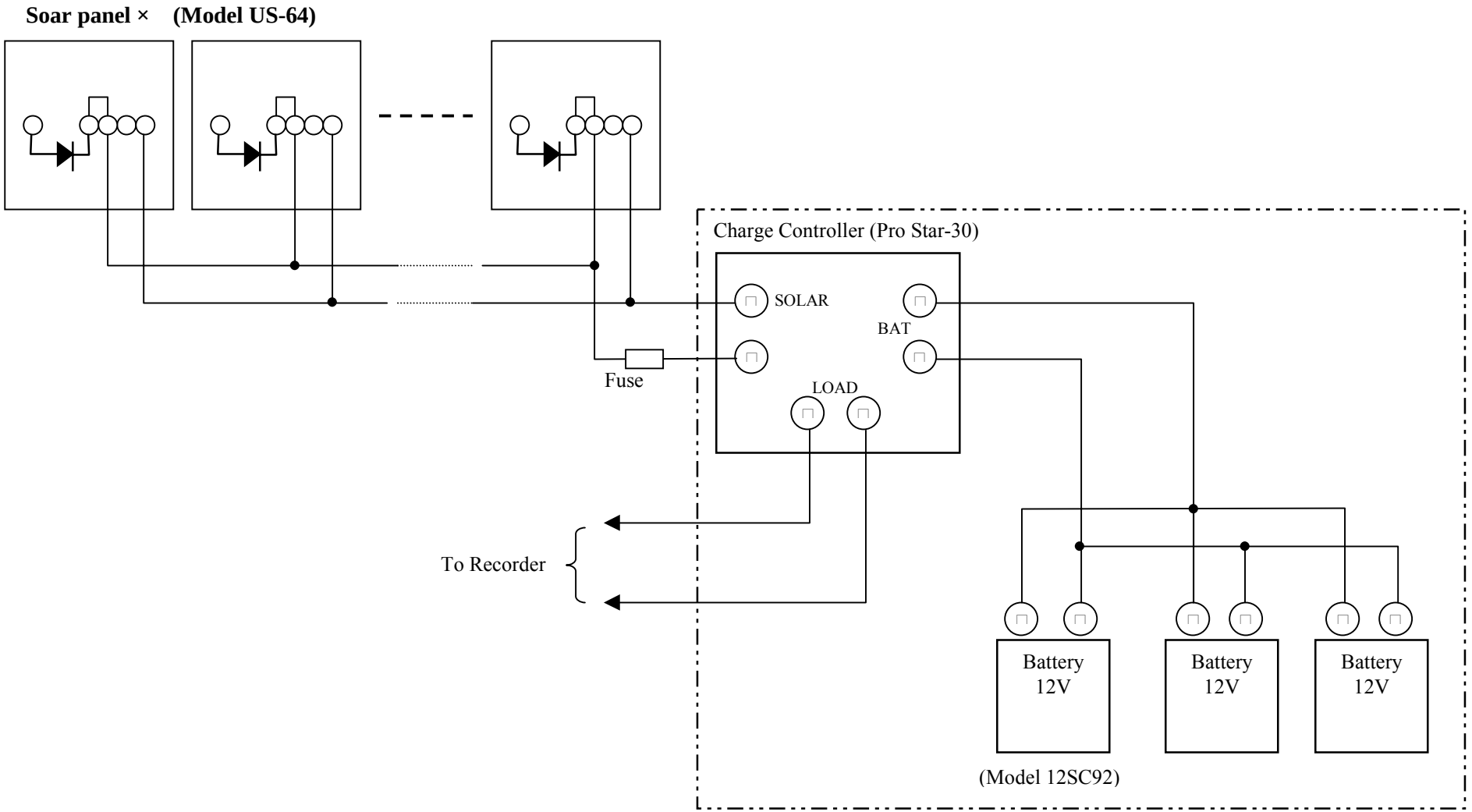

Figure 3.32: Schematic Diagram of Solar Power Supply System at Jamboree Road Overcrossing

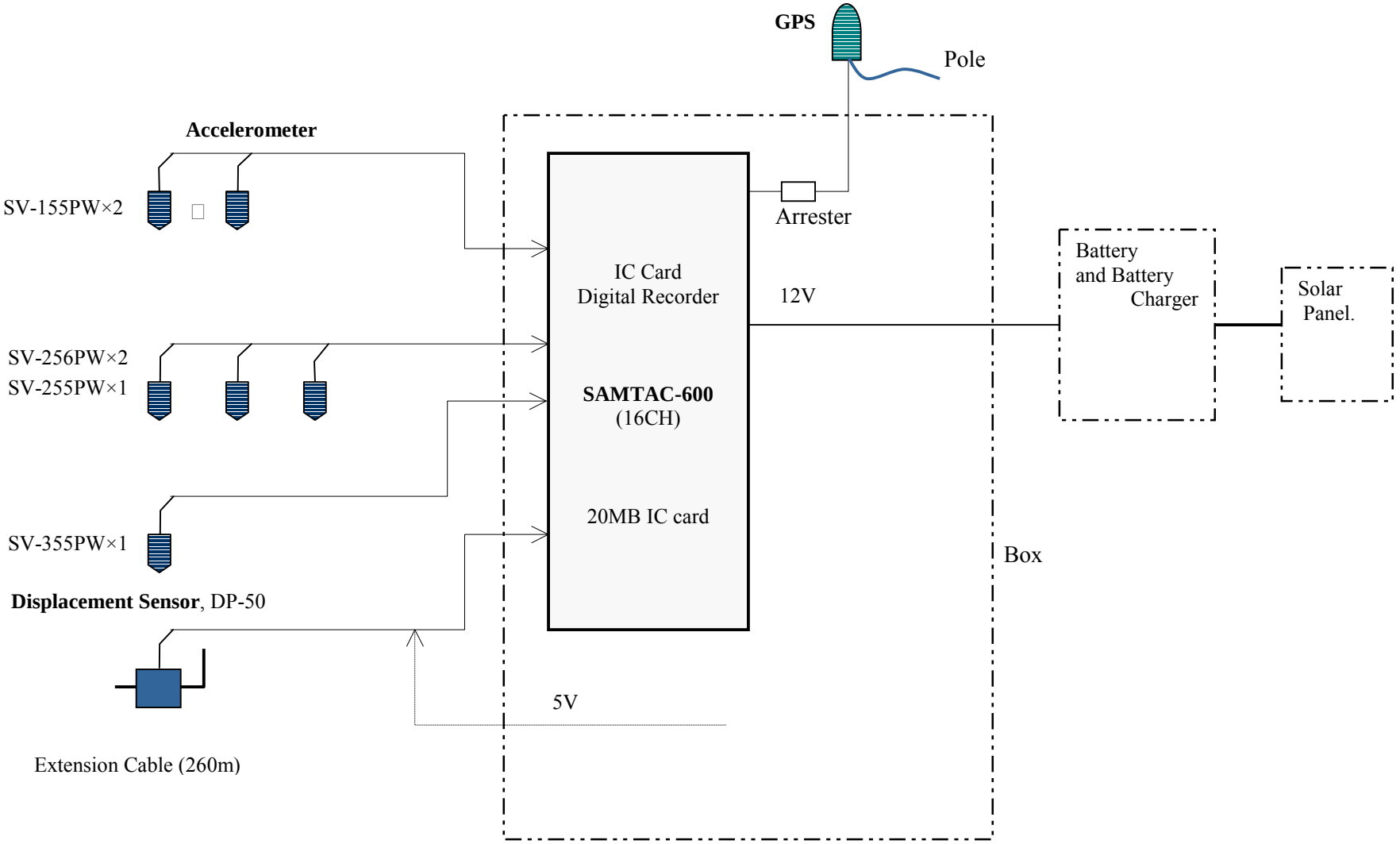

Figure 3.33: Monitoring System at Jamboree Road Overcrossing

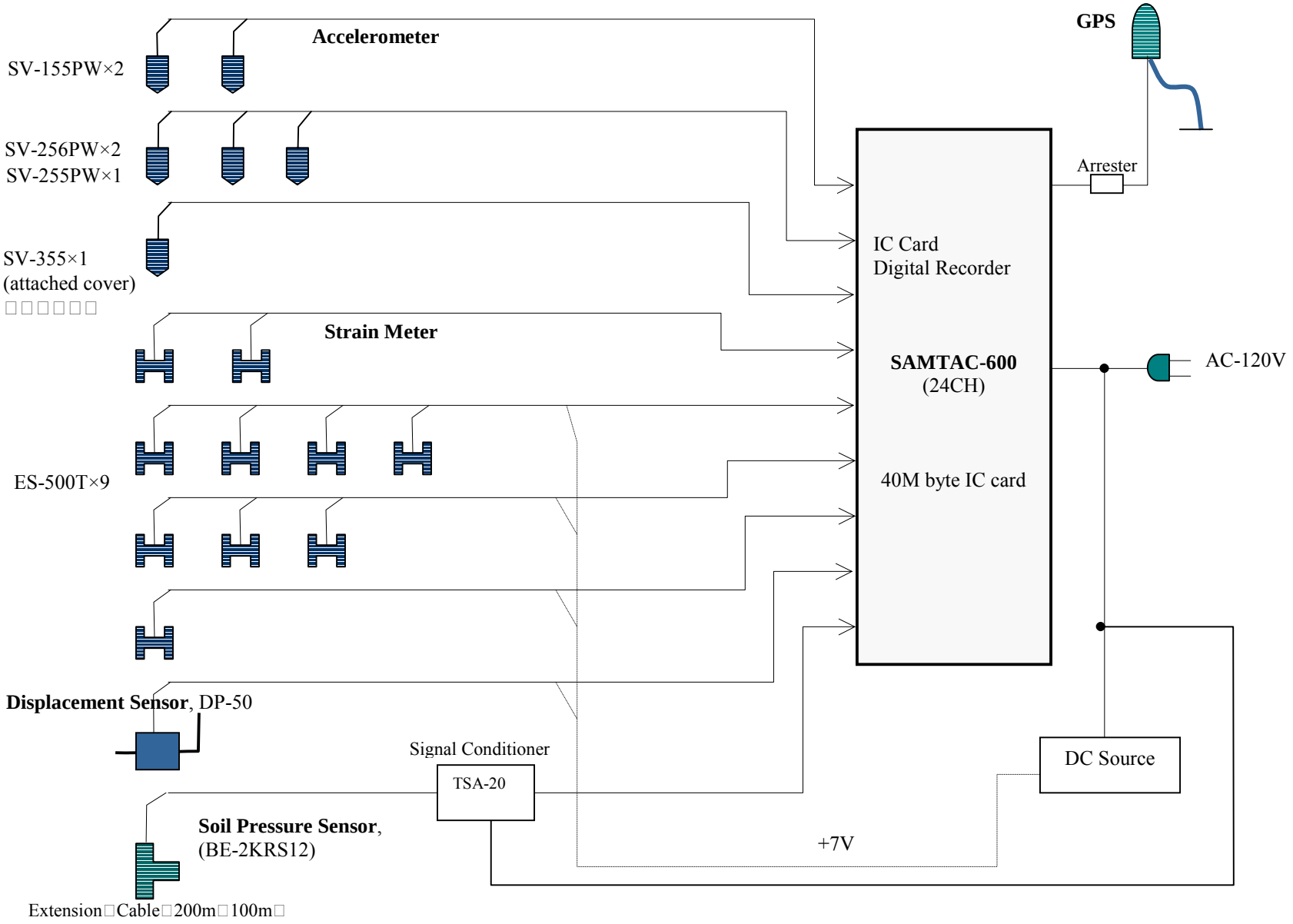

Figure 3.34: Monitoring System at West Street On-Ramp

Figure 3.35: Block of Traffic under Jamboree Road Overcrossing

Figure 3.36: Installation of Accelerometers Using a Cherry Picker

Figure 3.37: Installation of Cable Ducts Using a Cherry Picker

Figure 3.38: Embedment of a Strain Gauge During Construction at West Street On-Ramp

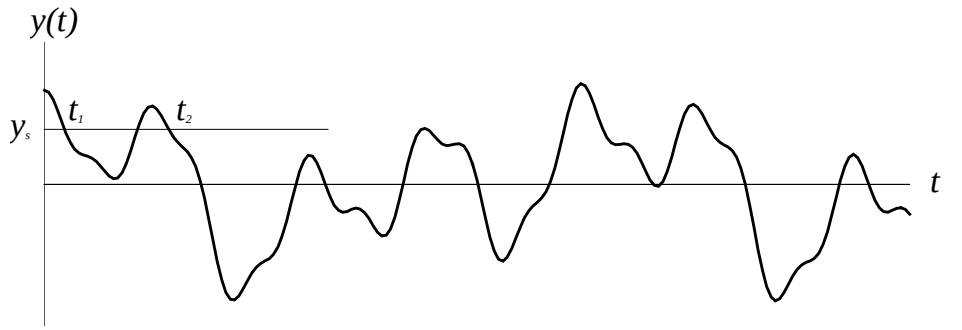

(a) A Random Response

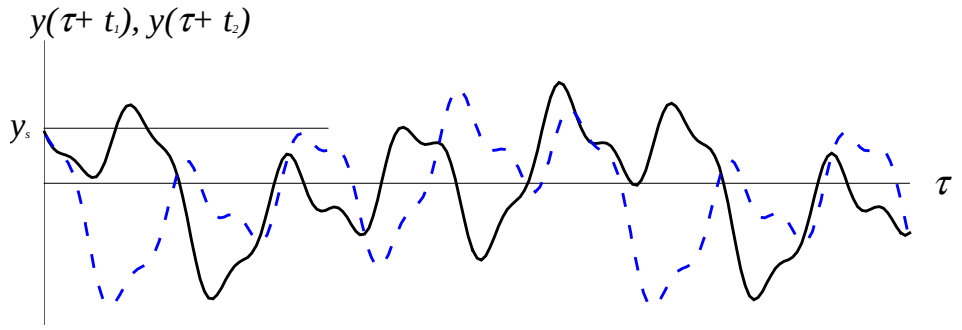

(b) Segments with Same Initial Conditions

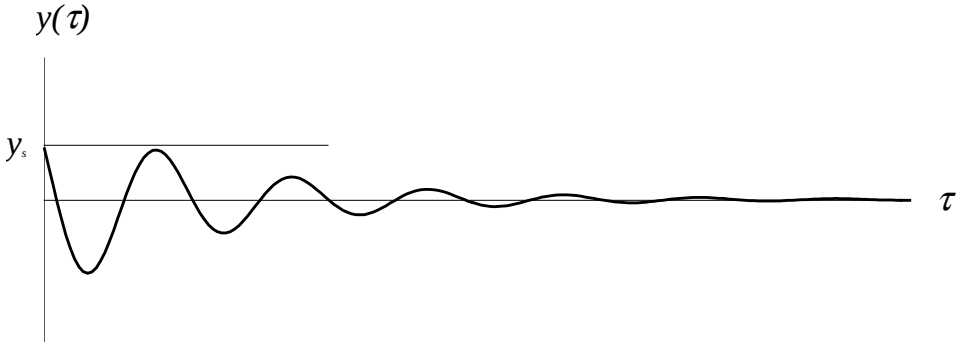

(c) Signature after *N* averages

Figure 4.1: Extraction of Randomdec Signature from a Random Response

Table 5.1: Comparison of Natural Frequencies of Jamboree Road Overcrossing (Hz)

Mode Number	In-plane modes				Out-of-plane modes	
	FE	PP	RD	FDD	FE	FDD
1	2.889	2.954 (0.065)	2.954 (0.065)	2.954 (0.065)	3.126	2.612 (0.514)
2	3.716	3.979 (0.263)	4.077 (0.361)	3.979 (0.263)	4.535	5.004 (0.469)
3	4.654	4.660 (0.006)	4.638 (0.016)	4.638 (0.529)	6.111	6.640 (0.529)
4	5.721	6.250 (0.529)	6.323 (0.602)	6.250 (0.529)		
5	9.400	8.957 (0.443)	8.813 (0.587)	8.911 (0.489)		
6	14.521	12.793(1.728)	12.866(1.655)	12.793(1.728)		

Where The values in the parentheses are the difference between the analytical and the experimental natural frequencies.

In-plane modes = modes in the vertical and in the longitudinal directions

Out-of-plane modes = modes in the transverse direction

FE = initial finite element analysis

PP = peak picking method

RD = random decrement method

FDD = frequency decomposition method

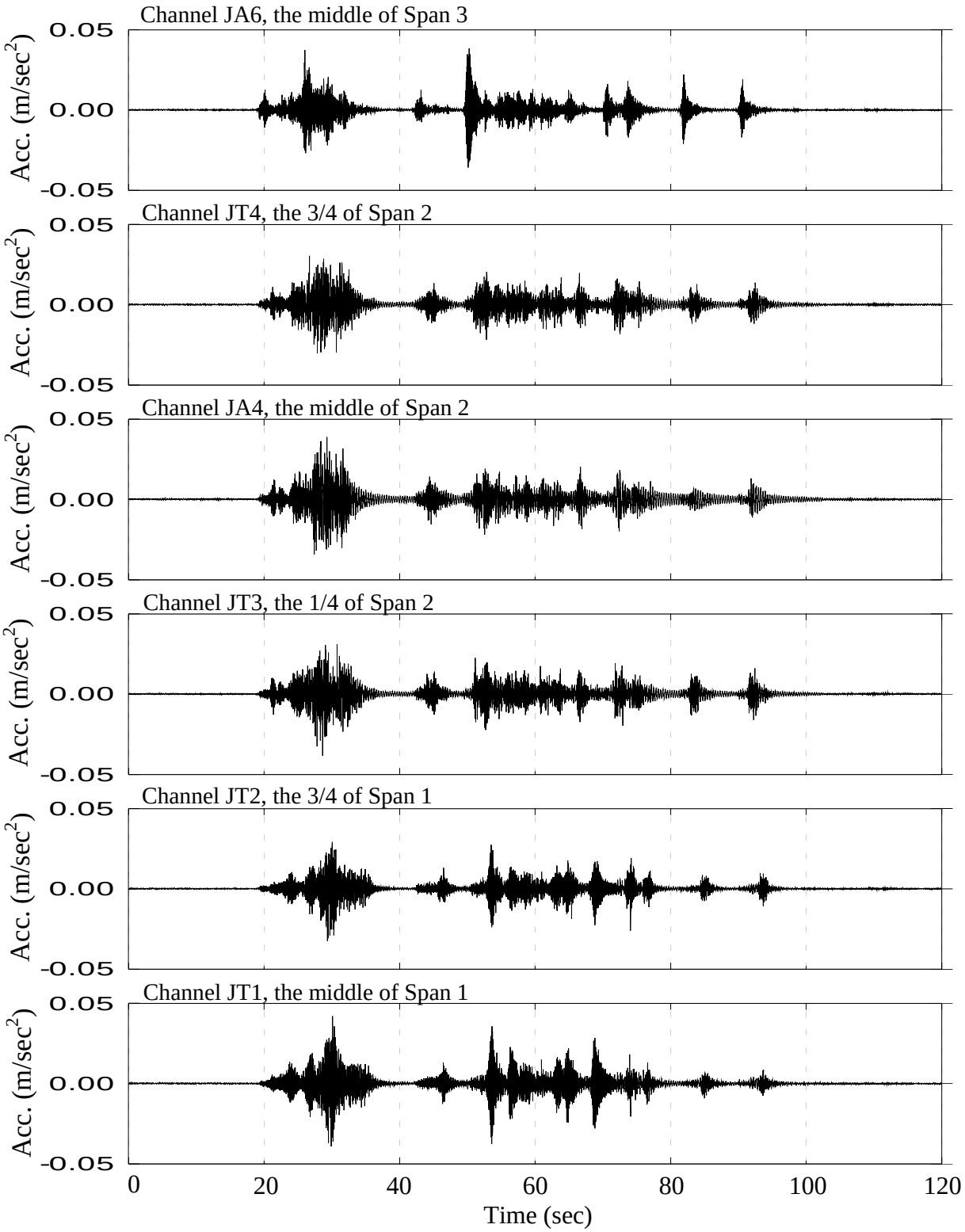

Figure 5.1: Typical Vertical Acceleration Time Histories
of Super-Structure at Jamboree Road Overcrossing

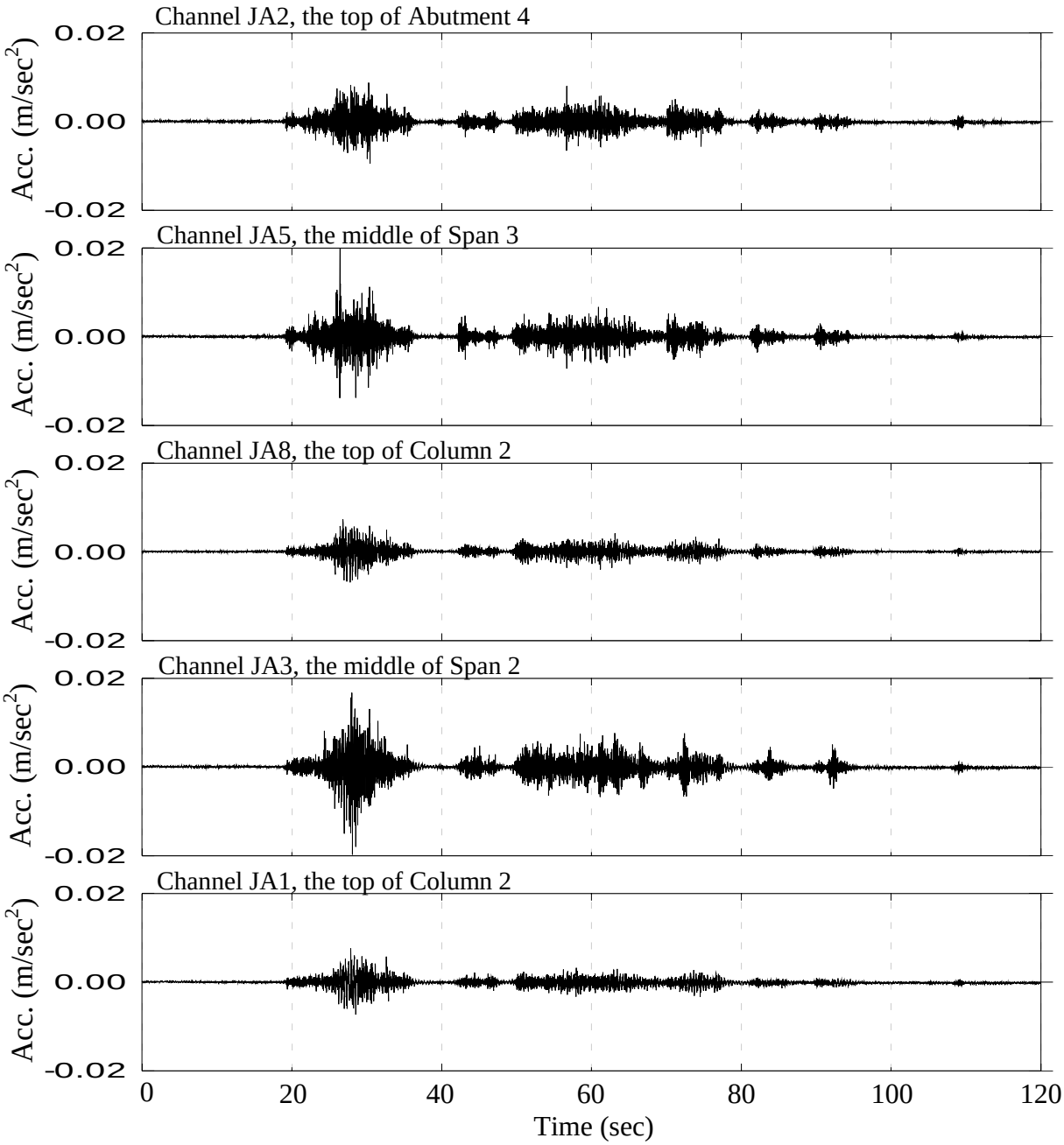

Figure 5.2: Typical Transverse Acceleration Time Histories
of Super-Structure at Jamboree Road Overcrossing

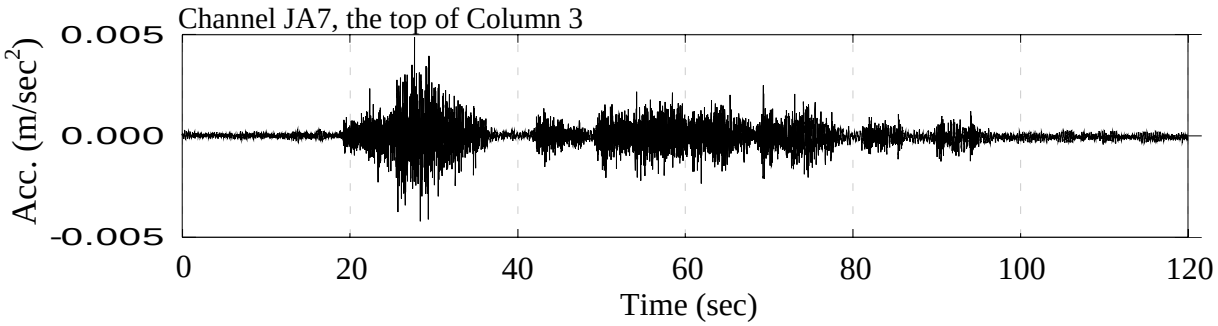

Figure 5.3: Typical Longitudinal Acceleration Time History
of Super-Structure at Jamboree Road Overcrossing

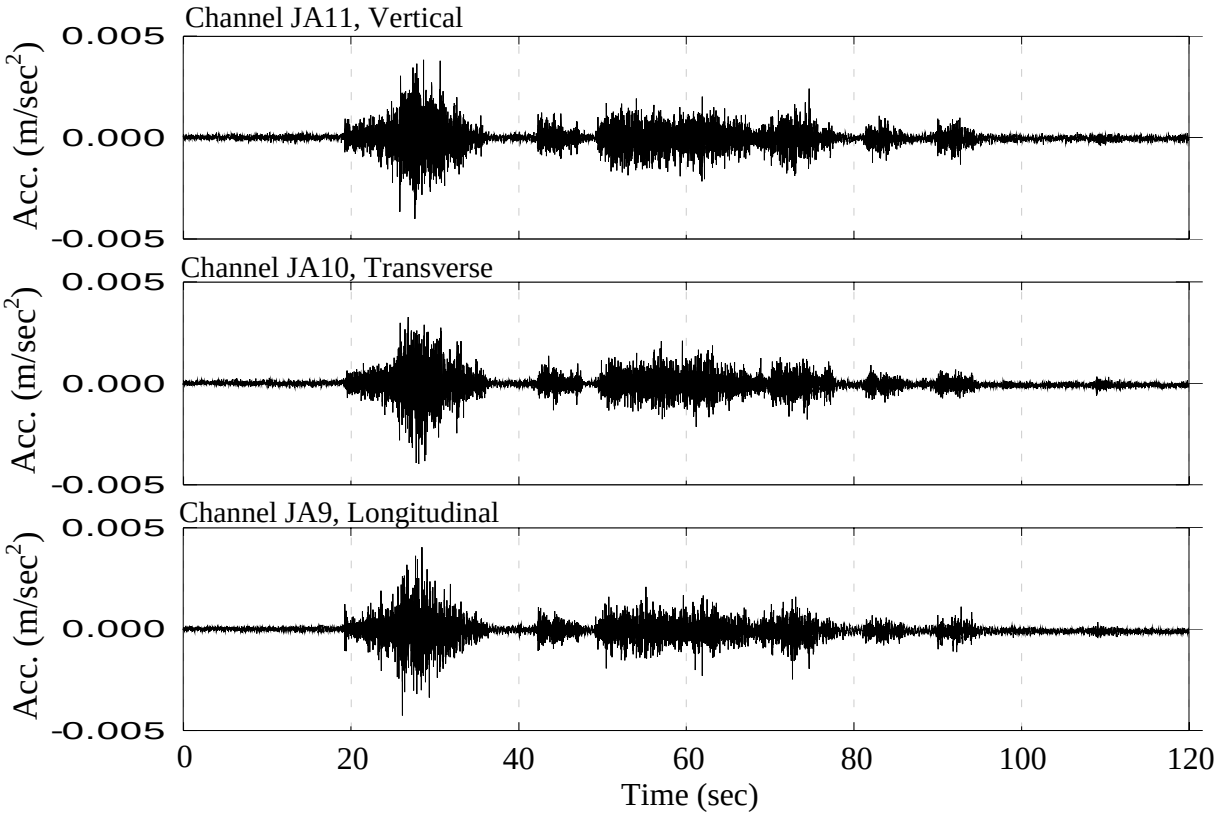

Figure 5.4: Typical Acceleration Time Histories
at the Bottom of Column 3 at Jamboree Road Overcrossing

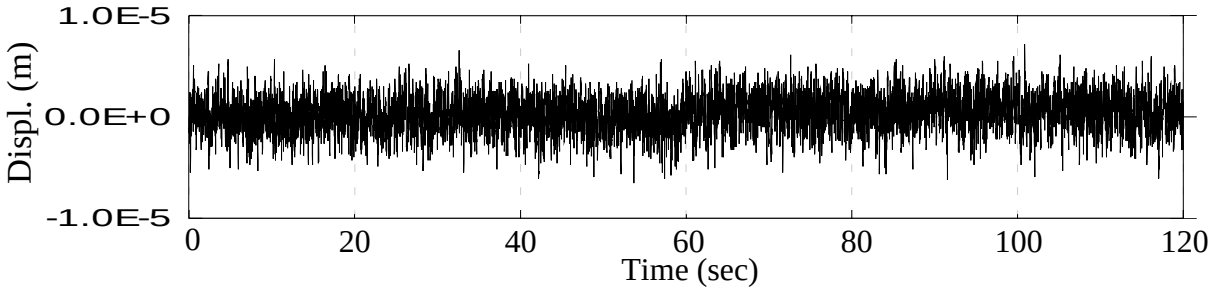

Figure 5.5: Typical Longitudinal Displacement Time History
of Super-Structure at Abutment 4 at Jamboree Road Overcrossing

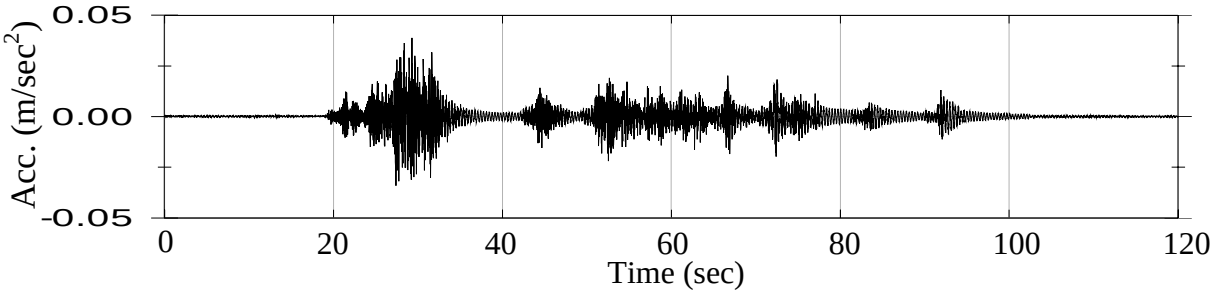

Figure 5.6: Typical Vertical Acceleration Time History
in the Middle of Span 2 at Jamboree Road Overcrossing

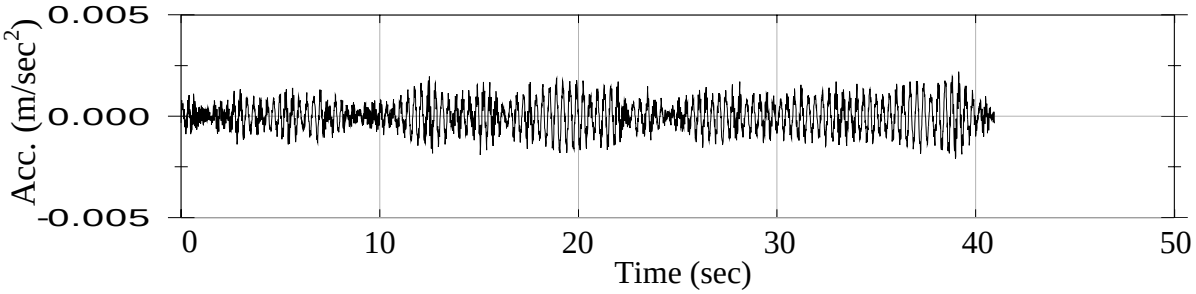

Figure 5.7: Typical Averaged Vertical Acceleration Time History
in the Middle of Span 2 at Jamboree Road Overcrossing; 25% overlapping

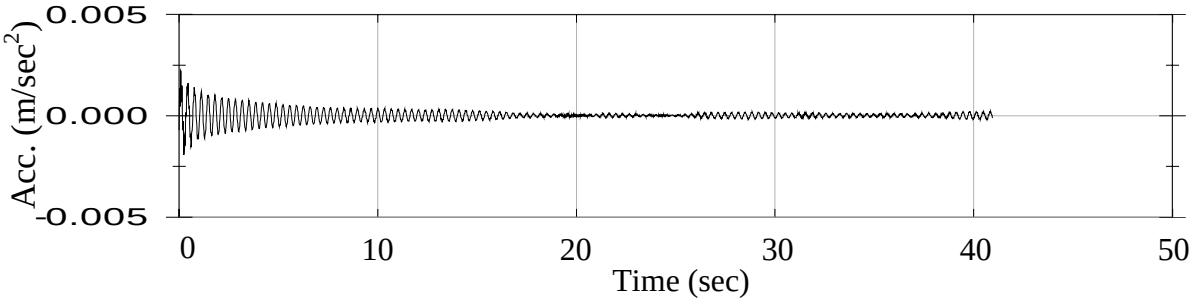

Figure 5.8: Typical Randomdec Vertical Acceleration Time History
in the Middle of Span 2 at Jamboree Road Overcrossing

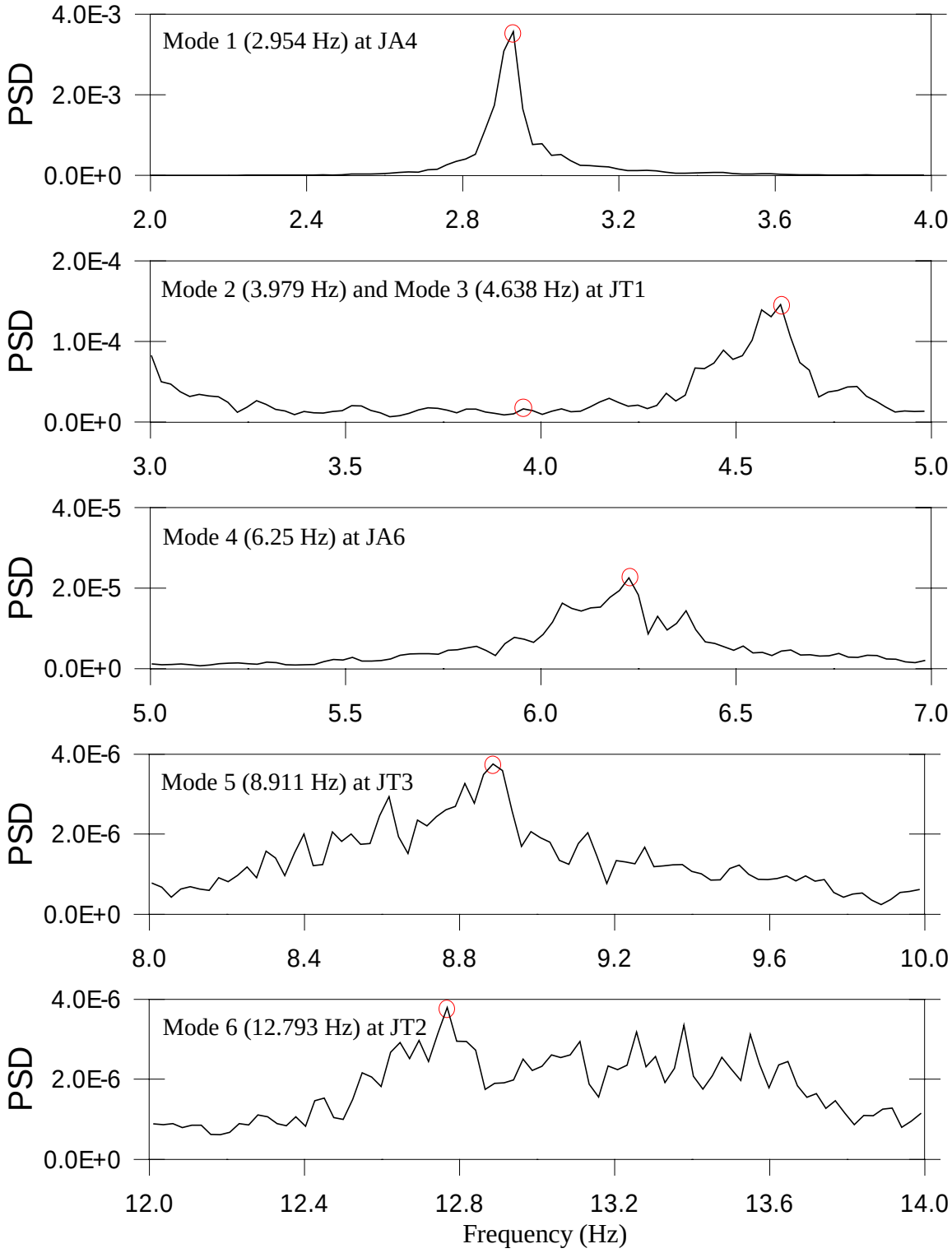

Figure 5.9: Power Spectral Density Functions of Averaged Vertical Accelerations

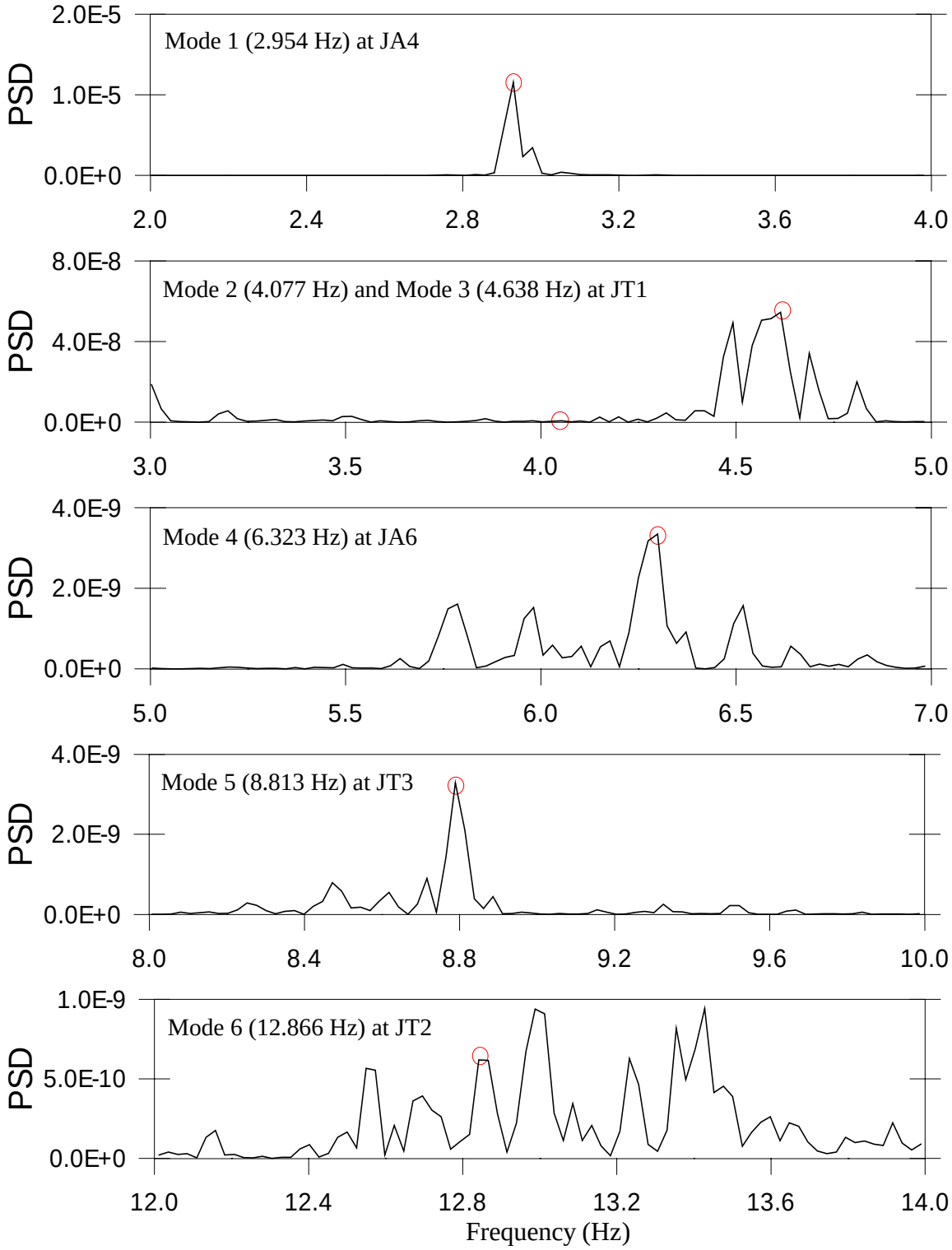

Figure 5.10: Power Spectral Density Functions of Randomdec Vertical Accelerations

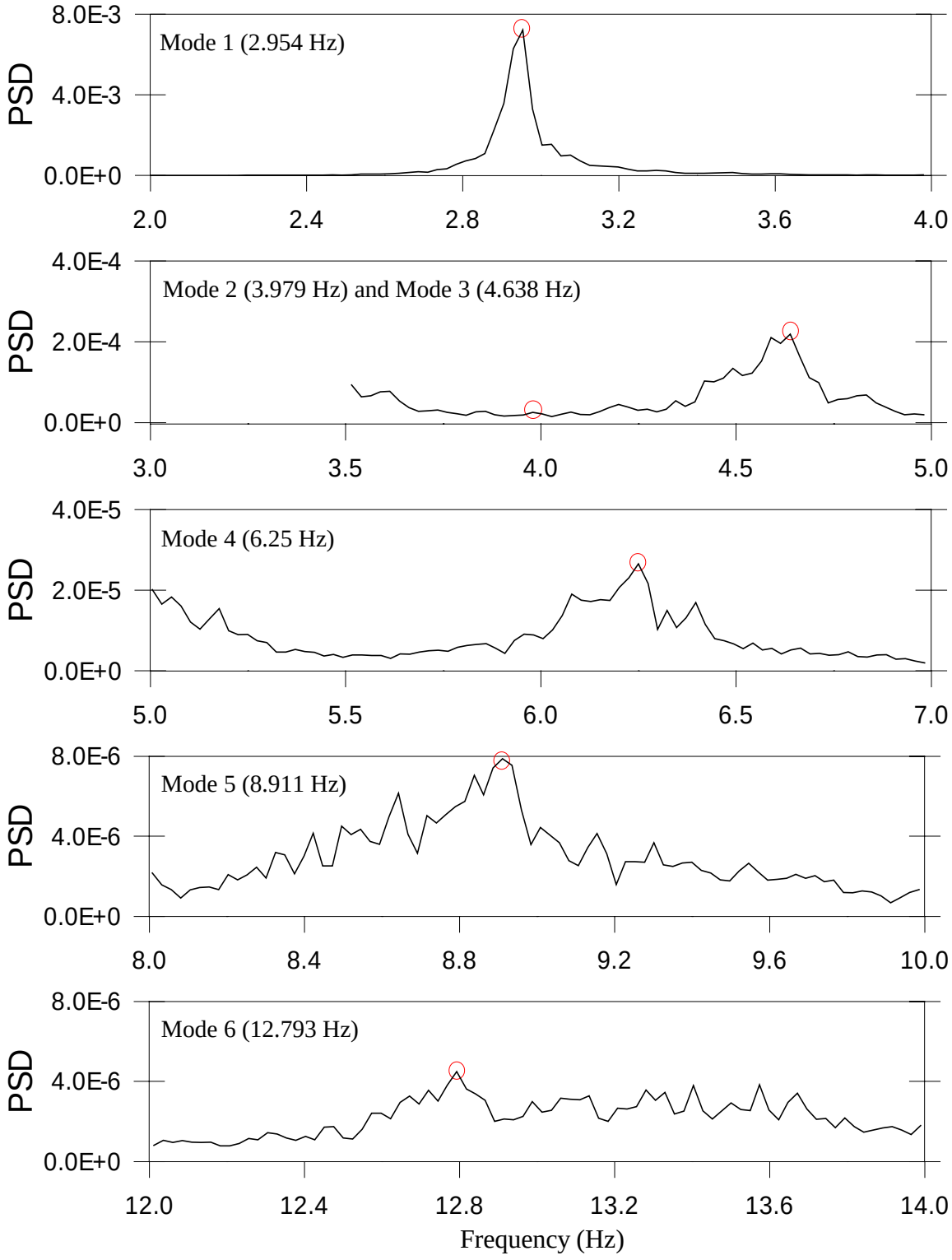

Figure 5.11: Power Spectral Density Functions of Vertical Accelerations Using Frequency Decomposition Method

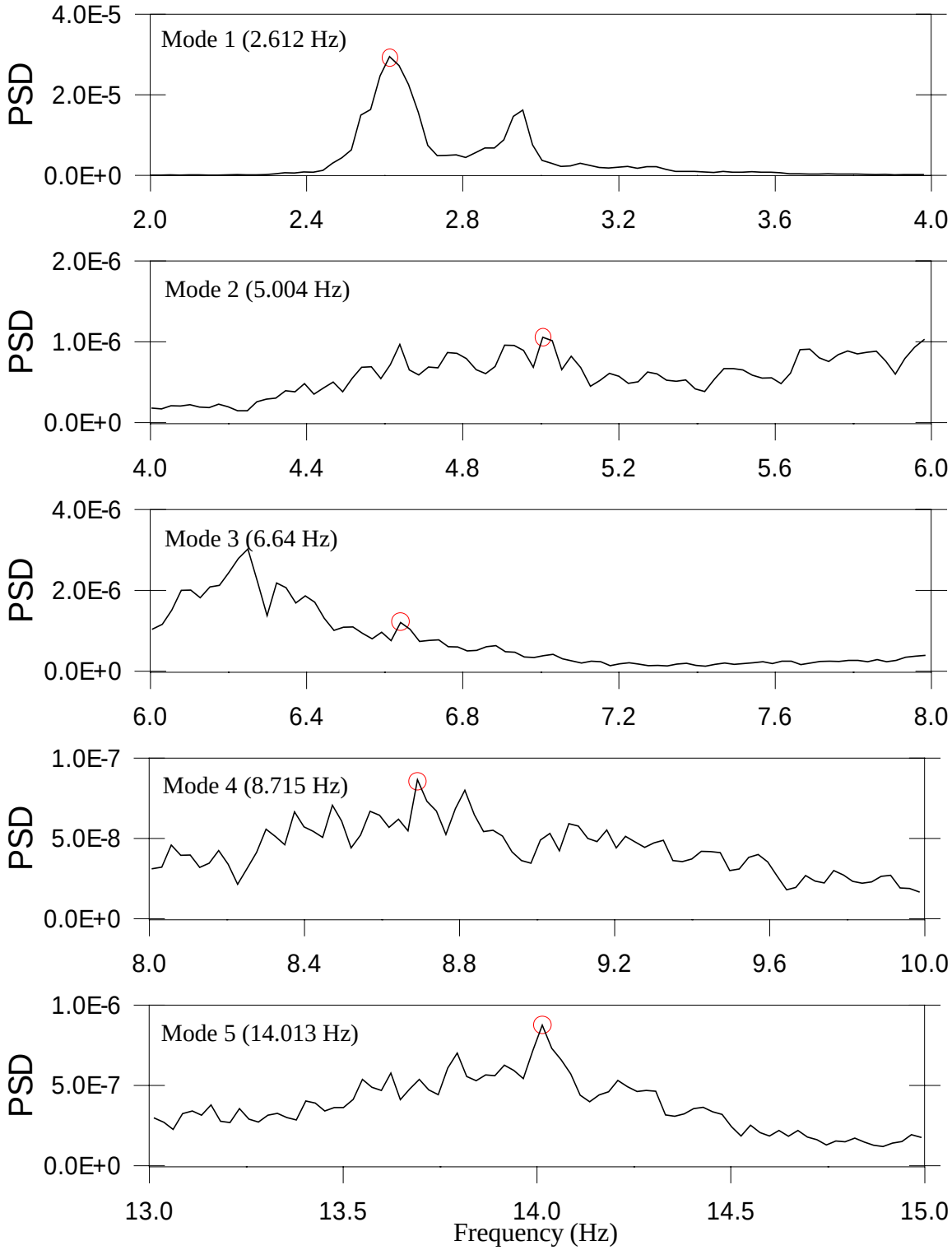

Figure 5.12: Power Spectral Density Functions of Transverse Accelerations Using Frequency Decomposition Method

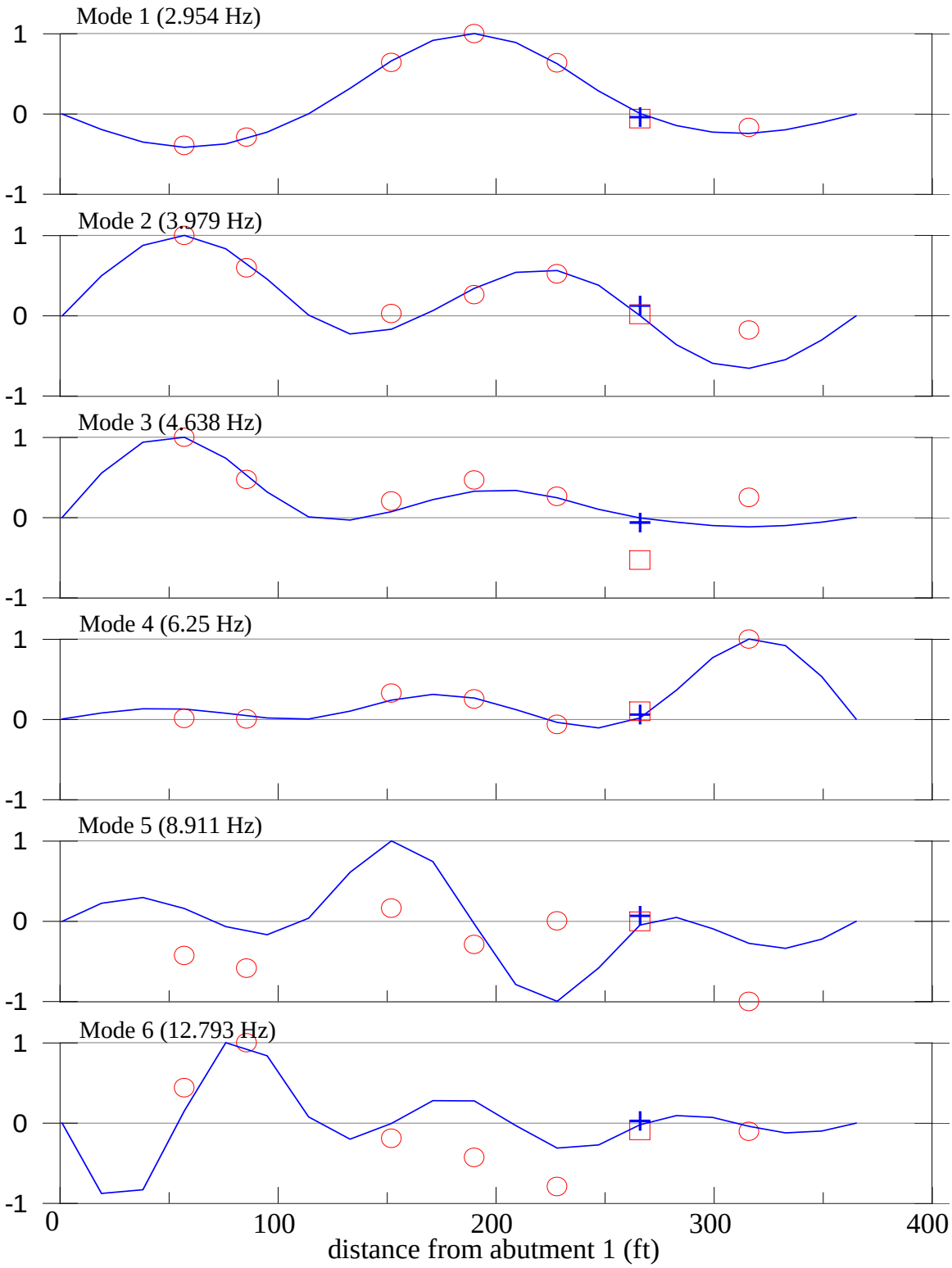

Figure 5.13: Vertical Mode Shapes by Peak Picking Method

Analytical vertical mode

Experimental vertical mode

Analytical longitudinal mode

Experimental longitudinal mode

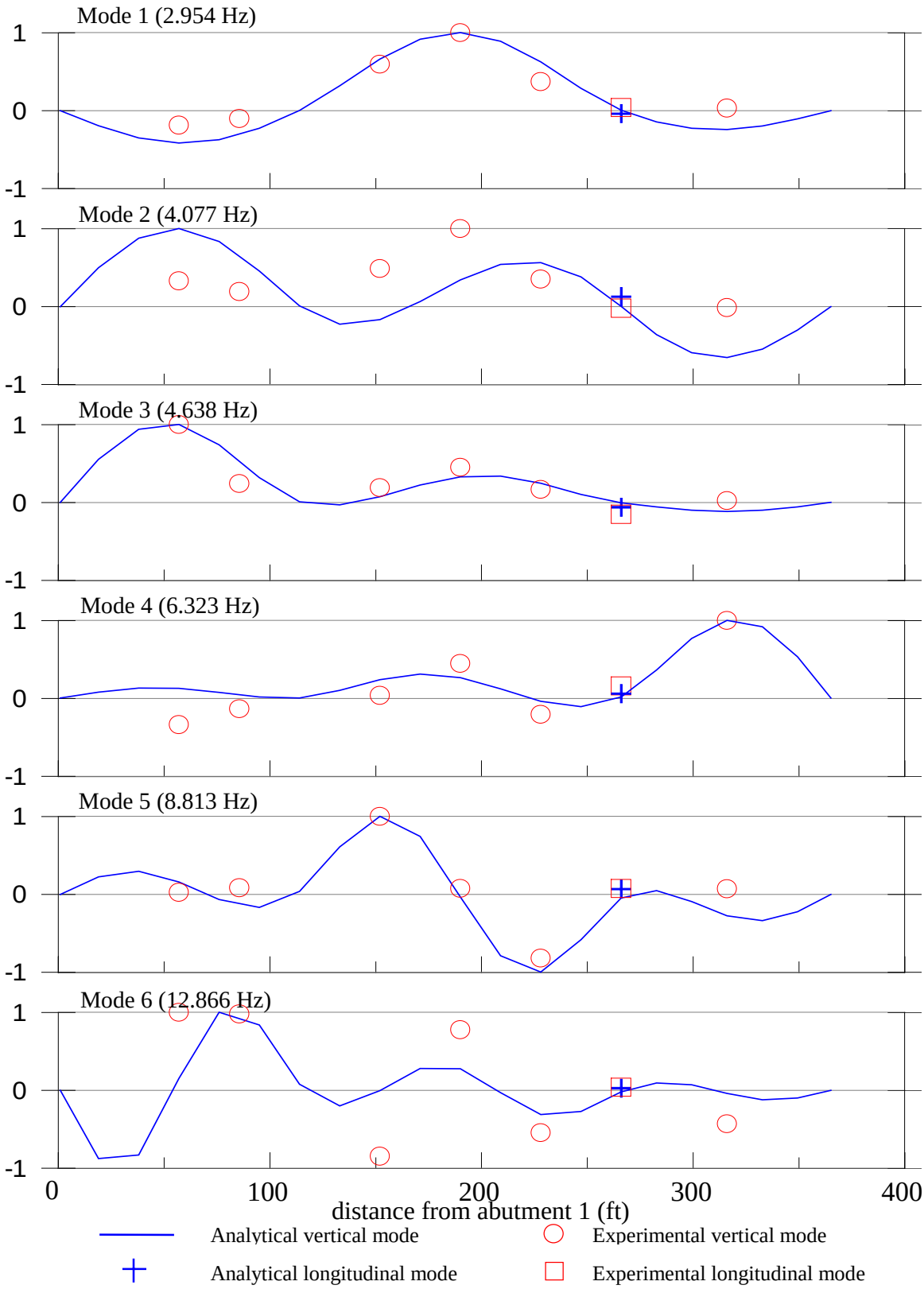

Figure 5.14: Vertical Mode Shapes by Random Decrement Method

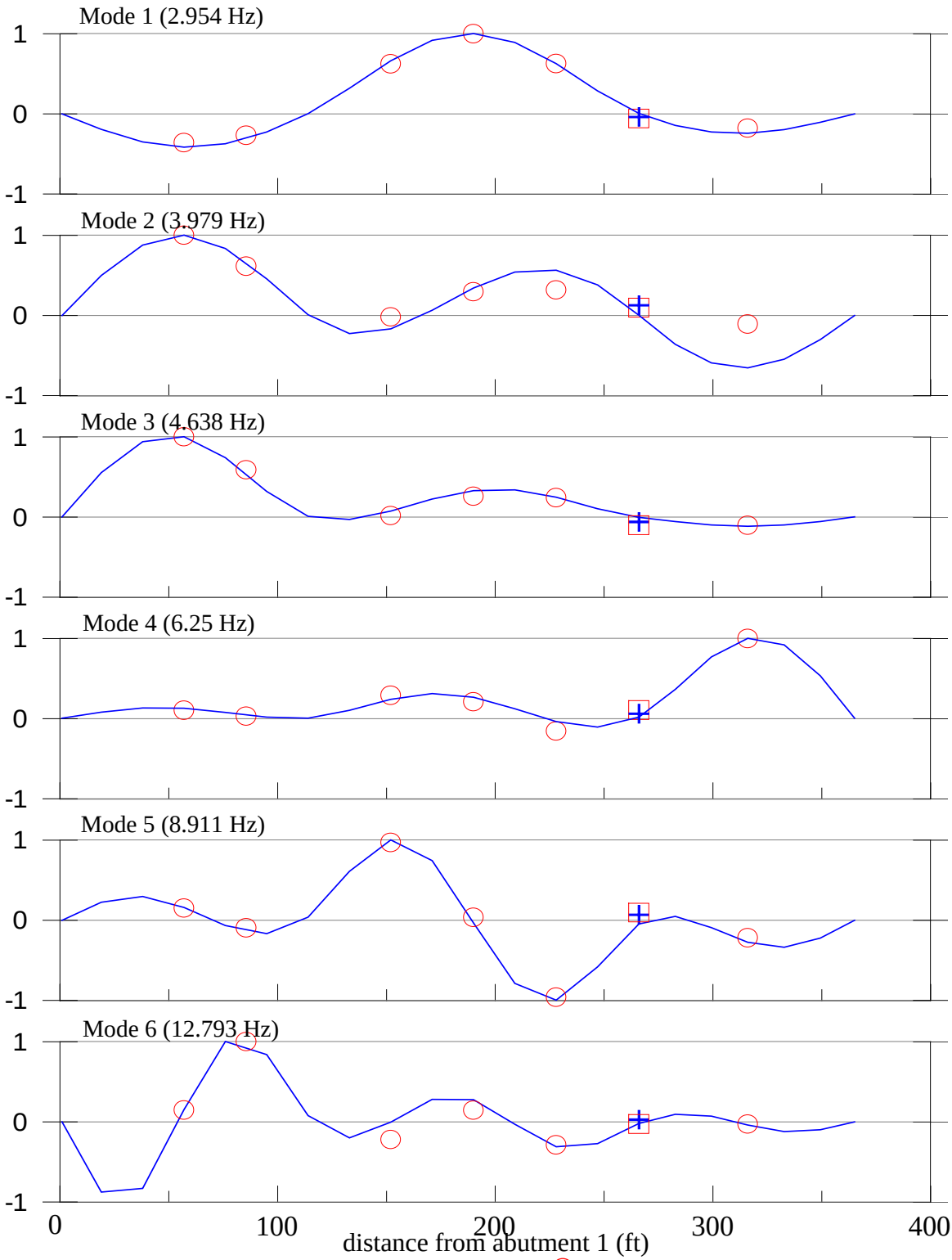

Figure 5.15: Vertical Mode Shapes by Frequency Decomposition Method

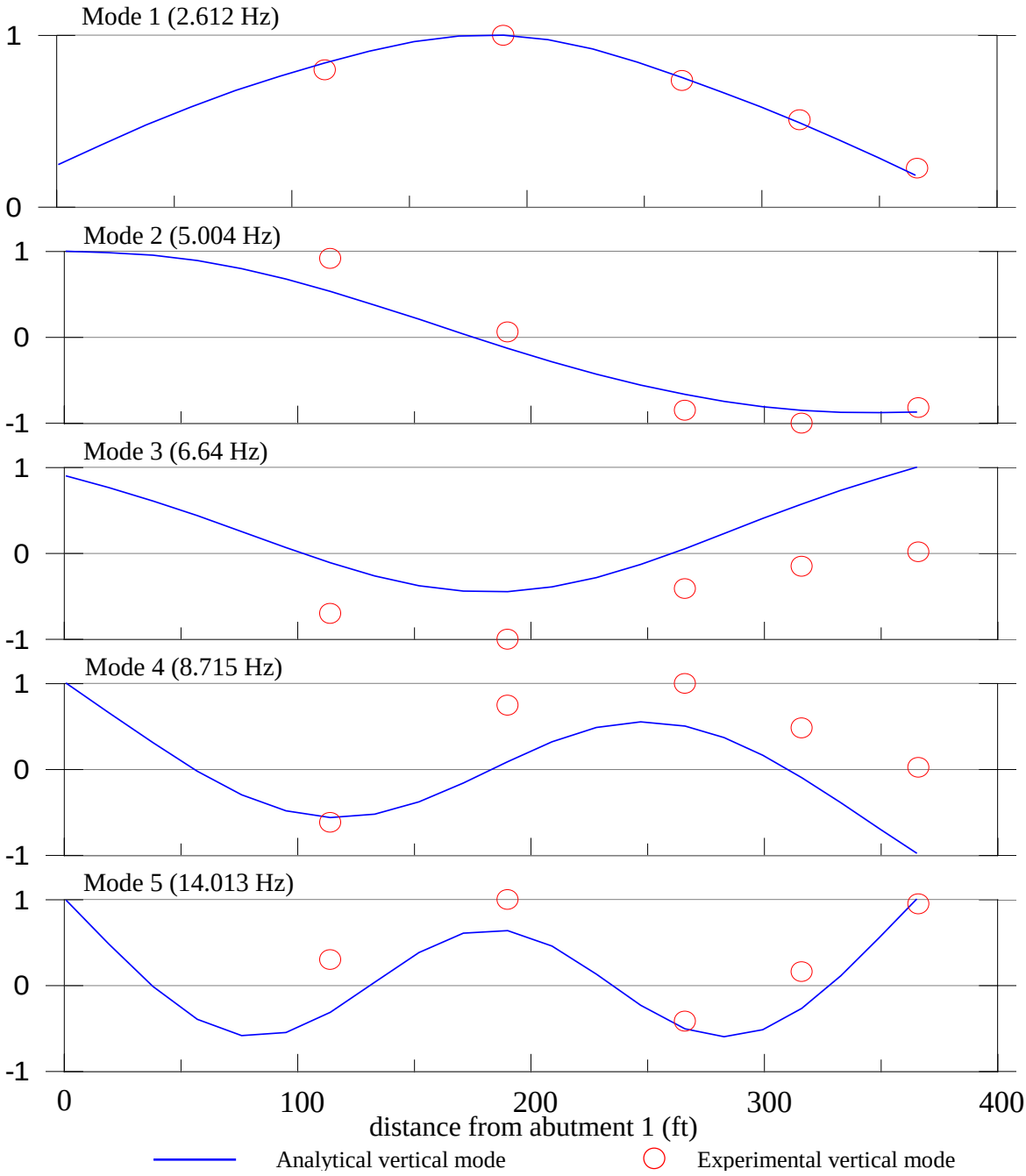

Figure 5.16: Transverse Mode Shapes by Frequency Decomposition Method

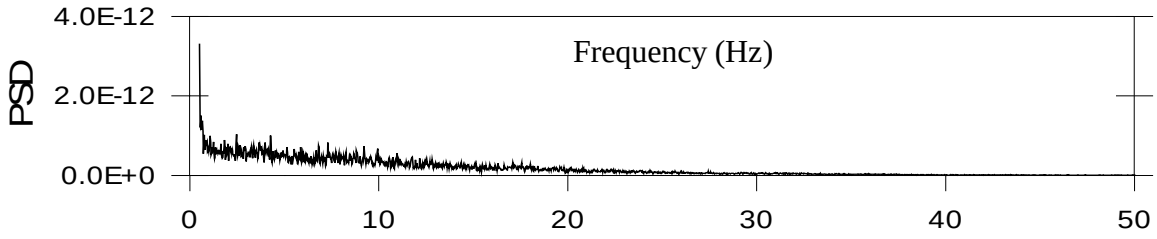

Figure 5.17: Power Spectral Density Function of Averaged Displacement

Table 6.1: Comparison of Natural Frequencies of West Street On-Ramp (Hz)

Test	Braking Vibration Test		Bumping Vibration Test	
Mode	Vertical	Transverse	Vertical	Transverse
1	2.148	2.148	2.075 (-0.073)	2.124 (-0.024)
2	2.465	2.465	2.441 (-0.024)	2.441 (-0.024)

Where '*Vertical*' and '*Transverse*' mean the direction of vibration measurements, and the values in the parentheses are the difference between two test results.

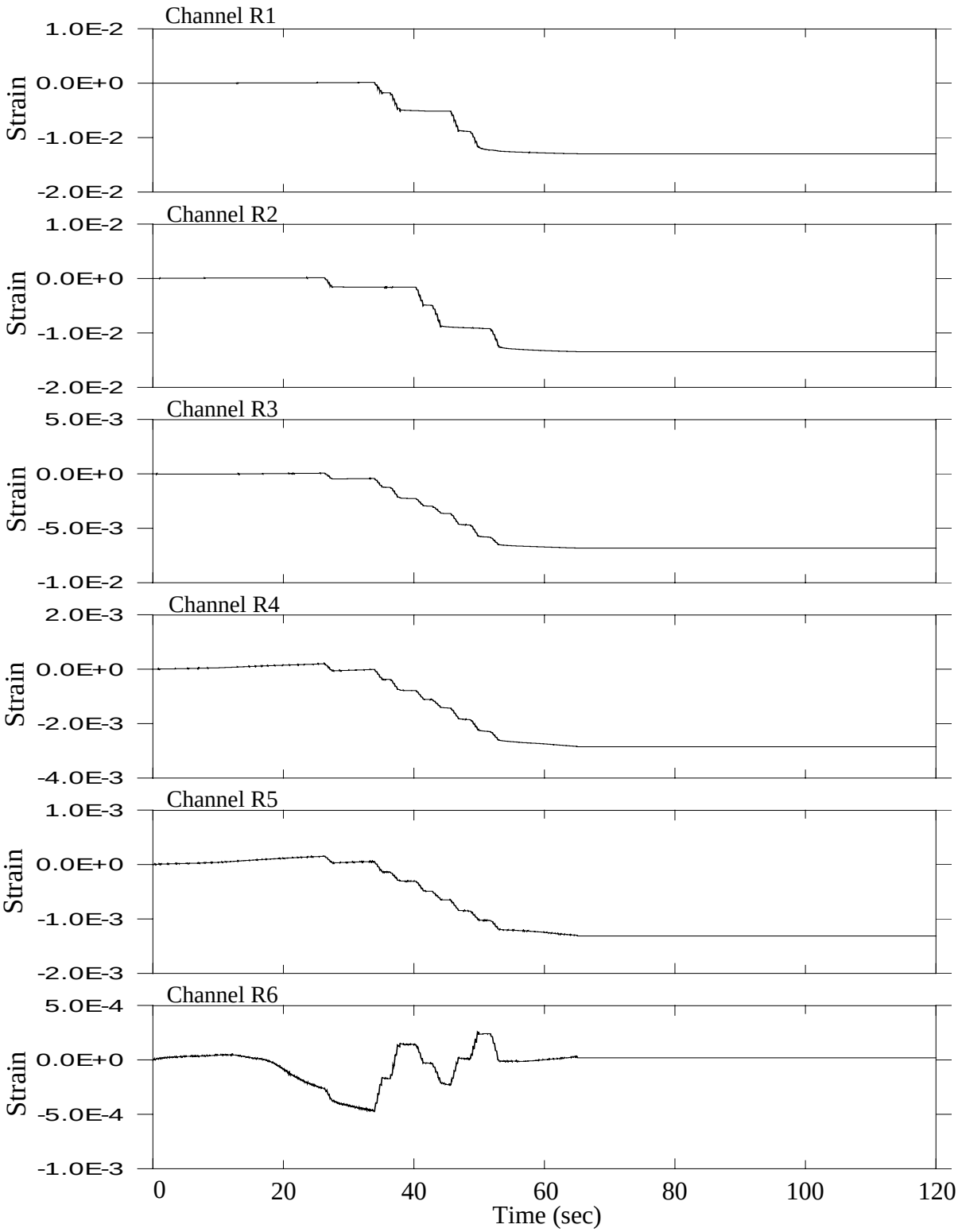

Figure 6.1: Typical Strain Time History During Post Tension at West Street On-Ramp

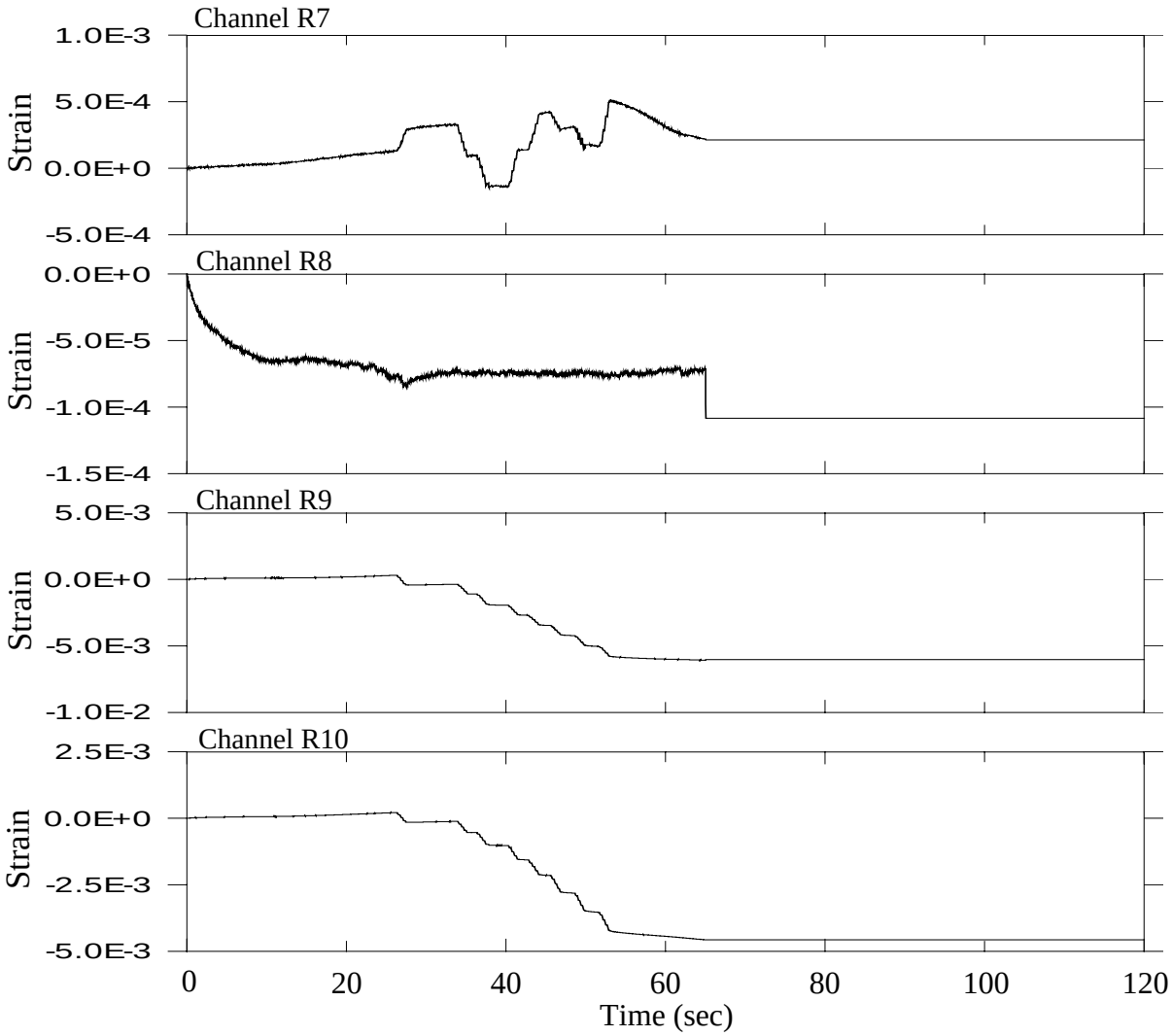

Figure 6.2: Typical Strain Time History During Post Tension at West Street On-Ramp

Figure 6.3: Water Truck for Braking and Bumping Tests at West Street On-Ramp

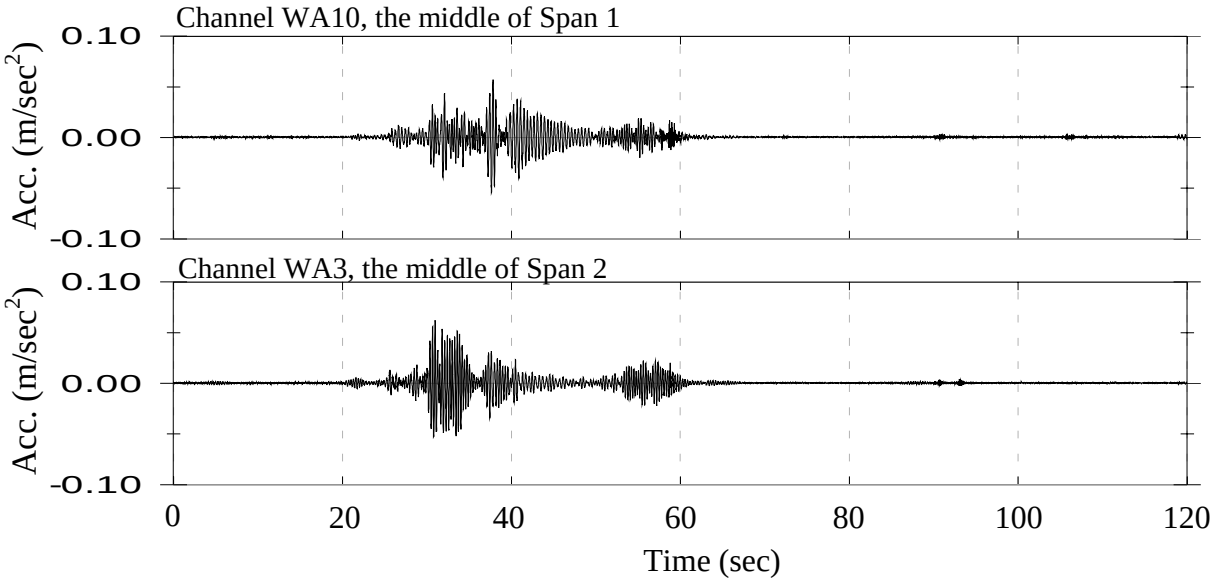

Figure 6.4: Typical Vertical Acceleration Time History
of Super-Structure at West Street On-Ramp

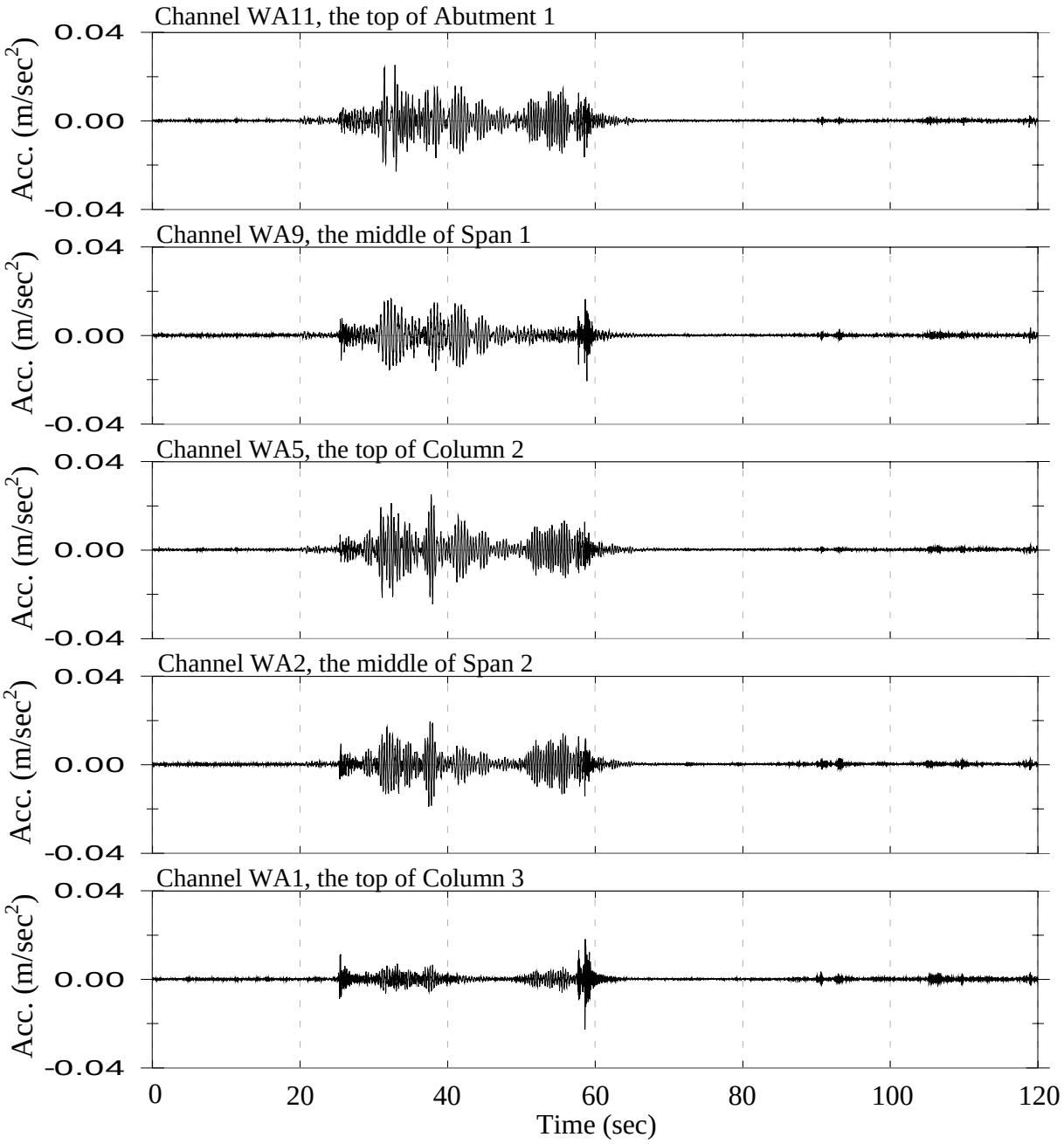

Figure 6.5: Typical Transverse Acceleration Time History
of Super-Structure at West Street On-Ramp

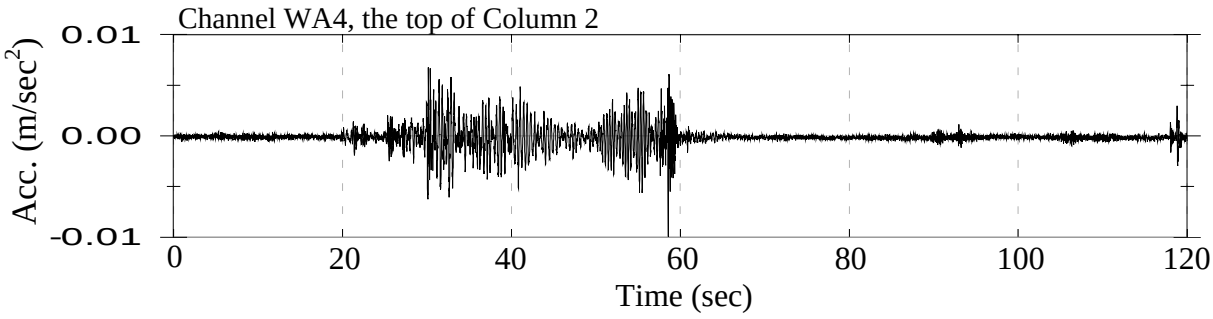

Figure 6.6: Typical Longitudinal Acceleration Time History
of Super-Structure at West Street On-Ramp

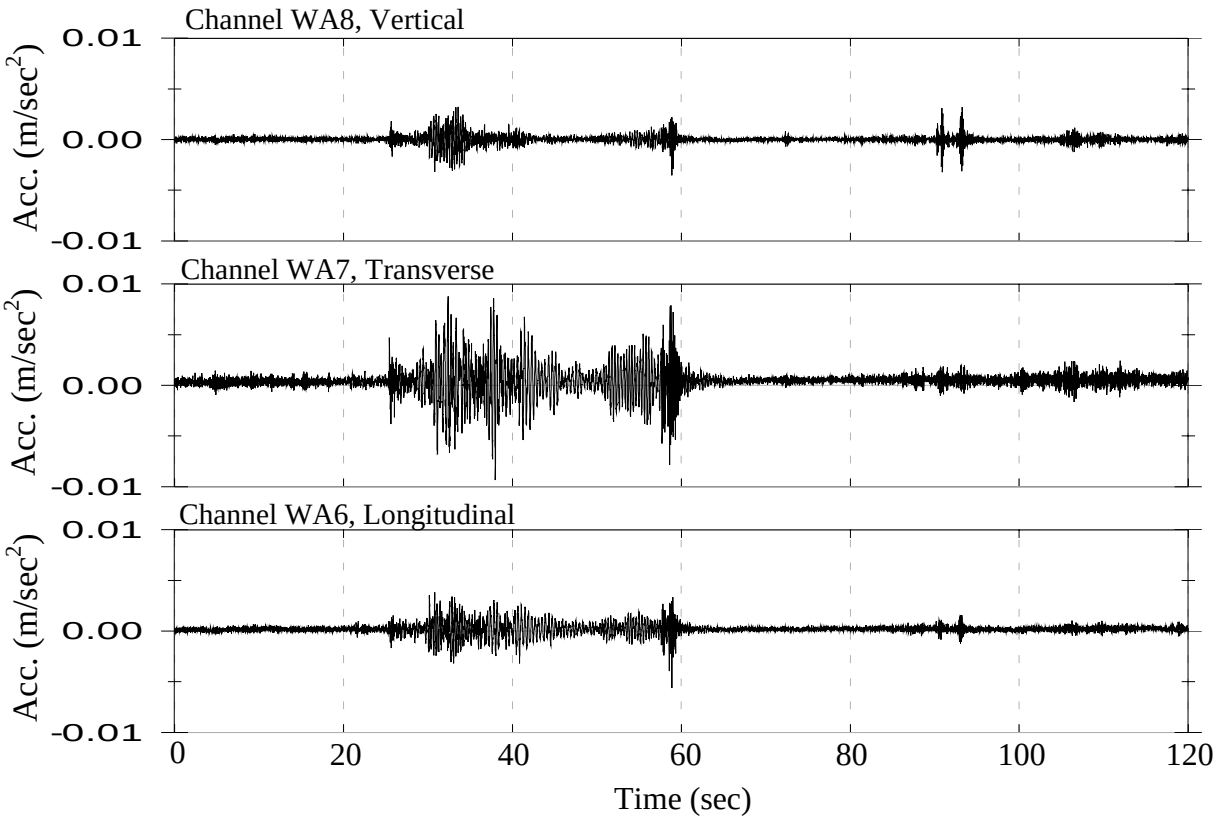

Figure 6.7: Typical Acceleration Time History at the Bottom of Column 2 of West Street On-Ramp

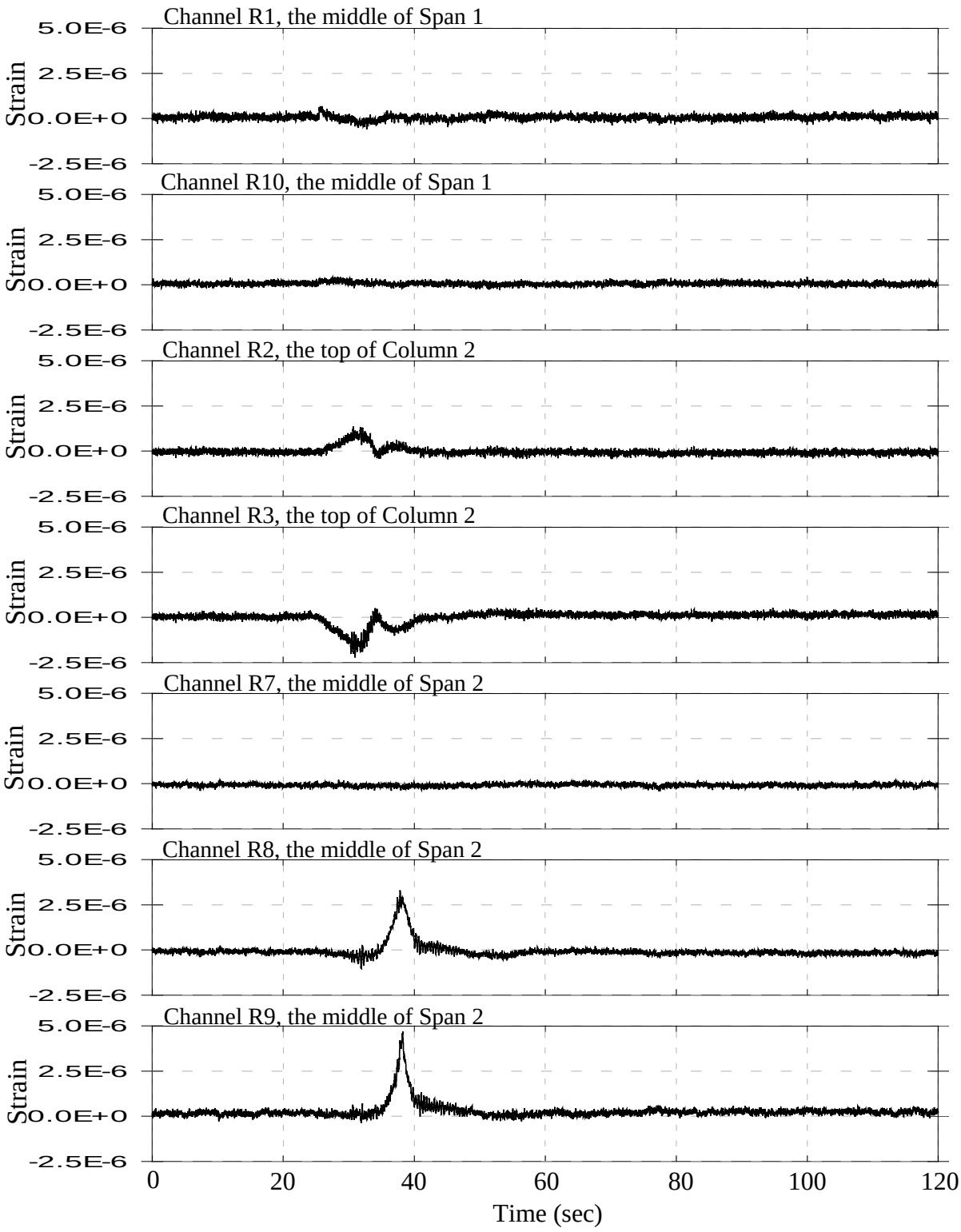

Figure 6.8: Typical Strain Time History of Super-Structure at West Street On-Ramp

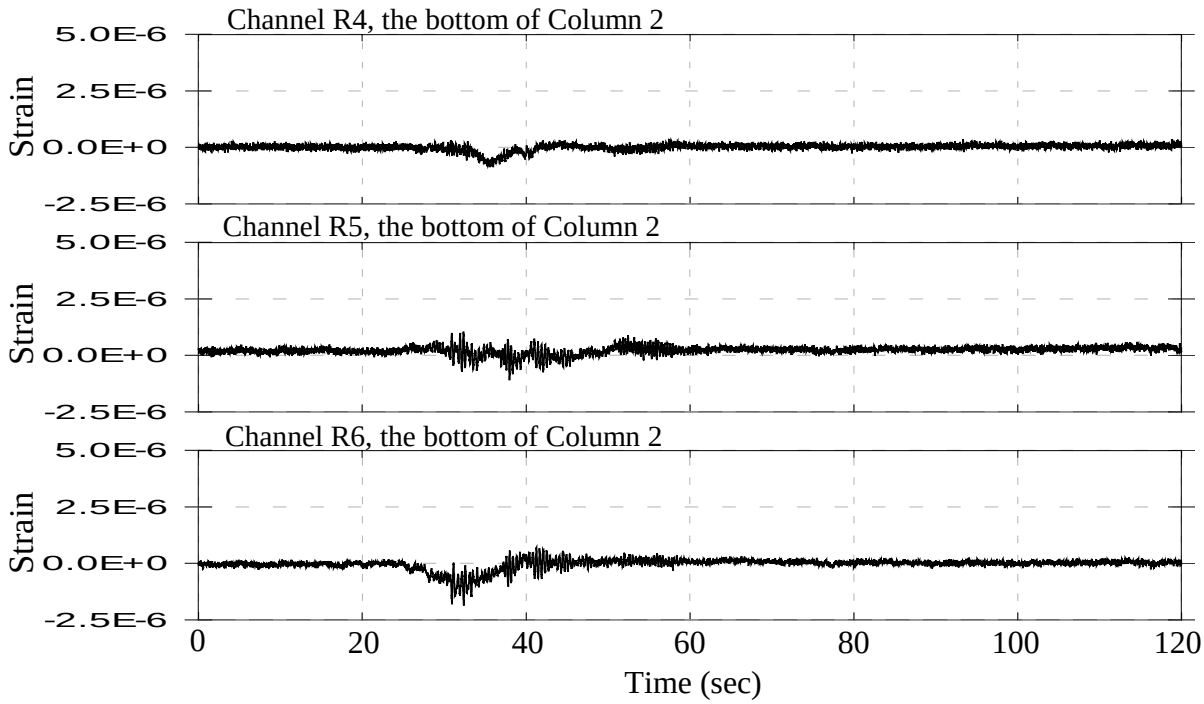

Figure 6.9: Typical Strain Time History at the Bottom of Column 2 of West Street On-Ramp

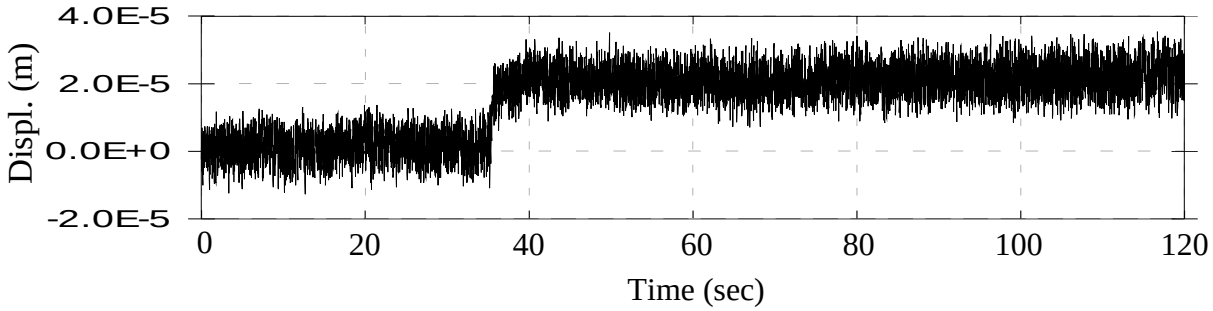

Figure 6.10: Typical Longitudinal Displacement Time History
of Super-Structure at Abutment 1 of West Street On-Ramp

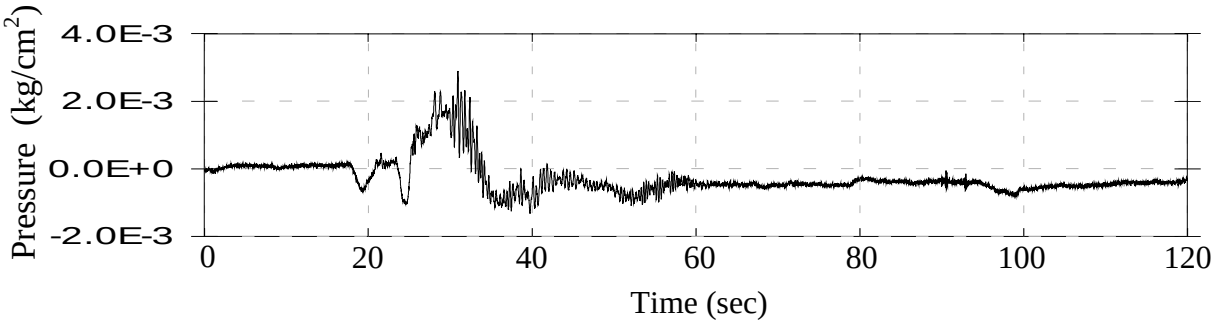

Figure 6.11: Typical Soil Pressure Time History at Abutment 1 of West Street On-Ramp

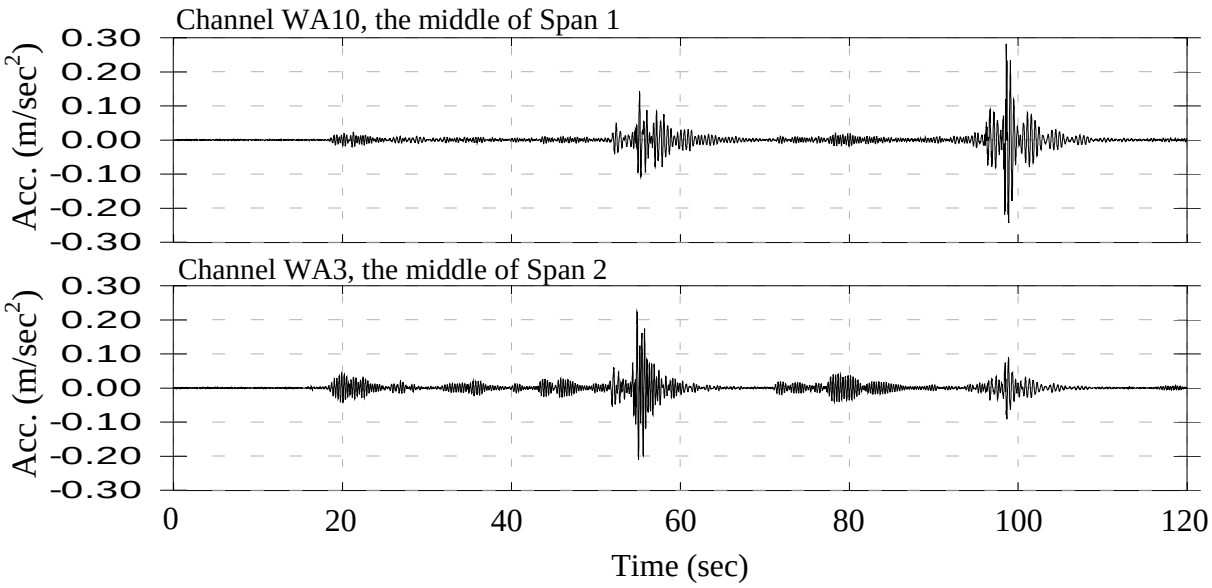

Figure 6.12: Typical Vertical Acceleration Time History
of Super-Structure at West Street On-Ramp

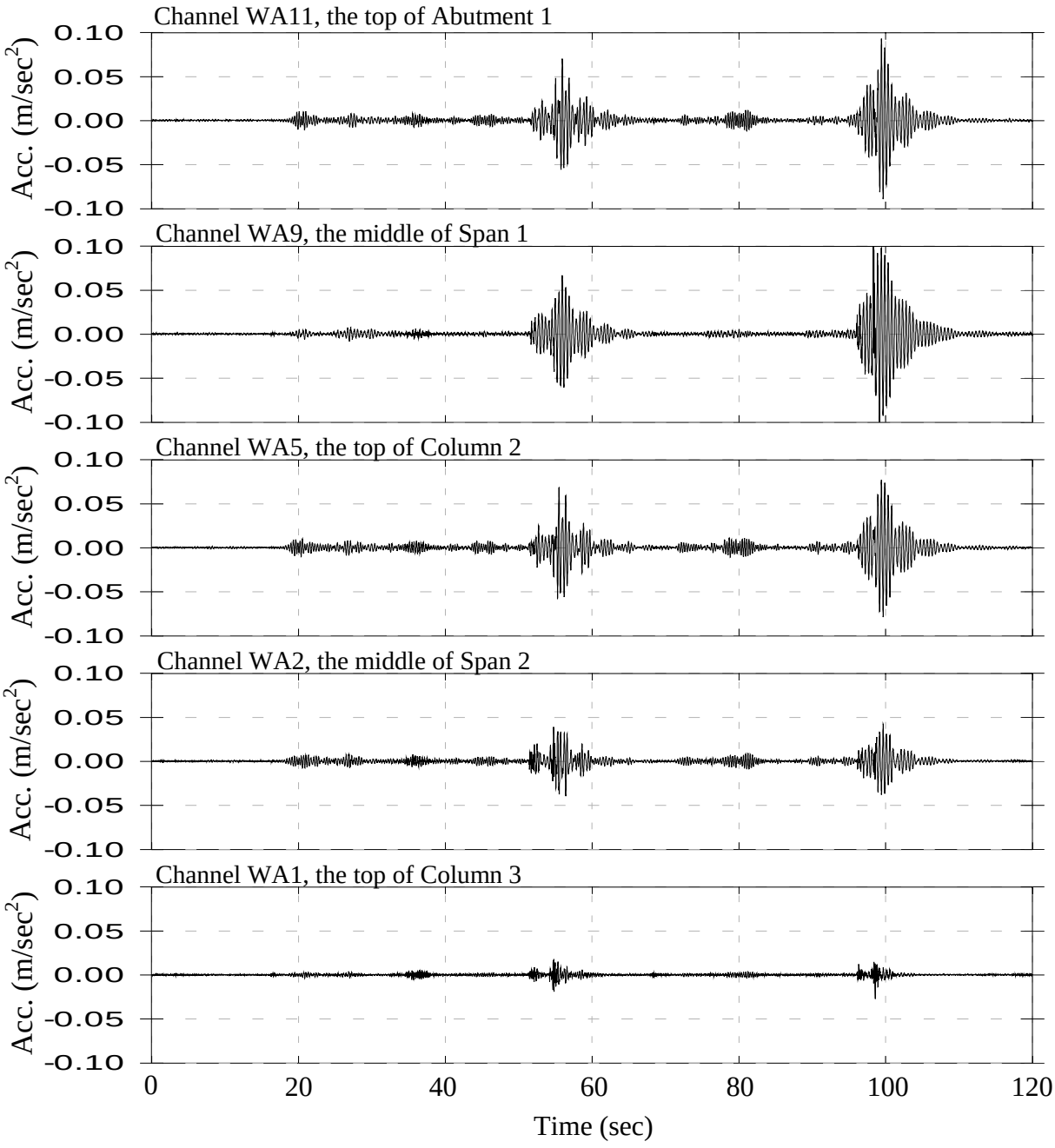

Figure 6.13: Typical Transverse Acceleration Time History
of Super-Structure at West Street On-Ramp

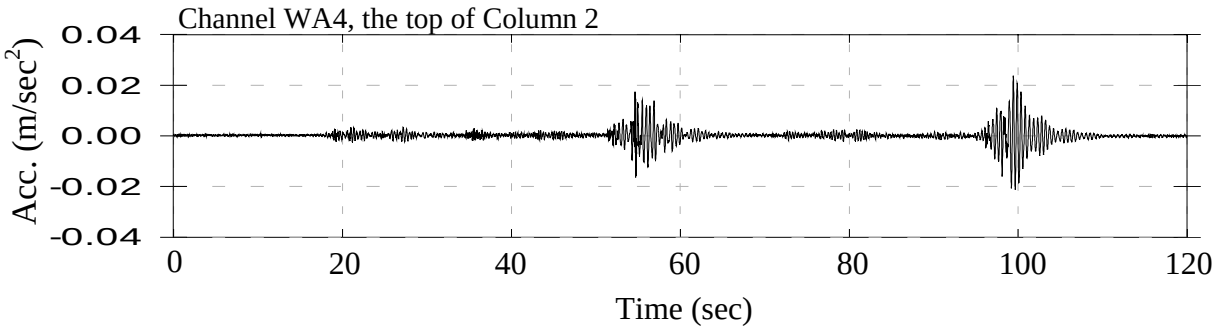

Figure 6.14: Typical Longitudinal Acceleration Time History
of Super-Structure at West Street On-Ramp

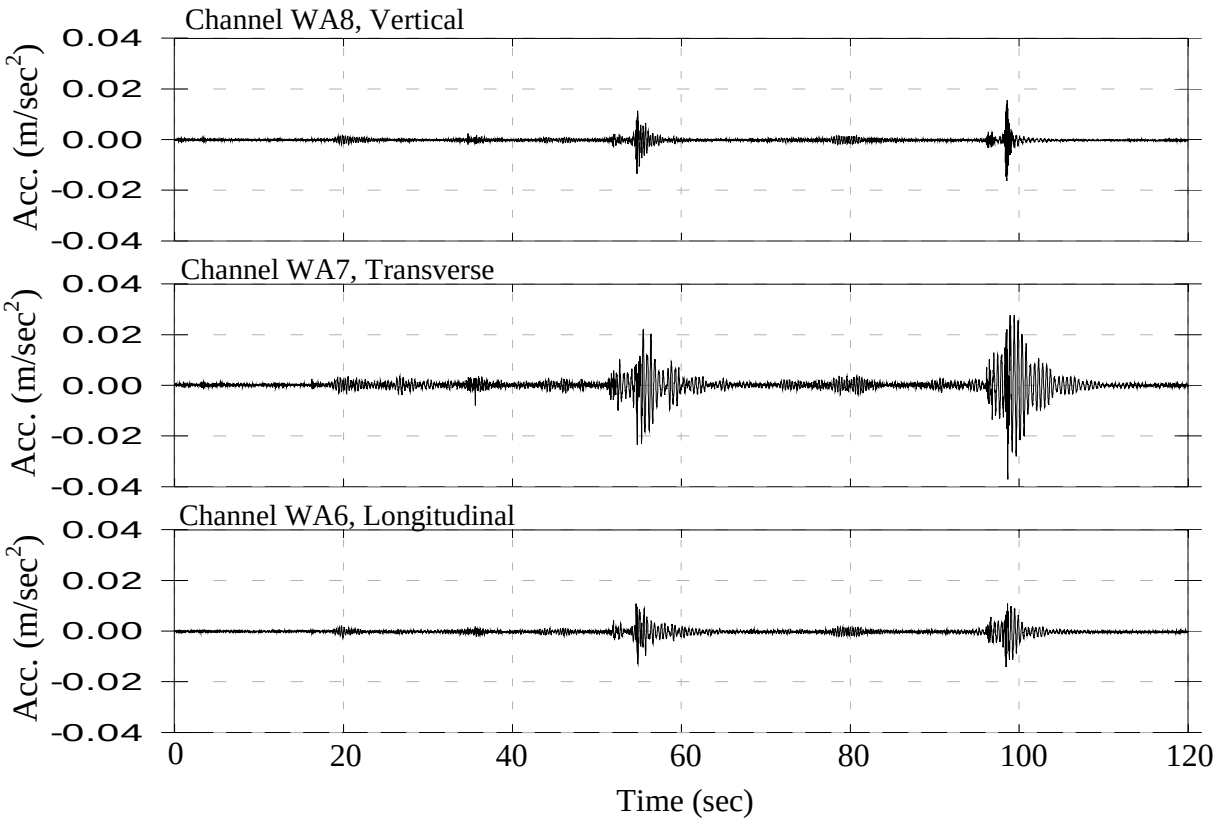

Figure 6.15: Typical Acceleration Time History
at the Bottom of Column 2 of West Street On-Ramp

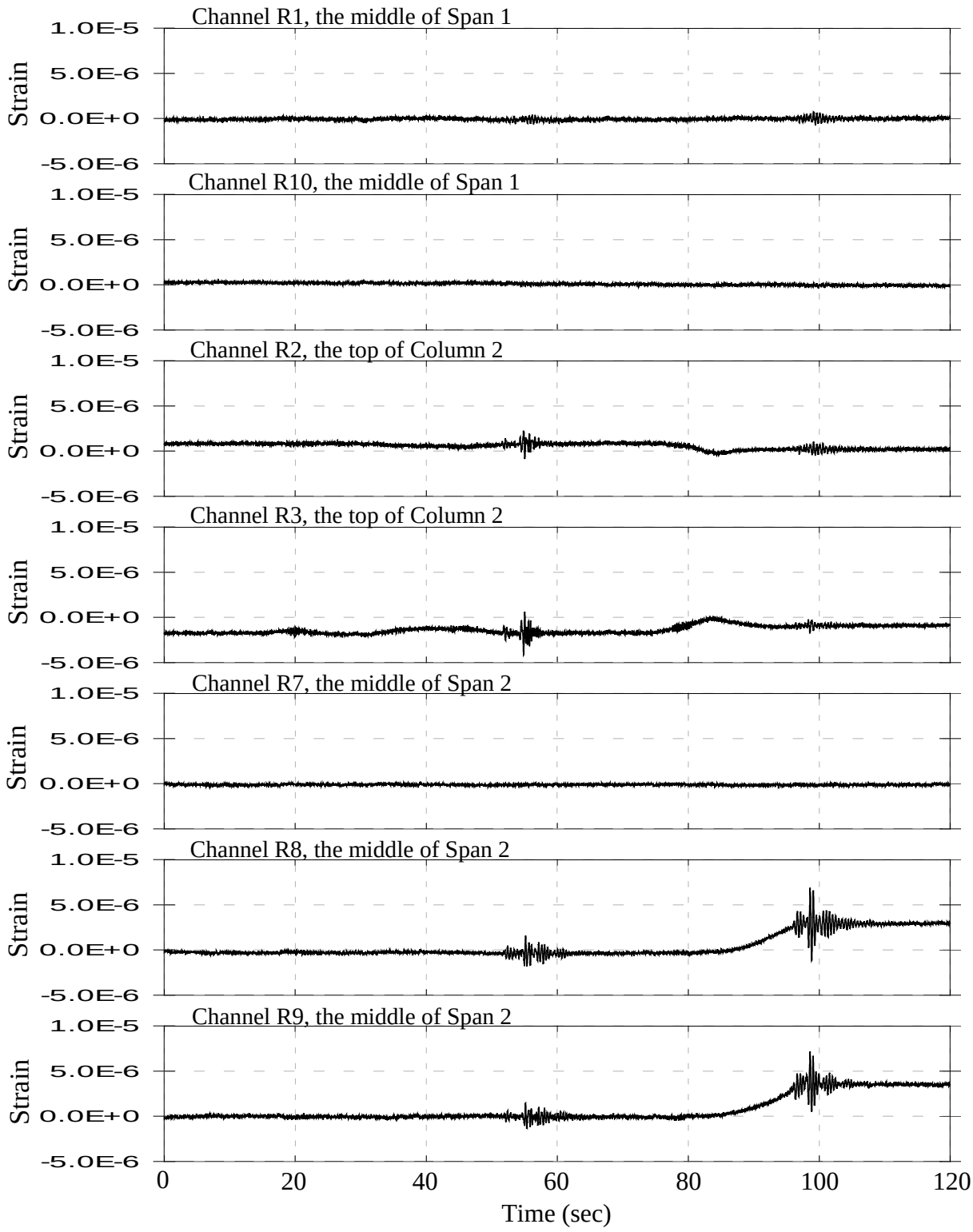

Figure 6.16: Typical Strain Time History
of Super-Structure at West Street On-Ramp

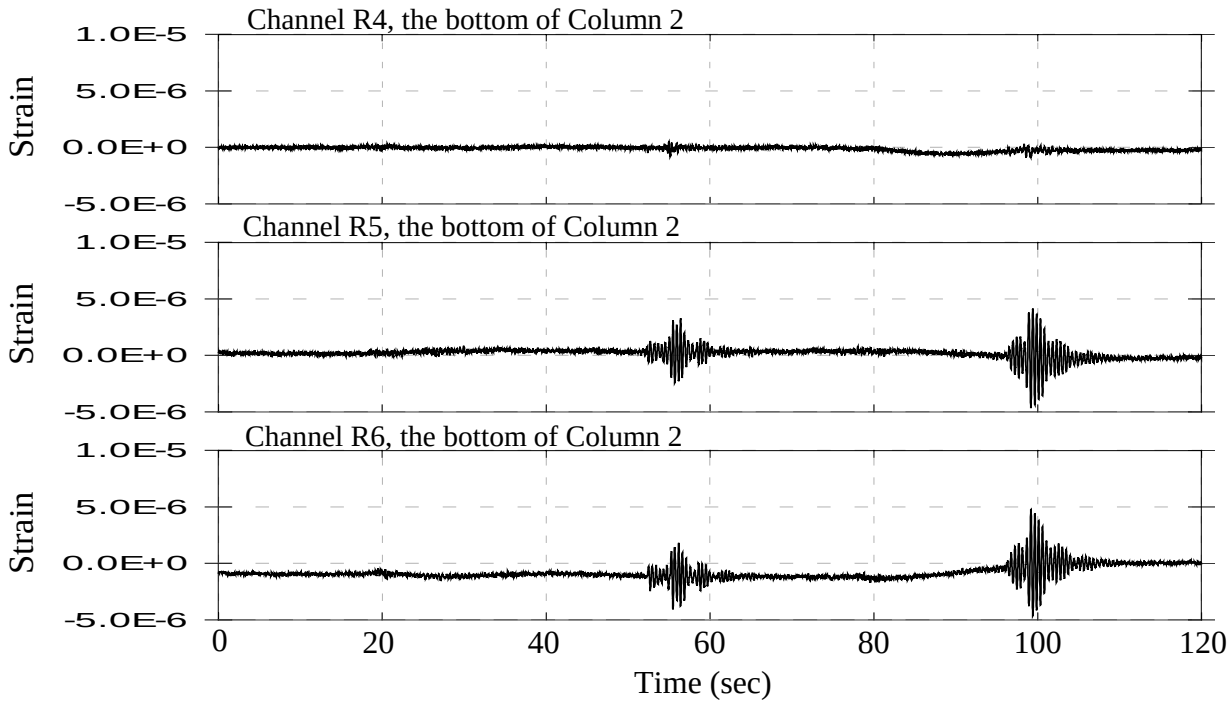

Figure 6.17: Typical Strain Time History
at the Bottom of Column 2 of West Street On-Ramp

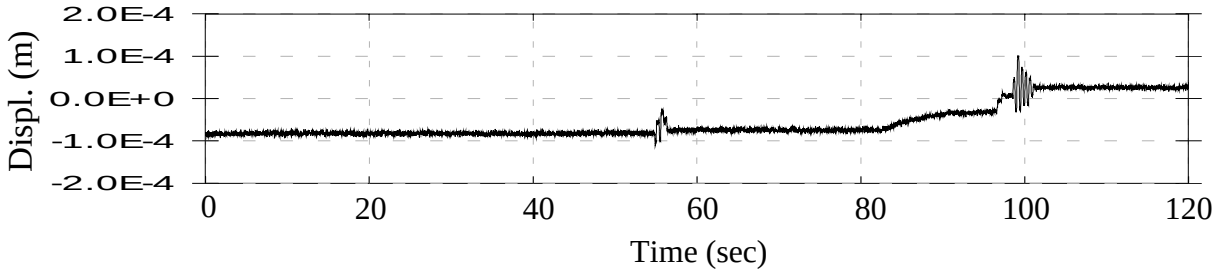

Figure 6.18: Typical Longitudinal Displacement Time History
of Super-Structure at Abutment 1 at West Street On-Ramp

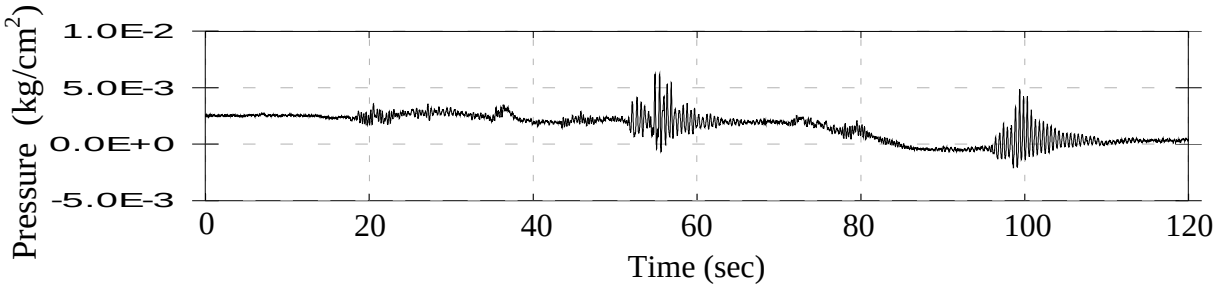

Figure 6.19: Typical Soil Pressure Time History at Abutment 1 at West Street On-Ramp

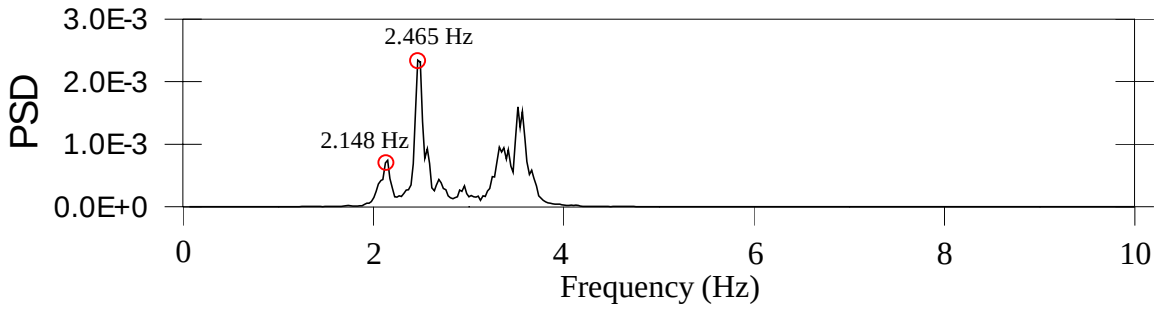

Figure 6.20: Power Spectral Density Function of Vertical Accelerations During Braking Vibration Tests

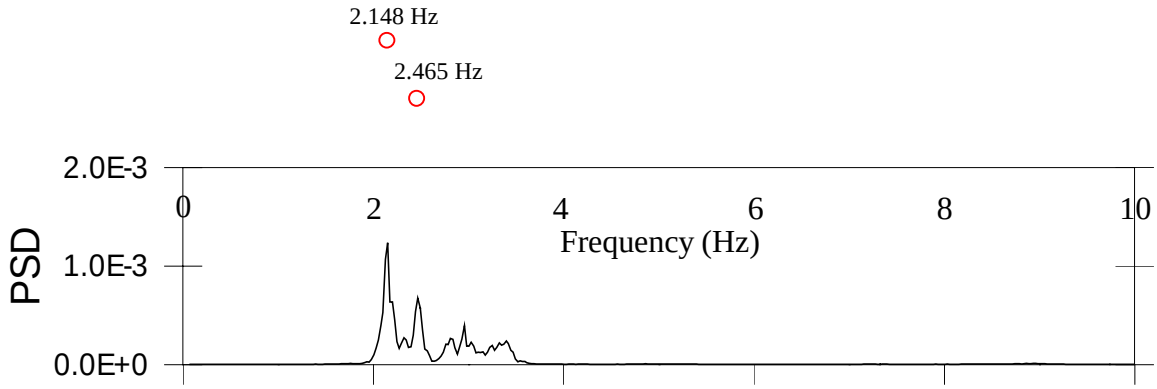

Figure 6.21: Power Spectral Density Function of Transverse Accelerations During Braking Vibration Tests

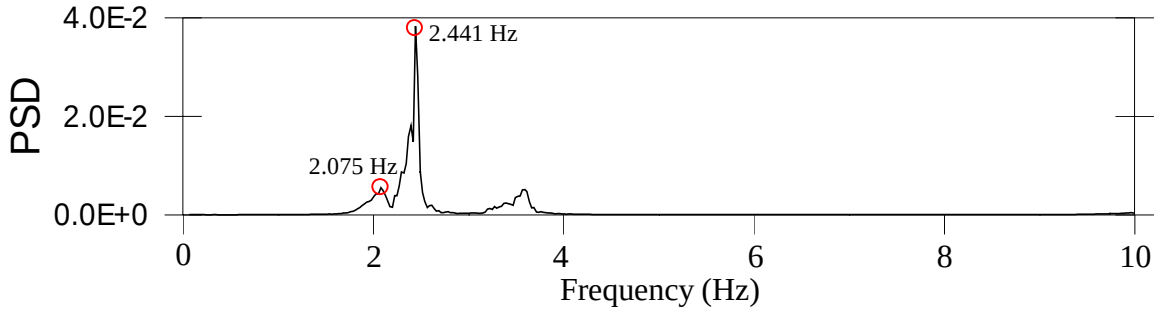

Figure 6.22: Power Spectral Density Function of Vertical Accelerations During Bumping Tests

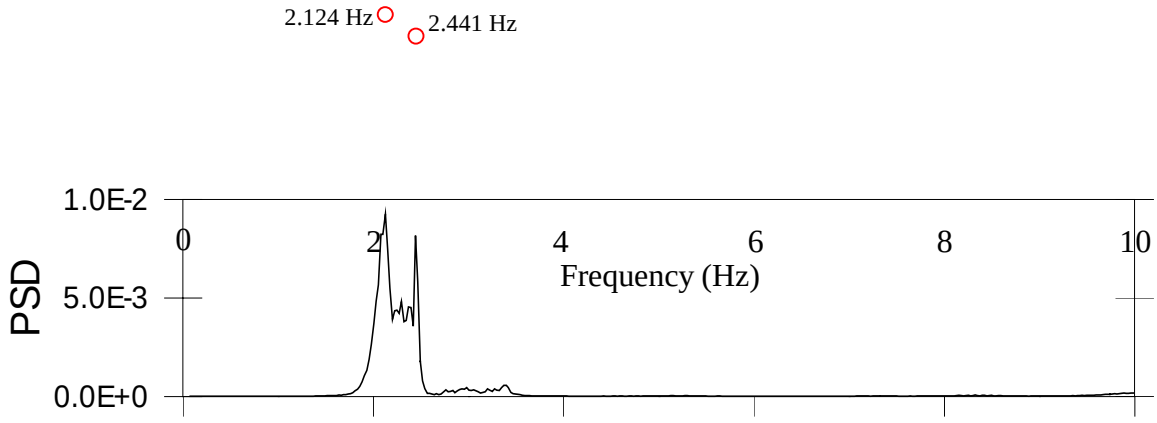

Figure 6.23: Power Spectral Density Function of Transverse Accelerations During Bumping Tests